Miocene basin development and volcanism along a strike-slip to flat-slab subduction transition: Stratigraphy, geochemistry, and geochronology of the central Wrangell volcanic belt, Yakutat–North America collision zone

Jeffrey M. Trop[1], William K. Hart[2], Darin Snyder[2], and Bruce Idleman[3]
[1]*Department of Geology, Bucknell University, Moore Avenue, Lewisburg, Pennsylvania 17837, USA*
[2]*Department of Geology and Environmental Earth Science, Miami University, Oxford, Ohio 45056, USA*
[3]*Department of Earth and Environmental Sciences, Lehigh University, Bethlehem, Pennsylvania 18015, USA*

ABSTRACT

New geochronologic, geochemical, sedimentologic, and compositional data from the central Wrangell volcanic belt (WVB) document basin development and volcanism linked to subduction of overthickened oceanic crust to the northern Pacific plate margin. The Frederika Formation and overlying Wrangell Lavas comprise >3 km of sedimentary and volcanic strata exposed in the Wrangell Mountains of south-central Alaska (United States). Measured stratigraphic sections and lithofacies analyses document lithofacies associations that reflect deposition in alluvial-fluvial-lacustrine environments routinely influenced by volcanic eruptions. Expansion of intrabasinal volcanic centers prompted progradation of vent-proximal volcanic aprons across basinal environments. Coal deposits, lacustrine strata, and vertical juxtaposition of basinal to proximal lithofacies indicate active basin subsidence that is attributable to heat flow associated with intrabasinal volcanic centers and extension along intrabasinal normal faults. The orientation of intrabasinal normal faults is consistent with transtensional deformation along the Totschunda-Fairweather fault system. Paleocurrents, compositional provenance, and detrital geochronologic ages link sediment accumulation to erosion of active intrabasinal volcanoes and to a lesser extent Mesozoic igneous sources. Geochemical compositions of interbedded lavas are dominantly calc-alkaline, range from basaltic andesite to rhyolite in composition, and share geochemical characteristics with Pliocene–Quaternary phases of the western WVB linked to subduction-related magmatism. The U/Pb ages of tuffs and $^{40}Ar/^{39}Ar$ ages of lavas indicate that basin development and volcanism commenced by 12.5–11.0 Ma and persisted until at least ca. 5.3 Ma. Eastern sections yield older ages (12.5–9.3 Ma) than western sections (9.6–8.3 Ma). Samples from two western sections yield even younger ages of 5.3 Ma.

Integration of new and published stratigraphic, geochronologic, and geochemical data from the entire WVB permits a comprehensive interpretation of basin development and volcanism within a regional tectonic context. We propose a model in which diachronous volcanism and transtensional basin development reflect progressive insertion of a thickened oceanic crustal slab of the Yakutat microplate into the arcuate continental margin of southern Alaska coeval with reported changes in plate motions. Oblique northwestward subduction of a thickened oceanic crustal slab during Oligocene to Middle Miocene time produced transtensional basins and volcanism along the eastern edge of the slab along the Duke River fault in Canada and subduction-related volcanism along the northern edge of the slab near the Yukon-Alaska border. Volcanism and basin development migrated progressively northwestward into eastern Alaska during Middle Miocene through Holocene time, concomitant with a northwestward shift in plate convergence direction and subduction collision of progressively thicker crust against the syntaxial plate margin.

INTRODUCTION

The evolution of continental-margin volcanic belts is typically difficult to reconstruct from stratigraphic studies. Erosion of high-standing volcanic belts removes much of the volcanic record, leaving only an expression of the subvolcanic plumbing of eruptive centers. Alternatively, subsidence of volcanic centers and subsequent burial by younger volcanic rocks obscures older phases of the stratigraphic record. Thus, exhumed sedimentary basins formed within volcanic belts offer valuable records of the long-term evolution of processes, environments, and climates. However, basins associated with such volcanic belts have not received the same rigorous analysis as other basin types, partly due to the paucity of well-exposed outcrops, postdepositional modification by deformation and intrusive activity, and abrupt lithofacies changes that complicate stratigraphic analyses (e.g., Smith and Landis, 1995; Bassett and Busby, 2005; Busby and Bassett, 2007). Previously unstudied sedimentary and volcanic strata exposed in high-relief regions of southern Alaska and adjacent parts of Canada offer insight on volcanic-related basin development. In particular, Holocene–recent deglaciation of the eastern Wrangell Mountains provides exceptional cross-sectional exposures of Neogene sedimentary and volcanic strata in the central part of the >500-km-long Wrangell volcanic belt (WVB) (Figs. 1–3). The depositional, geochronologic, petrologic, and geochemical characteristics of these strata are undocumented beyond the original regional-scale (1:63,360–1:250,000 scale) geologic mapping and a few K-Ar ages (Richter, 1976; MacKevett, 1978; Richter et al., 1990, 2000, 2006).

New geologic data from the WVB also contribute to reconstruction of the tectonic evolution of the northern Pacific margin, including subduction collision of the allochthonous Yakutat terrane. A >600-km-long segment of the Yakutat terrane was subducted at a shallow angle beneath south-central Alaska, prompting high rates of seismicity, crustal shortening, and erosion (Ferris et al., 2003; Eberhart-Phillips
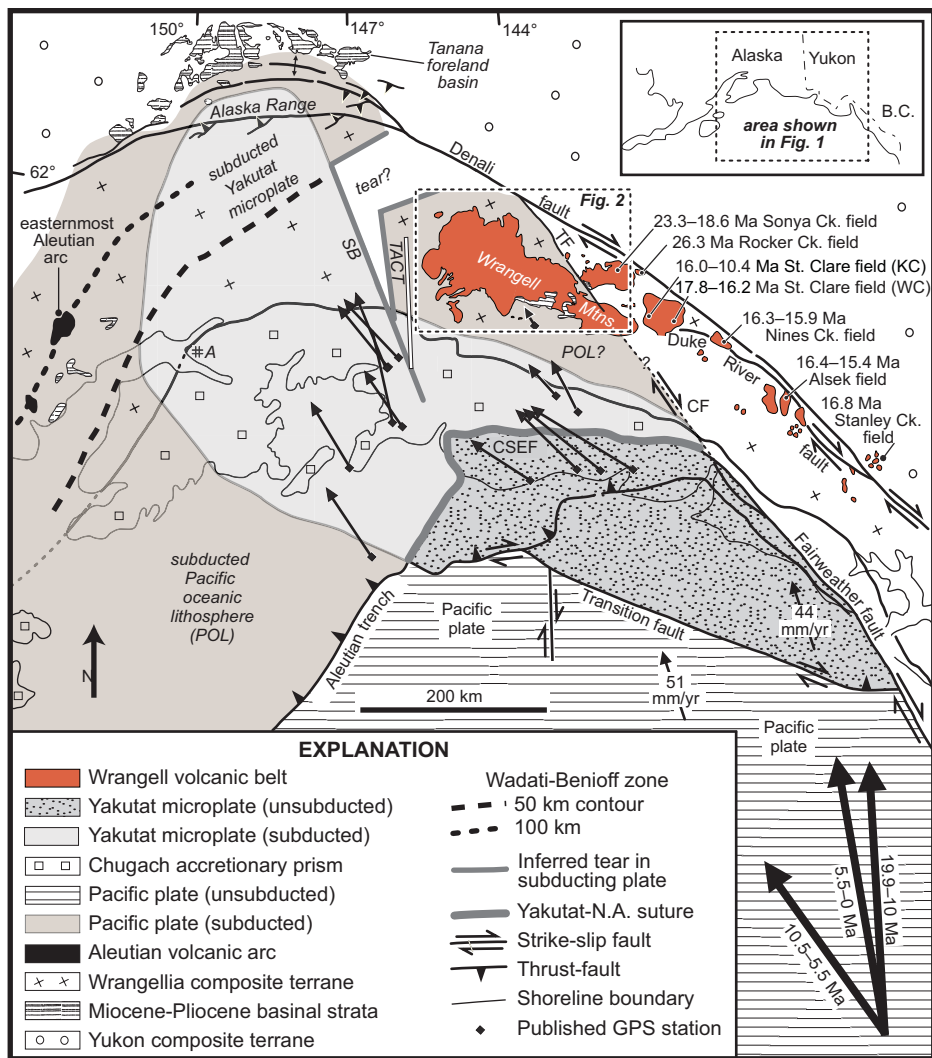
Figure 1. Map of southern Alaska and western Canada showing the Wrangell volcanic belt (WVB, red), easternmost Aleutian volcanic arc, Yakutat microplate, Wrangellia composite terrane, and major fault systems. Vector arrows in lower right corner show net displacement for Pacific plate with respect to North America during Miocene–recent time. Abbreviations: A—Anchorage, CF—inferred Fairweather-Totschunda connecting fault, Ck.—Creek, CSEF—Chugach–Saint Elias fault, GPS—global positioning system, KC—Klutlan volcanic center, N.A.—North America, SB—seismic anomaly that defines eastern boundary of subducted Yakutat microplate, TACT—Trans-Alaska Crustal Transect (a geophysical survey that constrains the crustal structure along the western margin of WVB) (Fuis et al., 2008), TF—Totschunda fault, WC—Wolverine volcanic center. Adapted from Pavlis et al. (2004), Kalbas et al. (2008), and Fuis et al. (2008).

stratigraphic observations, sediment provenance, geochemistry, and geochronology of Miocene sedimentary and volcanic strata exposed in the eastern Wrangell Mountains (MacKevett, 1978; Richter et al., 1990). This study reports (1) detailed stratigraphic and sedimentological data characterizing conditions of deposition and volcanism; (2) sedimentary provenance data (conglomerate and sandstone modal analyses, paleocurrents, and detrital zircon ages); (3) major and trace element geochemical compositions of lavas; and (4) $^{40}Ar/^{39}Ar$ and U/Pb ages of tuffs and lavas that bracket the timing of volcanism and basin development. Integration of these data sets with published studies from the eastern and western WVB provides the basis for understanding basin development and volcanism of the entire WVB in a regional tectonic context and offers an exceptional example of the stratigraphy and long-term evolution of a volcanic-related sedimentary basin.

GEOLOGIC AND TECTONIC FRAMEWORK

Active Tectonics

The northern Pacific plate margin is characterized by a west to east transition from normal subduction to flat-slab subduction to transform tectonics (Chapman et al., 2008; Haeussler, 2008). In the western region, subduction of the Pacific oceanic plate along the Aleutian megathrust produces a moderately dipping Wadati-Benioff zone that reaches depths of 100–150 km within ~400 km of the trench and active volcanism in the Aleutian Arc (Fig. 1). The central region is distinguished by relatively high topography, a lack of active volcanism, and a shallowly dipping Wadati-Benioff zone produced by flat-slab subduction of thickened oceanic crust, referred to as the Yakutat microplate or Yakutat terrane. Following Haeussler (2008), we use Yakutat terrane when the allochthonous nature of the crust is being emphasized and Yakutat microplate when plate kinematics is being highlighted. Currently subducting northwestward at a rate of 4.0–4.9 cm/yr, the shallow slab extends nearly horizontally for ~250 km northwestward beneath Alaska at a subduction angle of ~6° before reaching a depth of 150 km more than 600 km inboard of the Aleutian Trench (Eberhart-Phillips et al., 2006; Leonard et al., 2007). The microplate is separated from the North American plate by the Fairweather right-lateral fault to the east, the Aleutian megathrust to the northwest, and the Chugach–Saint Elias thrust to the north (Fig. 1). The Chugach–Saint Elias Range records deformation and exhumation within the zone of convergence between the Yakutat microplate and

et al., 2006; Haeussler, 2008). Recent studies provide major advances in our understanding of Neogene deformation, exhumation, and sediment accumulation along the suture zone between the Yakutat terrane and the former continental margin of Alaska (Sheaf et al., 2003; Bruhn et al., 2004; Pavlis et al., 2004; Gulick et al., 2007; Berger et al., 2008a, 2008b; Chapman et al., 2008; Meigs et al., 2008; Enkelmann et al., 2008, 2009, 2010; McAleer et al., 2009;

Perry et al., 2009; Witmer, 2009, Christeson et al., 2010; Koons et al., 2010; Worthington et al., 2010, 2012). In contrast, links between the subducted northeastern edge of the Yakutat terrane and deformation, volcanism, and sediment accumulation in the adjacent WVB remain largely unexplored, especially compared with continental U.S. standards.

In this paper, we investigate basin development and volcanism in the central WVB through

Figure 2. Map of the western and central part of the Wrangell volcanic belt (WVB) with known major vents. Note westward younging of volcanic centers with the exception of Mount Churchill and interior cinder cones in the western volcanic belt that are oriented subparallel to the trend of the volcanic belt. BP—before present. Adapted from Preece and Hart (2004).
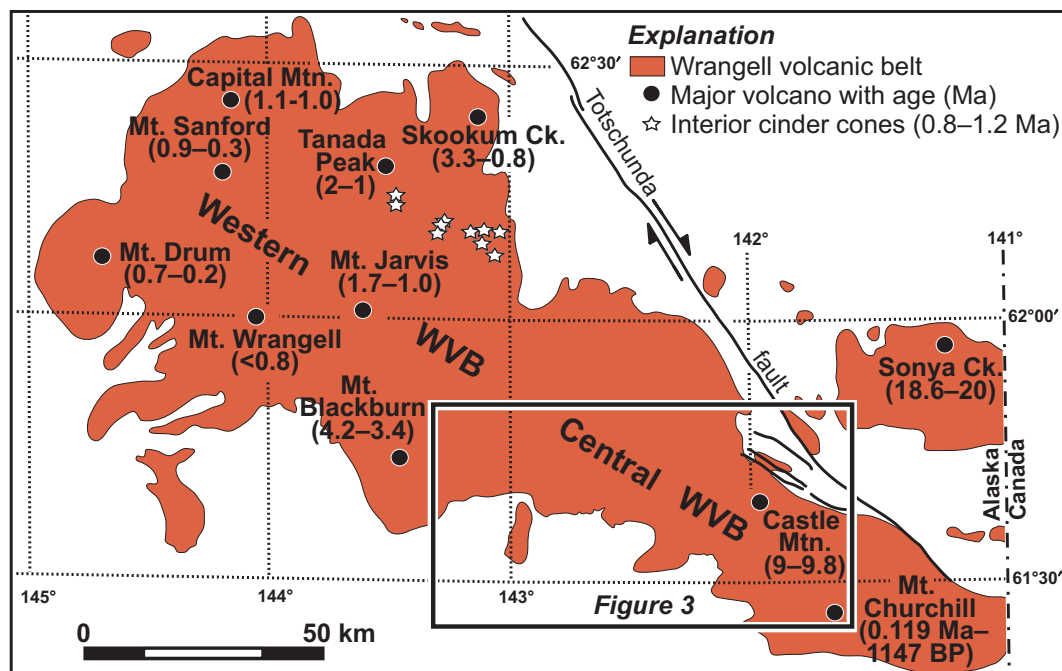
North American plate (Bruhn et al., 2004; Pavlis et al., 2004; Haeussler, 2008; Chapman et al., 2008). Regional tomographic (Eberhart-Phillips et al., 2006) and receiver function studies (Ferris et al., 2003) image the subducted portion of the Yakutat crust as a 15–20-km-thick low-velocity zone. The crystalline crust composing the unsubducted portion of the Yakutat terrane increases in thickness west to east from 15 km to 30 km (Worthington et al., 2012). Based on the crustal thickness, velocity structure, and shallow subduction angle, the Yakutat terrane is interpreted as an oceanic plateau composed of anomalously thick, and therefore more buoyant, oceanic crust (e.g., Bruhn et al., 2004; Pavlis et al., 2004; Gulick et al., 2007; Worthington et al., 2012).

The eastern region is marked by active volcanism in the WVB, shallow seismicity (<50 km), and right-lateral displacement along the Denali, Totschunda, and Fairweather faults (Page et al., 1991; Eberhart-Phillips et al., 2003; Preece and Hart, 2004). The Wrangell Mountains record volcanism, deformation, and exhumation along the northeastern edge of the subducted microplate (Miller and Richter, 1994; Preece and Hart, 2004; Enkelmann et al., 2010). Seismicity studies record few earthquakes along the eastern Denali fault, suggesting that this segment of the fault is relatively inactive (Page et al., 1991; Matmon et al., 2006). Instead, the Totschunda and Fairweather faults cut the WVB and transfer right-lateral shear from the Queen Charlotte fault in southeastern Alaska and British Columbia northward to the Denali fault in central Alaska. The Fairweather and Totschunda faults

may be joined by an unnamed southeast-striking fault (Richter and Matson, 1971; Kalbas et al., 2008); alternatively, the Fairweather fault may merge westward with numerous thrust faults (Doser and Lomas, 2000). The Fairweather fault, Totschunda fault, and possibly a Fairweather-Totschunda connecting fault constitute a northward extension of the Queen Charlotte–Fairweather transform system that accommodates right-lateral motion of the Pacific plate and Yakutat microplate relative to North America (Kalbas et al., 2008).

Geologic Framework

Southern Alaska consists of a collage of accreted terranes, magmatic belts, exhumed sedimentary basins, and subduction complex rocks that amalgamated during Mesozoic to Cenozoic time (Nokleberg et al., 1994; Trop and Ridgway, 2007). Three composite terranes make up much of the crust. From north to south, these include the Yukon, Wrangellia, and Southern Margin composite terranes (Fig. 1). The Yukon composite terrane consists of Proterozoic–Paleozoic metamorphic rocks (Yukon-Tanana terrane) and igneous rocks (Stikine terrane). The Wrangellia composite terrane consists of Mesozoic island-arc assemblages (Wrangellia and Peninsular terranes) and Paleozoic–Precambrian rifted continental-margin assemblages (Alexander terrane) that accreted to the Yukon composite terrane by Cretaceous time (Rioux et al., 2007; Trop, 2008). Mesozoic basinal strata in the suture zone record collision and exhumation of

the Wrangellia and Yukon composite terranes (Hampton et al., 2010). The Denali fault bisects the suture zone and accommodates as much as 400 km of Cretaceous–recent right-lateral displacement (Nokleberg et al., 1994; Matmon et al., 2006). The Wrangellia composite terrane is juxtaposed against the Southern Margin composite terrane along the Border Ranges fault system, which records as much as several hundred kilometers of Late Cretaceous–Paleogene right-lateral displacement (Pavlis and Roeske, 2007). From north to south, the Southern Margin composite terrane includes the Chugach, Prince William, and Yakutat terranes. The Chugach and Prince William terranes consist chiefly of Cretaceous–Eocene metasedimentary strata interpreted as offscraped seafloor strata associated with subduction of oceanic crust beneath the Wrangellia composite terrane prior to collision of the allochthonous Yakutat terrane (Plafker et al., 1994). The Yakutat terrane is sutured against the Prince William terrane along the Chugach–Saint Elias fault (Fig. 1; Chapman et al., 2008).

Geology of the WVB

The WVB extends >500 km across eastern Alaska, northwestern British Columbia, and southwestern Yukon Territory, making up much of the high relief of the Wrangell Mountains, including ice-capped volcanoes with elevations exceeding 4600 m (Figs. 1–3). The volcanic belt consists of Miocene–Holocene lava flows, lava domes, and pyroclastic deposits erupted from
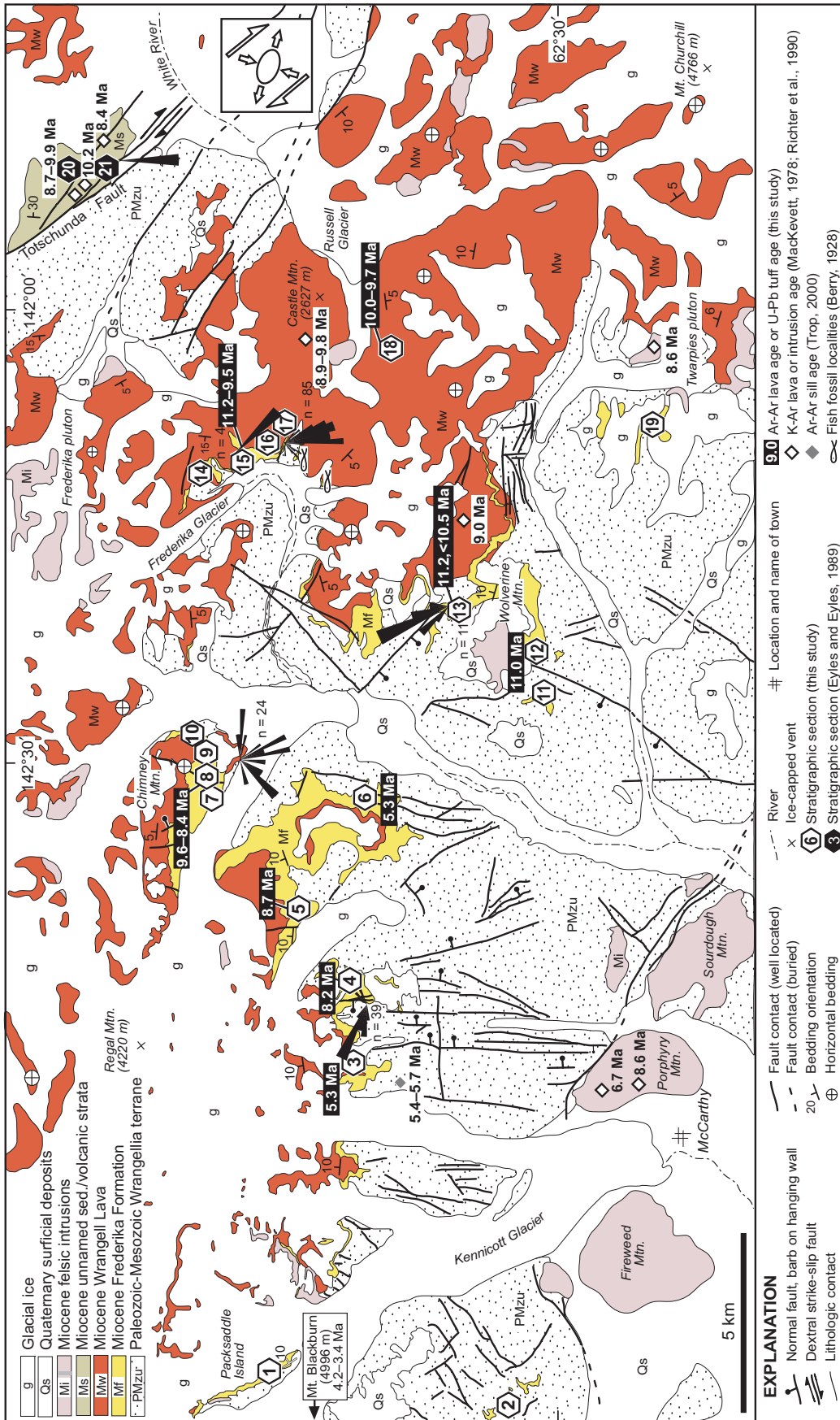
Figure 3. Geologic map of the eastern Wrangell Mountains showing Miocene deposits, isotopic ages, measured section locations, and paleocurrent data. Miocene strata include interbedded siliciclastic sedimentary and volcanic strata (Mf—yellow pattern, Frederika Formation) and thick successions of volcanic strata (Mw—red pattern, Wrangell Lavas). Miocene shallow-level intrusions (Mi—purple) overlap the age of Miocene sedimentary and volcanic strata. Numbered locations 1–21 on the map represent measured section locations where samples were collected for analytical studies. See Figure 1 for map location and Figures 5–6 for generalized sections and sample locations. Detailed sections are presented in Supplemental Figures 1–4 (see footnotes 1–4). Note north-striking normal faults with known pre-Cenozoic displacement are not depicted. Strain ellipse shows directions of shortening and extension that would be expected in response to right-lateral simple shear along a fault with the same orientation as the Totschunda fault. Rose diagrams show paleocurrent directions from cross-stratification and clast imbrication; n—number of paleocurrent measurements per locality. Rose diagram at station 21 represents south-directed paleocurrents reported by Eyles and Eyles (1989); quantitative data were not reported. Geology adapted from MacKevett (1970a, 1970b, 1978) and Richter et al. (2000).

shield volcanoes, stratovolcanoes, caldera complexes, and cinder cones along with subordinate siliciclastic strata that accumulated in volcanic-related sedimentary basins (Skulski et al., 1991, 1992; Richter et al., 2006). WVB deposits unconformably overlie the Wrangellia composite terrane, exhibit maximum preserved thicknesses >3 km, and yield geochronologic ages ranging from 26 Ma to 1500 ka (Fig. 4; Richter, 1976; MacKevett, 1978; Richter et al., 2006).

The ages, geochemical compositions, and structural framework of WVB strata vary from east to west. WVB deposits in the Yukon Territory and northwestern British Columbia crop out discontinuously for >300 km along the Duke River fault splay of the Denali fault (Figs. 1–3). Individual volcanic centers include the Stanley Creek, Alsek, Nines Creek, and Saint Clare centers (Fig. 1). Previous studies define two stratigraphic packages: a lower succession of Eocene–Oligocene sedimentary strata (Amphitheater Formation) and an upper succession of chiefly Miocene lavas and subordinate pyroclastic, intrusive, and sedimentary rocks (Wrangell Lavas; Skulski et al., 1991, 1992; Cole and Ridgway, 1993; Ridgway and DeCelles, 1993a, 1993b). The Duke River fault cuts the lower part of the WVB lavas and possibly related faults cut the entire lava pile. Eastern WVB volcanism is interpreted chiefly as the product of eruptions along leaky strike-slip faults, based on the dominance of alkaline to transitional geochemical compositions and close spatial association of the volcanic rocks with strike-slip faults that cut the volcanic pile (Souther and Stanciu, 1975; Skulski et al., 1991, 1992).

The central WVB, the focus of this study, extends from the Alaska-Yukon border region to Mount Blackburn, a Pliocene volcano in the Wrangell Mountains (Figs. 2 and 3). Previous studies define two stratigraphic packages: a lower succession of Miocene sedimentary strata with subordinate lavas, pyroclastic rocks, and intrusive rocks (Frederika Formation) and an upper succession of chiefly Miocene lavas and subordinate pyroclastic, intrusive, and sedimentary rocks (Wrangell Lavas; Figs. 4 and 5; Denton and Armstrong, 1969; MacKevett, 1978; Eyles and Eyles, 1989; Richter et al., 2000). Both successions are cut by north-striking high-angle faults that exhibit small amounts of normal separation (mostly <10–20 m) and the northwest-striking Totschunda fault, which reveals ~10 km of right-lateral offset (Richter and Matson, 1971; Plafker et al., 1977). The central WVB includes at least three known eruptive centers: Sonya Creek, Castle Mountain, and Mount Churchill (Figs. 2 and 3). Miocene intrusions within the belt likely represent the dissected subvolcanic roots of remnant eruptive centers (Porphyry, Sourdough, Twarpies intrusions in Fig. 3).

The western WVB consists of Pliocene–Holocene shield volcanoes, stratovolcanoes, and cinder cones in the western Wrangell Mountains (Fig. 2; Richter et al., 1990, 1994, 2006). Extensive icefields and glaciers partially cover Quaternary volcanoes with summit calderas at elevations >3500–4900 m above sea level. Western WVB volcanism is attributed to subduction-related processes based on transitional to calc-alkaline geochemical compositions and the spatial association of shield and stratovolcanoes above a geophysically imaged northward-dipping subducting slab (Page et al., 1989; Miller and Richter, 1994; Preece and Hart, 2004; Fuis et al., 2008). In summary, the western WVB records Miocene–Holocene subduction-related volcanism, whereas the eastern WVB records Oligocene–Miocene volcanism and basin development associated with displacement along strike-slip faults. New geochronologic, geochemical, and stratigraphic data from previously undocumented Miocene strata of the central WVB permit comprehensive evaluation of the tectonic evolution of the entire 500-km-long length of the volcanic belt, including the transition zone from strike-slip to subduction tectonics.

DEPOSITIONAL SYSTEMS

Stratigraphic Context

Central WVB deposits are well exposed in recently deglaciated cirques below the Nabesna icefield, plateaus between the Chitistone and

Figure 4. Chronostratigraphic chart summarizing all published isotopic ages of volcanic strata and shallow-level intrusions in the Wrangell volcanic belt (WVB). Black vertical lines show ages and calculated errors reported from individual vents. The ranges of new ages reported in this study are depicted by orange circles. Asterisks represent U/Pb ages of detrital zircons from Miocene sandstone from the Frederika Formation (see Fig. 12; Supplemental Table 1 [see footnote 5]). Age compilation includes 91 K/Ar ages compiled by Richter et al. (1990; the publications from which these data were originally reported range from 1969 to 1990). Additional plotted data include one $^{40}Ar/^{39}Ar$ age from Richter et al. (1990), six $^{40}Ar/^{39}Ar$ ages from Skulski et al. (1992), six $^{40}Ar/^{39}Ar$ ages from Ridgway et al. (1996), and twelve $^{40}Ar/^{39}Ar$ and two U/Pb ages from this study. Ages that the original authors deemed questionable or reset are not depicted here. Ages were not recalibrated using modern standards. Tectonics and basin development are adapted from Pavlis et al. (2004), Trop and Ridgway (2007), and Finzel et al. (2011). Time scale is from Gradstein et al. (2004). Quat.—Quaternary; Oligo.—Oligocene.
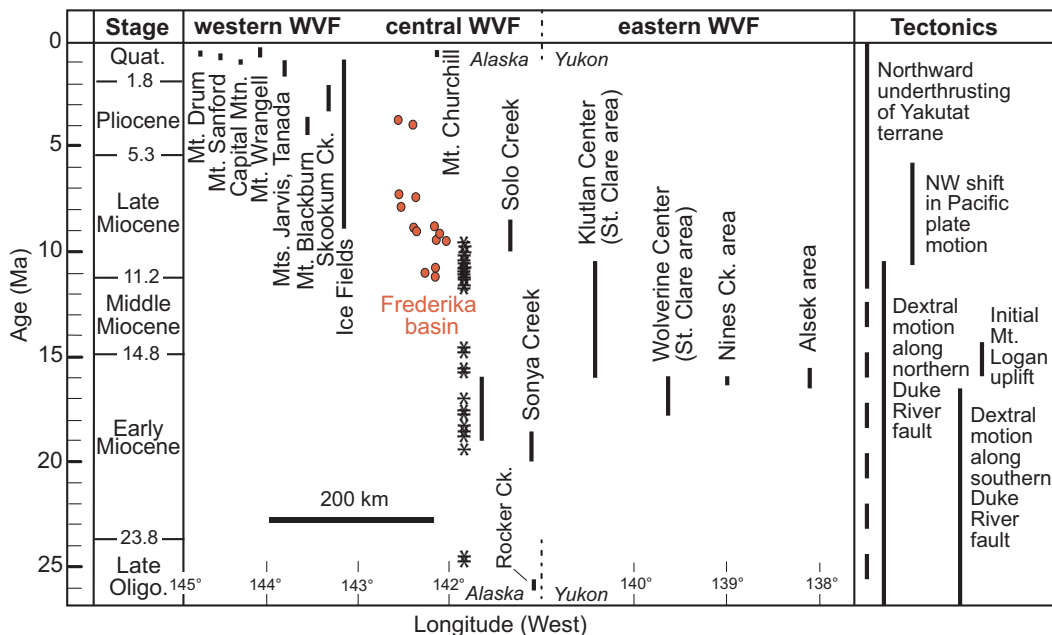
Nizina Rivers, and foothills along the White River (Fig. 3). Bedded strata exhibit consistently low-angle bedding dips (<15°) except for outcrops cut by the Totschunda fault. Figure 5 shows generalized sections for most of the studied outcrops. The Frederika Formation overlies, in angular unconformity, Mesozoic rocks with onlap relationships and an altitudinal range for the basal contact, reflecting an incised paleotopography with local relief >400 m (Figs. 3, 7A, and 7B). The maximum preserved thickness of the Frederika Formation in our measured sections is ~600 m (section 5 in Fig. 5). Upsection transitions from mostly sedimentary strata of the Frederika Formation to chiefly volcanic strata of the Wrangell Lavas vary from abrupt (sections 3–5 in Fig. 5) to gradational (sections 9, 13, 15 in Fig. 5). Uppermost strata are largely inaccessible due to steep, glaciated relief, so our measured sections span only several hundred meters of the upper succession (e.g., section 18 in Fig. 5). The maximum preserved thickness of the Wrangell Lavas is estimated as >3000 m (MacKevett, 1978).

Sedimentary and Volcanic Lithofacies Associations

Detailed sedimentologic observations were made while measuring a total of >5.5 km of stratigraphic sections on a bed-by-bed basis using a Jacob staff. Sections were correlated by tracing marker beds in the field and applying chronostratigraphy from isotopic ages of volcanic rocks. Complex lateral facies changes, paleotopography preserved along the basal erosional surface, and modern high-relief topography precluded more detailed stratigraphic correlations.

The Frederika Formation and lower Wrangell Lavas can be divided into four main lithofacies associations on the basis of grain size, lithology, and sedimentary structures. The lithofacies record deposition in proximal volcanic aprons and alluvial fans and more distal braided streams, anastomosing streams, and floodplains. Key aspects of each lithofacies association are summarized in the following. Table 1 summarizes common lithofacies and corresponding standard interpretations of depositional processes and environments. Key sedimentological features are shown in detailed sections in Figure 6 and Supplemental Figures 1[1], 2[2], 3[3], and 4[4], and photographs in Figures 7, 8, and 9.

Lithofacies Association 1: Braided Stream Deposits

Description. This association consists chiefly of moderately to well-organized, moderately sorted, clast-supported pebble-cobble conglomerate (Gcm, Gcmi), and subordinate massive to cross-stratified sandstone (Sm, St, Sp), tuffaceous sandstone (Smv), and sparse siltstone (Fsm) (see Fig. 5). Strata comprise broadly lenticular (several to <15 m) upward-fining bodies with erosional bases that scoured tens of centimeters deep. Internally, beds are amalgamated and marked by reactivation surfaces, reworked organic debris, and clast imbrication. Lithofacies association 1 makes up the lower 100–130 m of sections 13 and 15 in the northeastern part of the outcrop belt (Figs. 5 and 6; Supplemental Figs. 3 and 4 [see footnotes 3 and 4]). Representative photos are shown in Figures 8A and 8B.

Interpretation. Lithofacies association 1 reflects subaqueous gravel deposition in braided stream channels and bar tops by tractive forces capable of routinely transporting pebble- and cobble-sized clasts. Evidence for fluvial bedload deposition includes the erosive bases, scours, upward-fining trends, unidirectional paleocurrent indicators, and laterally discontinuous sandstone and conglomerate. Sparse interbedded siltstones record overbank and waning-flood deposits. Characteristics of lithofacies association 1 are diagnostic of gravelly braided streams characterized by streamflow and flood flow (Lunt and Bridge, 2004; Miall, 2006). The moderate degree of sorting and/or rounding, lack of mass flow deposits, and upsection transitions to fine-grained fluvial-lacustrine strata (sections 13, 15 in Figs. 5 and 6 and Supplemental Figs. 3 and 4 [see footnotes 3 and 4]) indicate that braided streams formed within alluvial plain or distal alluvial fan environments as opposed to proximal alluvial fans.

Lithofacies Association 2: Anastomosing Stream, Floodplain, and Lacustrine Deposits

Description. Stratified volcanic-lithic sandstone (Sm, Sp, St, Sr), carbonaceous siltstone (Fsc), mudstone (Fsm), laminated shale (Fsl), bioturbated limestone and marl (Ls), coal, volcaniclastic strata (Smv, Vb, Vts, Vt), and subordinate pebble-cobble conglomerate (Gcm, Gcmi) typify association 2 (see Fig. 5). Lobate to wedge-shaped bed geometries dominate sandstone units, although coarser grained sandstone and conglomerate beds exhibit channelform geometries. Many sandstone interbeds exhibit nonerosive bases, horizontal stratification, load marks, current ripple lamination, and convolute lamination. Mudstones and siltstones exhibit mottling, variegated colors, and bioturbated and/or disrupted horizons, root traces, plant fossils, coalified wood, and petrified logs. Laminated mudstone and fissile shales contain abundant disseminated organic material and fish fossils (Fig. 3; Berry, 1928). Reworked pyroclastic and epiclastic deposits along with primary pyroclastic material are also present locally. Facies association 2 typifies the lower half of stratigraphic sections in the central and northwestern parts of the outcrop belt (sections 3–6, 11–15 in Figs. 5 and 6 and Supplemental Figs. 3 and 4 [see footnotes 3 and 4]). Representative photos of common lithofacies are shown in Figures 9A–9F.

Interpretation. Lithofacies association 2 reflects the deposits of anastamosing stream channels and vegetated floodplains. Channelform sandstone and conglomerate record deposition by subaqueous tractive transport in fluvial channels. Finer grained detritus was deposited from suspension as overbank and lacustrine sediments on floodplains, including crevasse splays, levees, vegetated overbank areas, mires, and ponds and/or lakes. Abrupt upsection transitions from channel sandstones to overbank deposits are comparable with multichannel anastomosing fluvial environments in humid high-latitude settings (Smith, 1983; Nadon, 1994; Morozova and Smith, 1999; Makaske, 2001). Breaching of channel margins prompted waning-flow and crevasse-splay deposition of massive to horizontally stratified sandstone with lobate, wedge, and channel-form geometries.

[1]Supplemental Figure 1. PDF file of log (in meters) of measured stratigraphic section 4 (PIL) in the central Wrangell volcanic belt. Mf—Miocene Frederika Formation; Mw—Miocene–Quaternary Wrangell Lavas. Refer to Figure 3 for location and Table 1 for explanation of lithofacies codes. If you are viewing the PDF of this paper or reading it offline, please visit http://dx.doi.org/10.1130/GES00762.S1 or the full-text article at www.gsapubs.org to view Supplemental Figure 1.

[2]Supplemental Figure 2. PDF file of log (in meters) of measured stratigraphic section 5 (BK1) in the central Wrangell volcanic belt. Mf—Miocene Frederika Formation; Mw—Miocene–Quaternary Wrangell Lavas. Refer to Figure 3 for section and Table 1 for explanation of lithofacies codes. If you are viewing the PDF of this paper or reading it offline, please visit http://dx.doi.org/10.1130/GES00762.S2 or the full-text article at www.gsapubs.org to view Supplemental Figure 2.

[3]Supplemental Figure 3. PDF file of log (in meters) of measured stratigraphic section 13 (DBT) in the central Wrangell volcanic belt. Mf—Miocene Frederika Formation; Mw—Miocene–Quaternary Wrangell Lavas. Refer to Figure 3 for location and Table 1 for explanation of lithofacies codes. If you are viewing the PDF of this paper or reading it offline, please visit http://dx.doi.org/10.1130/GES00762.S3 or the full-text article at www.gsapubs.org to view Supplemental Figure 3.

[4]Supplemental Figure 4. PDF file of log (in meters) of measured stratigraphic section 15 (FDN) in the central Wrangell volcanic belt. Mf—Miocene Frederika Formation; Mw—Miocene–Quaternary Wrangell Lavas. Refer to Figure 3 for location and Table 1 for explanation of lithofacies codes. If you are viewing the PDF of this paper or reading it offline, please visit http://dx.doi.org/10.1130/GES00762.S4 or the full-text article at www.gsapubs.org to view Supplemental Figure 4.
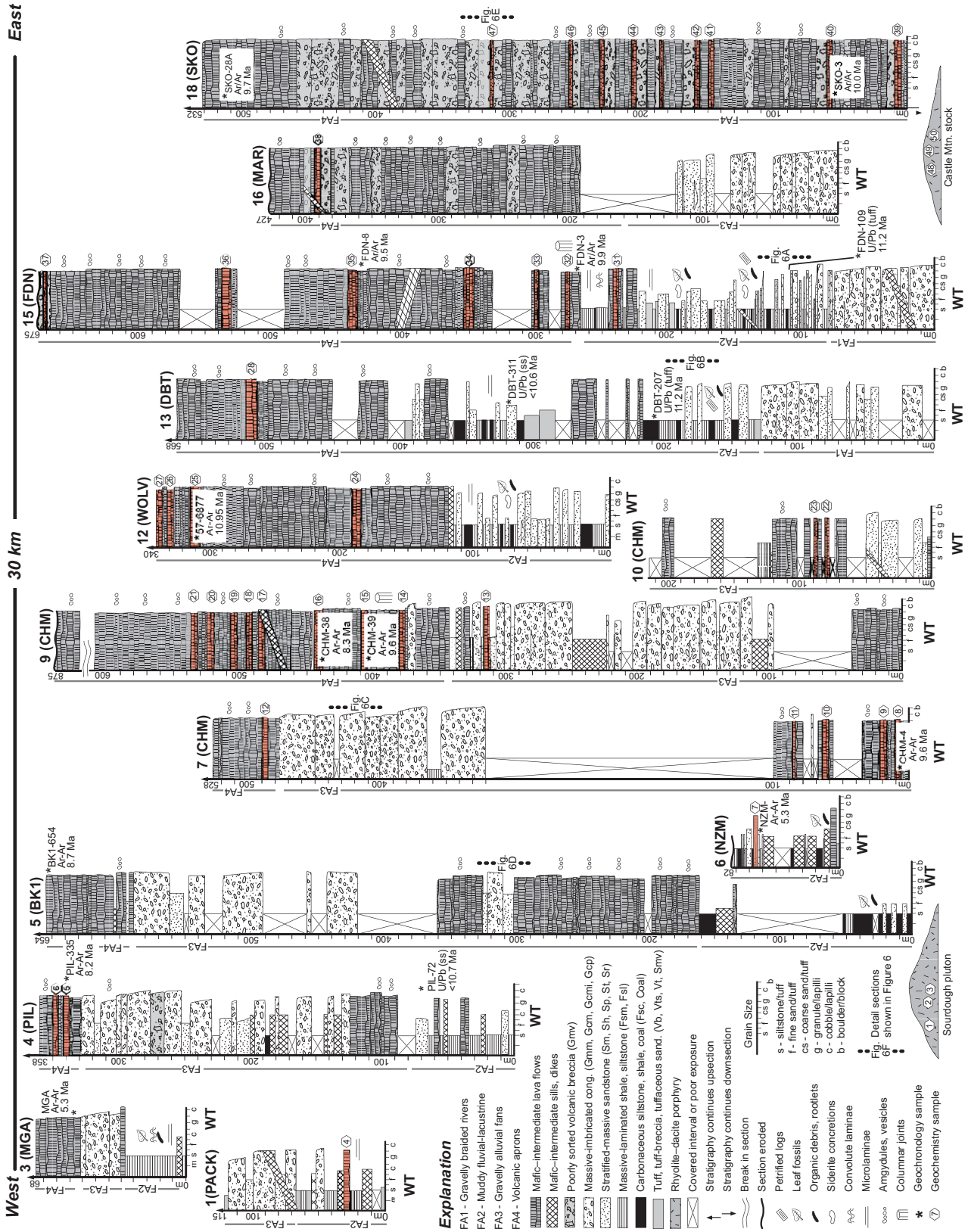
Figure 5. Simplified logs (in meters) of measured stratigraphic sections of Miocene sedimentary and volcanic strata in the central Wrangell volcanic belt. Only generalized sections are presented. Mf—Miocene Frederika Formation; Mw—Miocene Wrangell Lavas. Red units denote lavas sampled for geochemical analyses. Most sections overlie the Wrangellia terrane (WT) along an angular unconformity. See Figure 3 for geographic locations of measured sections and Table 1 for explanation of lithofacies codes, and Supplemental Figures 1–4 (see footnotes 1–4), Tidmore (2004), and Delaney (2006) for bed by bed measured sections and locality information.

TABLE 1. LITHOFACIES CHARACTERISTICS AND INTERPRETATIONS FOR MIOCENE STRATA OF THE WRANGELL VOLCANIC FIELD

Facies codes	Color, bedding, texture, structures, fossils	Facies interpretations
Gmv	Cobble to boulder breccia and conglomerate, unsorted or poorly sorted, angular to subrounded clasts, outsized clasts several meters long, block-supported to matrix-rich, exclusively volcanic-lithic clasts, matrix of volcanic-lithic grains, unstratified, most beds >4 m thick	Remobilization of unconsolidated volcanic material by volcanic debris avalanche and debris flow (lahar) on steep sides of volcanic edifices (Waythomas and Wallace, 2002; Busby and Bassett, 2007)
Gmm	Sandy pebble to boulder breccia and conglomerate, poorly sorted, angular to subrounded clasts, matrix-rich, mostly unstratified, rare inverse grading, mainly volcanic clasts, matrix mainly mudstone and volcanic-lithic sandstone, rare faceted, striated, and bullet-shaped clasts, most beds 1–10 m thick	Subaerial debris flow, high-concentration flood flow, and stream-bank collapse proximal to flanks of active volcanic centers; variable reworking of volcanic detritus with a previous phase of subglacial abrasion and transport (Eyles and Kocsis, 1988; Smith and Lowe, 1991)
Gcm	Granule to cobble conglomerate with rare boulder-sized clasts, moderately sorted, subangular to rounded clasts, clast-supported, unstratified to horizontally stratified, lenticular to tabular bed geometries, basal scours, mainly volcanic-lithic clasts, most beds 1–5 m thick and upward fining	Hyperconcentrated flood flow, stream flow, and sheetflood in shallow channels and bar tops (Pierson and Scott, 1985; Smith, 1986); variable reworking of pyroclastic debris
Gcmi	Pebble to cobble conglomerate, moderately sorted, clast-supported, subrounded to rounded clasts, unstratified to crudely horizontally stratified, imbricated, lenticular geometries, basal scours, predominantly volcanic-lithic clasts, most beds 1–5 m thick	Deposition by stream flow and high-concentration flood-flow in shallow channels and bar tops (Miall, 1978; Collinson, 1996), limited reworking of recently deposited pyroclastic debris
Gcp	Granule to pebble conglomerate and sandstone, moderately to well sorted, clast-supported, normal grading, large-scale planar foresets to 17 m high, downdip reduction in grain size along foresets, syndepositional soft-sediment deformation, predominantly volcanic clasts, medium to thick bedded	Subaqueous turbidity currents and traction flow on lake margin fan deltas (Postma, 1984; Eyles and Eyles, 1989)
Sm	Fine- to coarse-grained volcanic-lithic sandstone, beds lobate with sharp, nonerosive bases to channelized bodies with erosive bases, carbonaceous plant debris, medium to thick bedded, bioturbation and pedoturbation common	Stream flow and high-concentration flood flow in shallow channels and bar tops and crevasse splay (Miall, 1978; Collinson, 1996), limited reworking of recently deposited pyroclastic debris
Sh	Fine- to medium-grained volcanic-lithic sandstone, plane-parallel lamination, sparse reworked carbonaceous plant debris, medium to thick bedded	Deposition under upper plane bed conditions from very shallow or strong (>1 m/s) unidirectional flow conditions in fluvial channels, bar tops, crevasse channels, and sheetfloods (Miall, 1978)
Sp	Medium- to coarse-grained volcanic-lithic sandstone, planar cross-stratification, carbonaceous plant debris, medium to thick bedded	Migration of two-dimensional ripples and small dunes under moderately strong (~40–60 cm/s) unidirectional channelized flow in fluvial channels, bar tops, crevasse channels (Miall, 1978)
St	Medium- to coarse-grained volcanic-lithic sandstone, trough cross-stratification, carbonaceous plant debris, medium to thick bedded	Migration of three-dimensional ripples and dunes under moderately strong (40–100 cm/s), unidirectional channelized flow in fluvial channels, bar tops, crevasse channels (Miall, 1978)
Sr	Fine- to medium-grained volcanic-lithic sandstone, asymmetric two-dimensional and three-dimensional current ripples, minor mud drapes and convolute laminae, carbonaceous plant debris, thin to medium bedded	Migration of two-dimensional and three-dimensional ripples under weak (20–40 cm/s) unidirectional flow in shallow fluvial channels, bar tops, crevasse channels, and lake margins (Miall, 1978)
Smv	Tuffaceous sandstone, tan to purple, massive or horizontal stratification, minor cross-stratification or horizontal stratification, reworked organic matter, subangular to subrounded volcanic lithic grains, euhedral to subrounded plagioclase feldspar crystals, and minor glass shards	Reworking of tephra and subordinate nonvolcanic detritus in proximal alluvial-fluvial environments, mainly by flood flow (Fisher and Schmicke, 1984; Smith, 1986, 1987)
Fsm	Massive mudstone, gray, brown, and yellow-brown, locally variegated with iron-oxide mottles, plant fossils, coalified wood fragments and petrified logs, root traces, bioturbation, sparse desiccation cracks, smectite-rich units with popcorn weathering, thin bedded	Suspension settling, tephra fallout, and paleosol development in poorly drained floodplain environments (Collinson, 1996; Miall, 2006; Melchor, 2007)
Fsl	Coarsely laminated gray mudstone to finely laminated black shale, ripple laminae, climbing ripples, clay drapes, flame structures, convolute laminae, normal grading, thin bedded, delicately preserved plant leaf fossils of conifer and broad-leaf axes and leaves; sparse fish fossils (Berry, 1928)	Subaqueous suspension settling, episodic rapid aggradation, and minor desiccation in low-energy, suboxic to anoxic ponds and profundal lakes (Platt, 1989; Johnson and Graham, 2004; Pietras and Carroll, 2006)
Fsc	Carbonaceous mudstone, dark gray to black, lignite stringers, plant leaf fossils, coalified wood fragments, root traces bioturbation, thin bedded	Suspension settling and accretion of organic and clastic mud in floodplain ponds/lakes and mires (bogs, fens, moors, muskegs, or swamps; McCabe, 1984, 1991)
Coal	Rare, blocky lignite and bony coal, shaley coal, macerated and coalified organic debris, silicified logs and tree stumps, ironstone/siderite nodules and sparse larger concretions, thin to medium bedded	Vertical accretion and diagenesis of organic matter in poorly drained mires (bogs, fens, moors, muskegs, or swamps; McCabe, 1984, 1991)
Ls	Limestone, calcareous siltstone, and marl, white to bluish gray, fine-grained, bedding-parallel feeding traces, nonchannelized, thin bedded	Inorganic carbonate precipitation in floodplain lakes and ponds (Talbot and Allen, 1996)
Lava	Lava flows, dark gray, brown, or reddish brown, typically massive to weakly vesicular bases and vesicular or amygdaloidal tops, sparse pillows, phyric and nonphyric, mostly basaltic andesite and andesite, minor dacite and rhyolite, chiefly plagioclase, pyroxene, olivine, and Fe-Ti oxide crystals in fine matrix of devitrified glass and plagioclase, minor flow-banding or flow-aligned crystals, some plagioclase-phyric flows, most flow units 2–8 m thick	Subaerial lava-producing eruptions that flowed onto alluvial fans, streams, and lakes (Fisher and Schminke, 1984; Skulski et al., 1992; Cole and Ridgway, 1993)
Vb	Lithic-vitric tuff-breccia, white to tan, moderately sorted, nonwelded texture, subangular framework grains of pumice and tuff with minor rhyolite and andesite, ash matrix of pumice, glass, and felsic volcanic-lithic fragments, beds >8 m in channel axes to <40 cm in channel margins	Hot, gaseous, high-concentration density currents (pyroclastic flows; Fisher and Schminke, 1984; Freundt et al., 2000)
Vts	Vitric-crystal tuff with low-angle stratification and scours, white to tan, subangular to subrounded framework grains of pumice, vitric shards, volcanic-lithic grains, and euhedral to subhedral plagioclase and quartz crystals, minor reworked carbonaceous debris, most beds 10–50 cm thick	Pyroclastic ground-surge deposits associated with contemporary pyroclastic flows (Fisher and Schminke, 1984)
Vt	Vitric-crystal tuff and lapilli tuff, unstratified to laminated, white to tan, subangular framework grains of vitric shards, pumice, and euhedral to subhedral feldspar and quartz crystals, mottling and root traces, most beds <1 mm to 25 cm thick	Pyroclastic fallout deposition, mainly in floodplain swamps, ponds, and lakes (Cas and Wright, 1987); incipient pedogenic modification locally.

Figure 6. Representative detailed logs (in meters) of measured stratigraphic sections of Miocene sedimentary and volcanic strata in the central Wrangell volcanic belt. Sections are arranged spatially by geographic location from west to east. See Figure 5 for explanation of grain sizes and lithofacies patterns, Figure 3 for locations of sections, and Table 1 for explanation of lithofacies abbreviations. (For additional detailed measured sections and locality information, see Supplemental Figs. 1–4 [see footnotes 1–4]; Tidmore, 2004; Delaney, 2006.)

Figure 7. Photographs showing key stratigraphic relationships in the central Wrangell volcanic belt. Black symbols with heads indicate bedding. Black arrows indicate thick-bedded lavas interbedded within alluvial sedimentary strata. Solid white lines indicate angular unconformity that separates Miocene strata from deformed Paleozoic–Mesozoic strata. Dashed lines mark boundaries between lithofacies associations. (A) Basal unconformity and upsection transition from fluvial-lacustrine strata to volcanic strata. Mudstone (Fsl, Fsm, Fsc), sandstone (Sr), tuff (Vt) and lava of facies association 2 are overlain by lavas and volcanic breccia of facies association 4. See Table 1 for explanation of facies abbreviations. Height of outcrop is >900 m. Outcrop is near section 19 in Figure 3. (B) Upsection transition from fluvial-lacustrine strata to alluvial and volcanic strata. Mudstone (Fsl, Fsc) and sandstone (Sr) of facies association 2 are replaced upsection by conglomerate (Gcm, Gmm), lava, and volcanic breccia (Gmv) of facies association 3 and lava flows and volcanic breccia of facies association 4. White arrows (lower left) indicate felsic sills. Height of outcrop is >550 m. Refer to section 3 in Figure 5 for generalized measured section. (C) Upsection transition from alluvial conglomerate (Gcm, Gmm) and lava flows of lithofacies association 3 to exclusively lava flows and volcanic breccias of lithofacies association 4. Height of outcrop is >700 m. Refer to upper part of section 4 in Figure 5 and Supplemental Figure 1 (see footnote 1) for measured section of outcrop.
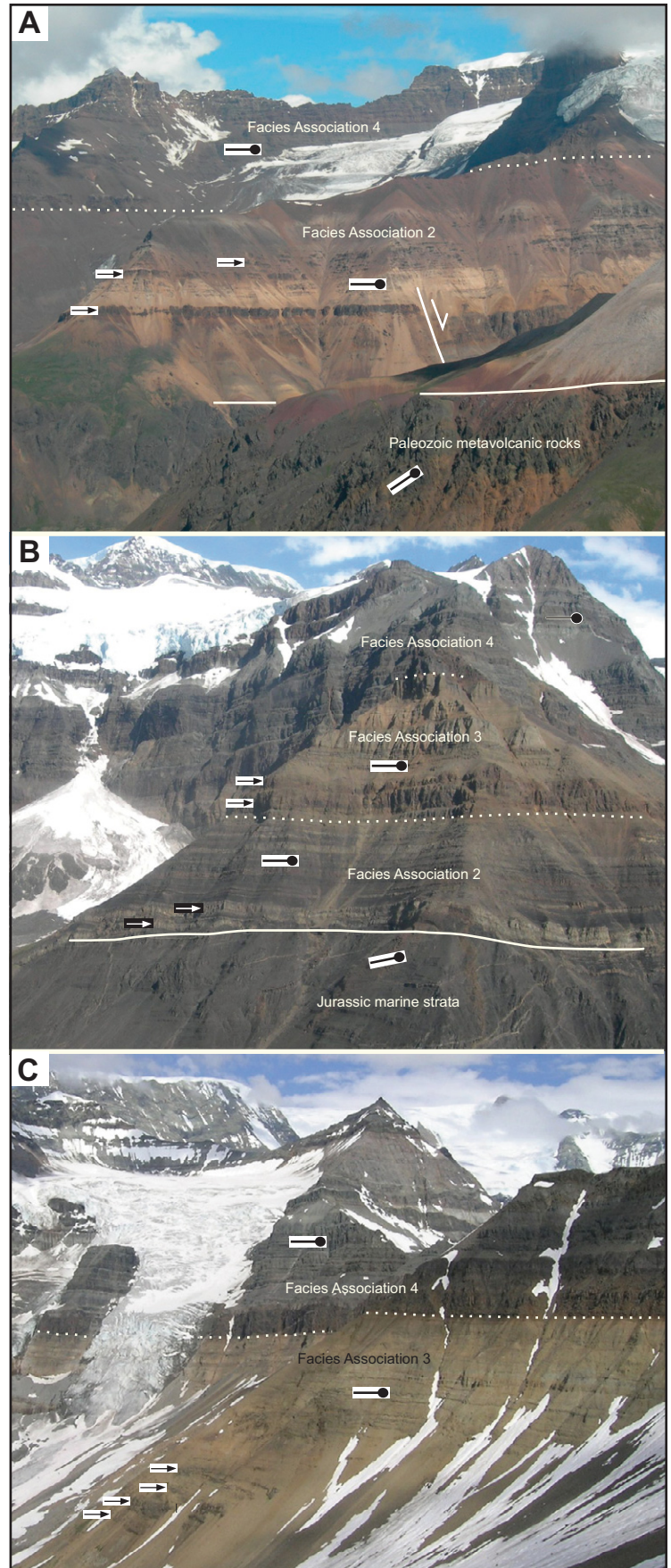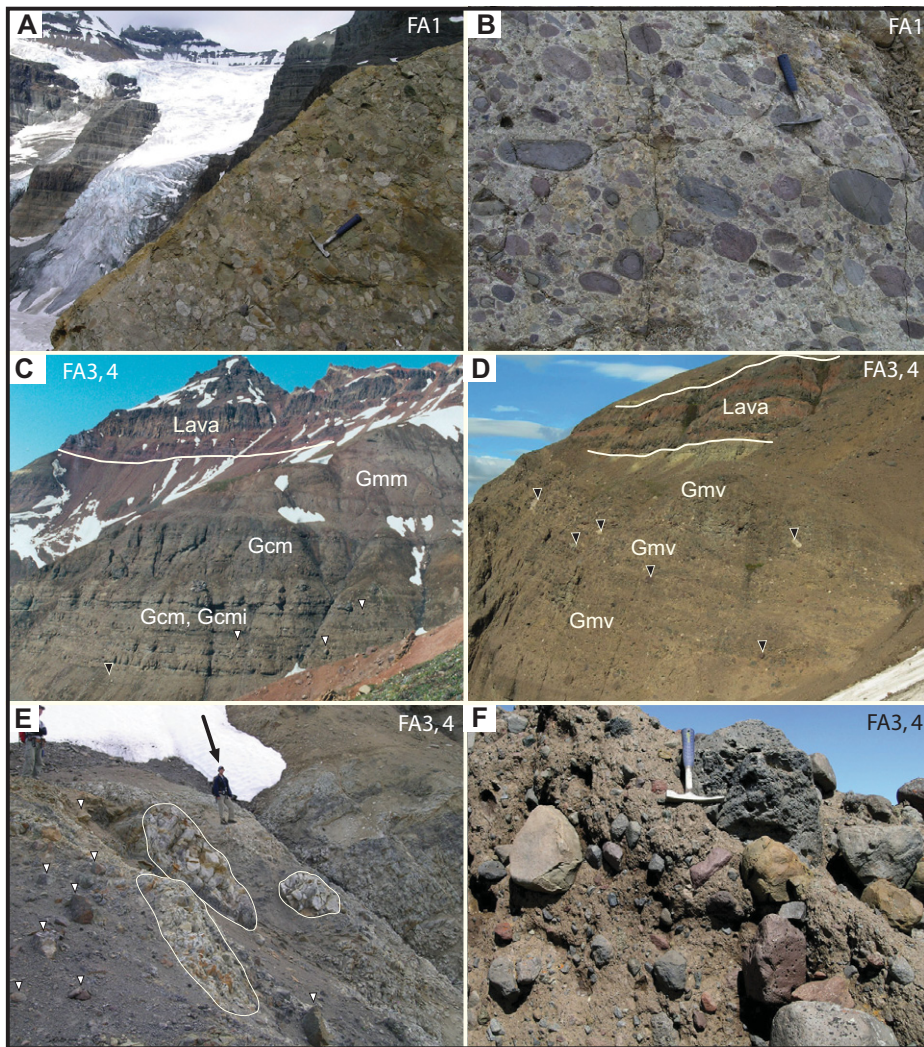
Figure 8. Photographs of coarse-grained lithofacies that characterize lithofacies associations 1, 3, and 4 (see text). (A) Imbricated pebble-cobble conglomerate (Gcmi) with dacite-rhyolite clasts (light colored clasts) and subordinate basaltic andesite and basalt clasts (dark colored clasts). This facies dominates lithofacies association 1. Hammer is 35 cm long. From ~220 m in section 4 in Figure 5. See Table 1 for explanation of facies abbreviations. (B) Cobble conglomerate (Gmm) with subrounded basaltic andesite clasts supported in a volcanic-lithic sandstone matrix. This facies is present in lithofacies association 1 but is more common in associations 3 and 4. Hammer is 35 cm long. From ~430 m in section 5 in Figure 5. (C) Massive clast-rich conglomerate (Gcm), imbricated conglomerate (Gcmi), and matrix-rich conglomerate (Gmm) that characterize association 3. Note upsection change from conglomerate to lava flows. Arrows mark boulders >2 m long. Height of outcrop is ~260 m. Interval 420–520 m of section 7 in Figure 5. (D) Unorganized volcanic breccia (Gmv) and massive lavas that characterize lithofacies association 4. Black arrowheads indicate >2-m-long clasts that range from basaltic andesite and andesite clasts (dark colored clasts) to dacite and rhyolite clasts (light colored clasts). Height of outcrop is ~40 m. Interval 430–470 m of section 18 in Figure 5. (E) Matrix-rich boulder breccias and conglomerate (Gmv) with outsized rhyolite/dacite clasts (outlined in white) and basaltic andesite clasts (white arrows). This poorly sorted facies is common in association 4 and to a lesser extent association 3. Person (black arrow) for scale. Interval 270–275 m of section 4 in Figure 5. (F) Close-up of matrix-supported cobble-boulder conglomerate (Gmm) dominated by volcanic clasts with vesicular textures and basalt to andesite compositions. This facies is common in association 4 and to a lesser extent association 3. Hammer is 35 cm long. From section 20 in Figure 3; not depicted in Figure 5.

Overbank mudstones with mottling, variegated colors, and bioturbated and/or disrupted horizons (Fsm) (see Fig. 5 for unit abbreviations) suggest pedogenesis between events of stream migration and/or avulsion and flooding. Floodplains were partly forested, based on the presence of coal and mudstone with root traces, plant fossils, coalified wood, and petrified logs (Fsc). Coal and carbonaceous shale with nodules indicate accretion of organic material under suboxic to anoxic conditions in floodplain bogs, fens, moors, muskegs, and/or swamps. Subaqueous suspension settling in lakes and ponds deposited laminated mudstone and black shale with fish fossils (Fsl, Fsc). Bioturbated limestone and marl (Ls) reflect subaqueous inorganic carbonate precipitation in lakes and ponds under suboxic conditions permissive of infaunal activity. Lower oxygen bottom conditions in deeper ponds and lakes enabled deposition of finely laminated organic-rich shale and tuff that imply the absence of burrowing infauna or resuspension of bottom sediment by currents. Sandstone interbeds with nonerosive bases, horizontal stratification, load marks, current ripple lamination, and convolute lamination record episodic higher energy lacustrine deposition from sediment-laden unidirectional flows derived from lake-margin fluvial-deltaic environments during floods (Johnson and Graham, 2004; Pietras and Carroll, 2006).

Lithofacies Association 3: Distal Volcanic Flank Deposits

Description. Association 3 consists of >200-m-thick successions of matrix- to clast-supported pebble-boulder conglomerate and breccia (Gmm, Gcm, Gcmi), tuffaceous sandstone (Smv), and lavas (see Fig. 5 for unit abbreviations). Subordinate massive to cross-stratified sandstone (Sm, St, Sp) and sparse massive siltstone (Fsm) are also present. Bedding contacts are dominantly subhorizontal erosive surfaces. Sandstone and conglomerate lithofacies typically comprise broadly lenticular (several meters to <15 m), 2–20 m-thick, upward-fining bodies with nonerosive to erosional bases that scoured tens of centimeters deep. Facies association 3 characterizes the lower and middle portions of sections in the northwestern and northeastern part of the outcrop belt (sections 3–5, 7–10, 20, and 21 in Figs. 5 and 6 and Supplemental Figs. 1 and 2 [see footnotes 1 and 2]). Figure 8C shows a representative photo of this association.

Interpretation. Facies association 3 records reworking of volcanic debris and lava deposition on distal volcanic aprons flanking active volcanoes. Poorly sorted, matrix-rich conglomerate and breccia indicate emplacement

Figure 9. Photographs of fine-grained lithofacies that characterize lithofacies association 2. (A) Stratified volcanic-lithic sandstone and carbonaceous siltstone. Thick-bedded massive (Sm) to horizontally stratified (Sh) sandstone are replaced upsection by thin-bedded ripple-stratified sandstone (Sr) and carbonaceous siltstone (Fsc). Outcrop is the base of section 4 in Figure 5. Person for scale. (B) Close-up of amalgamated lenses of trough cross-stratified volcanic-lithic sandstone (St). Black arrows mark individual cross beds. Outcrop is the base of section 4. Hammer is 35 cm long. (C) Cross-stratified tuffaceous sandstone (Smv) overlying coal. Note planar cross-beds (black arrowheads). Hammer is 35 cm long. Outcrop is ~120 m in section 15. (D) Laminated siltstone (Fsl) and very fine-grained ripple-laminated sandstone (Sr). Note ripple-laminae (white arrowheads) and convolute laminae (black arrowheads). Pen is 13 cm long. Outcrop is ~25 m in section 3. (E, F) Interbedded laminated ashfall tuff (white colored) and laminated siltstone (dark colored). Note unit with convolute laminae (black arrowheads) overlying finely laminated horizon (white arrowheads). Pen is 13 cm long. Outcrop E is 260 m on section 15 (E). Outcrop F is 20 m on section 1 in Figure 5. See Table 1 for explanation of facies abbreviations.
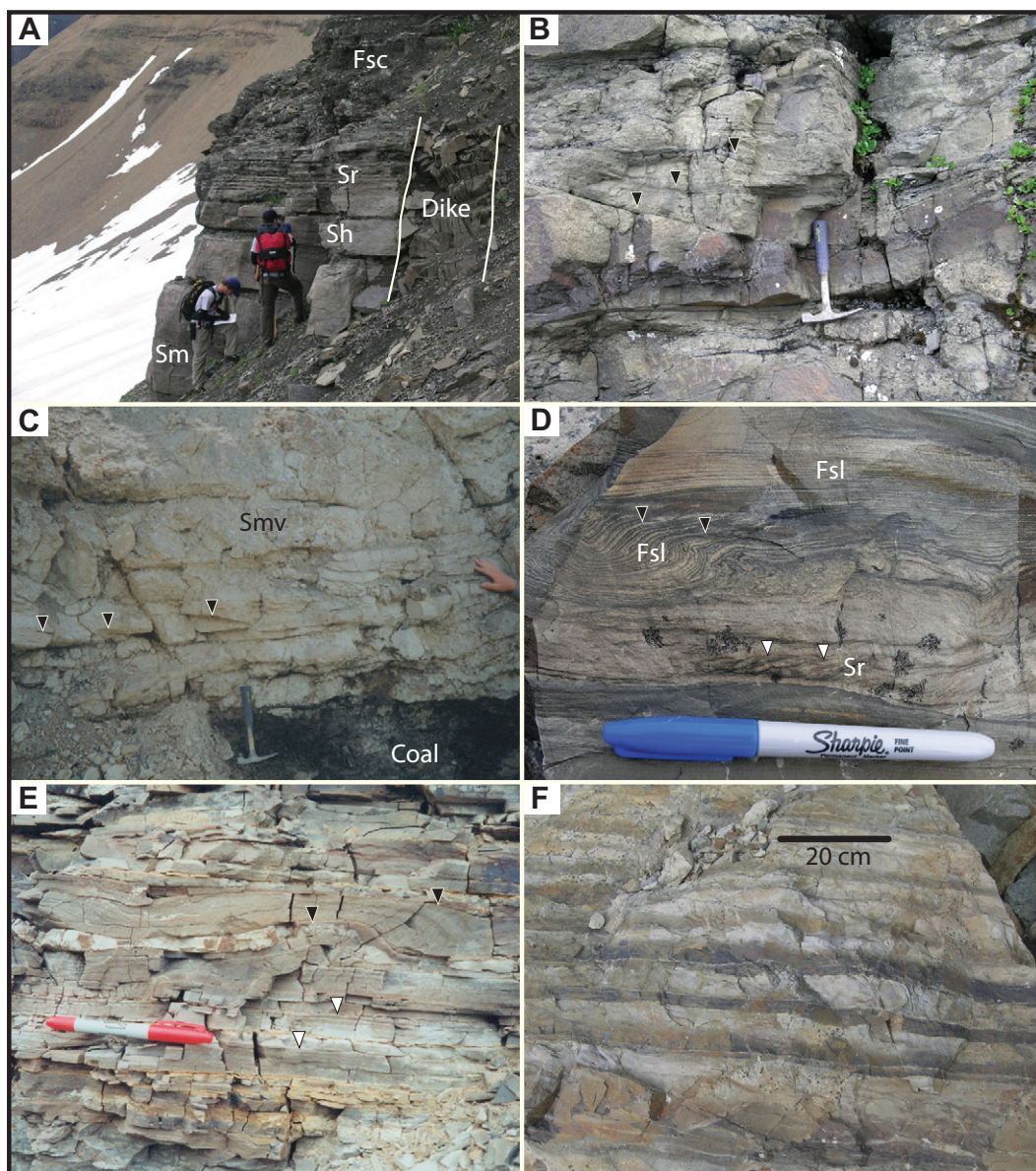
by debris flow, high-concentration flood flow, and stream-bank collapse. Clast-supported and imbricated conglomerates are best interpreted as waterlain bedload deposits within broad channels. Subordinate sandstone and siltstone reflect lower energy bar deposits formed between channels. Alluvial fans flanked active volcanoes judging by the presence of andesite and/or basalt lavas, dominance of basalt and/or andesite lithic clasts in conglomerate and sandstone (Figs. 10 and 11), and detrital zircon ages from sandstone that overlap the age of intrabasinal eruptive centers (Fig. 12). Juvenile volcanic detritus was mixed, remobilized, and transported downslope over relatively short distances (<10 km from active vents).

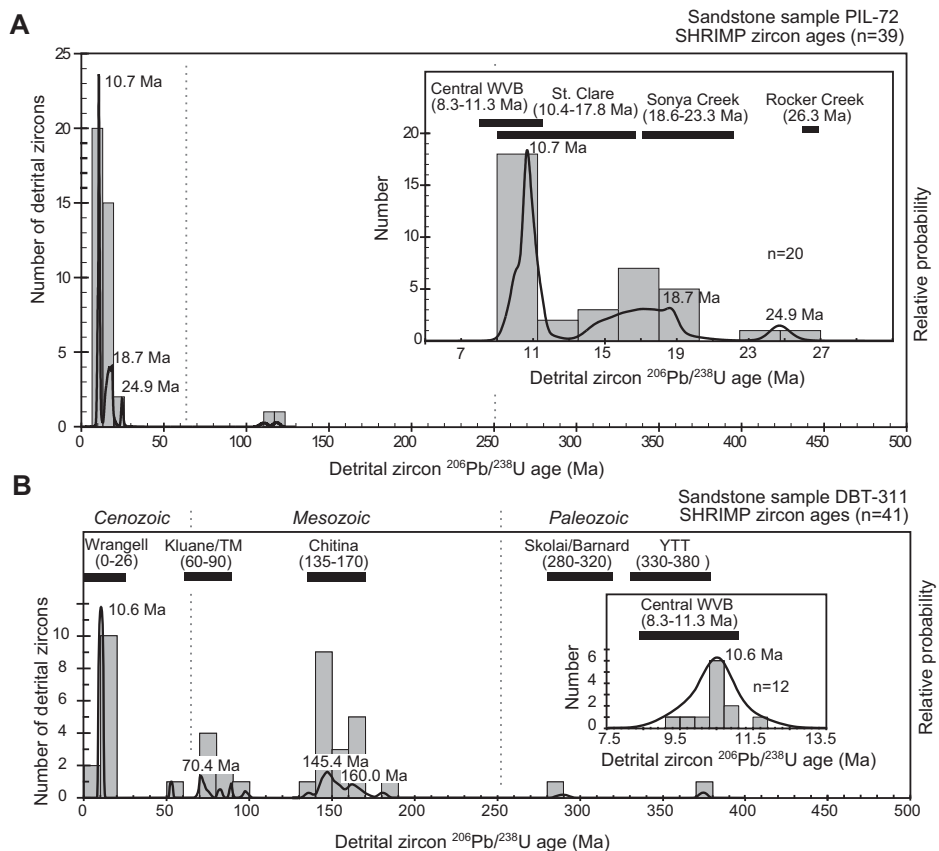### *Lithofacies Association 4: Proximal Volcanic Flank Deposits*

Description. This lithofacies association consists of thick successions of interbedded lavas, volcanic breccia (Gmv), lithic-vitric tuff breccia (Vts), vitric-crystal tuff (Vt), and unsorted to poorly sorted conglomerate (Gmv), and spatially associated aphanitic dikes and sills (e.g., section 18 in Fig. 6; see also Fig. 5). Many lavas grade upward from lower massive units to vesicular and/or amygdaloidal flow tops. Volcanic breccias are massive, unorganized, thick bedded, and poorly sorted with angular to subangular clasts of exclusively volcanic lithologies. Subordinate tuff breccia, tuff, and unsorted conglomerate are massive to horizontally stratified. Representative photos of common lithofacies are shown in Figures 8D–8F.
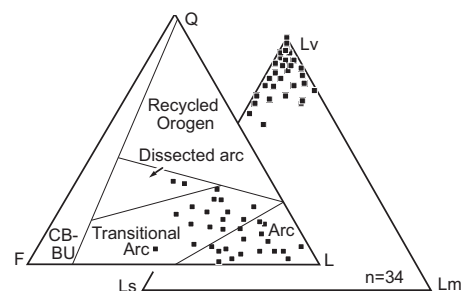
Interpretation. Volcanic breccias reflect remobilization of unconsolidated volcanic material by volcanic debris avalanche and debris flow (lahar) on high-gradient flanks of volcanic
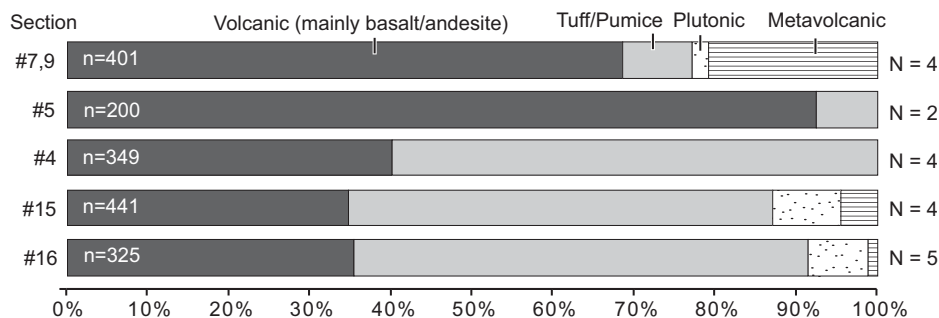
Figure 10. Histograms showing compositions of Miocene conglomerate in the central Wrangell volcanic belt. Note dominance of volcanic clast types (91% of all sampled clasts). Volcanic category includes mainly mafic to intermediate compositions (basalt and andesite) with subordinate felsic compositions (dacite and rhyolite). Section numbers correspond to measured sections shown in Figure 5. N—number of conglomerate beds sampled; n—total number of clasts counted. Refer to Tidmore (2004) and Delaney (2006) for clast descriptions and raw clast count data.

Figure 11. Sandstone point-count data from Miocene sandstone in the central Wrangell volcanic belt plotted on QFL and Lv-Lm-Ls ternary diagrams. Black squares represent individual samples; n—total number of samples point counted. A minimum of 400 grains were counted per sample. Q—monocrystalline quartz; F—plagioclase and potassium feldspar; L—total lithics, including polycrystalline quartz; Lv—volcanic lithics; Lm—metamorphic lithics; Ls—sedimentary lithics. Note enrichment of feldspar and volcanic lithic fragments. CB-BU—continental block-basement uplift. Provenance fields are from Dickinson (1985).

edifices (Waythomas and Wallace, 2002; Busby and Bassett, 2007). Tuff breccia and tuff record episodic pyroclastic flows, ground-surge deposits, and air fallout (Fisher and Schmincke, 1984; Freundt et al., 2000). These strata are interpreted as near-vent eruptive deposits (<2 km from central vents), primarily effusive eruptions and sparse pyroclastic eruptions and associated intrusive feeder bodies. Volcanic apron facies consist chiefly of event deposits related to stripping and light reworking of volcanic debris from the steep flanks of volcanoes during or soon after an eruption (Smith, 1987).

PROVENANCE

Quantitative provenance data have not been reported previously from the central WVB. New clast counts from conglomerate, modal analysis of sandstone thin sections, U/Pb geochronology of detrital zircons, and paleocurrent measurements permit reconstruction of the lithologies, ages, and locations of sediment sources.

Sediment Dispersal Patterns

Paleocurrent data were collected by measuring the orientation of imbricated clasts in conglomerate and cross-beds in sandstone, totaling 163 measurements. Corrections for bedding dip were not needed because sampled beds dip <10°. Rose diagrams summarizing paleocurrent

Figure 12. Detrital zircon histograms (light gray bars) and age probability curves (solid curve) for detrital zircon ages from Wrangell volcanic belt (WVB) sandstone samples. (A) PIL-72. (B) DBT-311. Age determinations represent individual spot analyses of separate zircons; n—total number of spot analyses. Relative heights of peaks correspond to statistical significance. Numbers above individual histograms represent peak ages. Note dominance of Miocene ages. Inset probability plots show details of main age population. Black horizontal bars above plots represent age ranges of igneous belts exposed in eastern Alaska. Refer to sections 4 (PIL) and 13 (DBT) in Figures 3 and 5 for geographic and stratigraphic location of sandstone samples. Plots calculated with Isoplot software (Ludwig, 2006). SHRIMP—sensitive high-resolution ion microprobe; TM—Talkeetna Mountains; YTT—Yukon-Tanana Terrane.

directions are shown in Figure 3. Paleocurrents reflect southwest- to southeast-directed sediment transport in the northern part of the outcrop belt, northward transport in southern outcrops, and west-directed paleoflow in western outcrops.

Conglomerate Composition

Compositional data were obtained from counts of 1316 individual clasts at 19 pebble-cobble conglomerate beds in the field by tabulating the lithology of all pebble-, cobble-, and boulder-sized clasts within a 1–5 m² outcrop face, yielding a minimum population of 80–100 clasts per bed to provide statistical significance (Van der Plas and Tobi, 1965). Figure 10 summarizes conglomerate compositional data; raw data were reported in Tidmore (2004) and Delaney (2006). The dominant volcanic category accounts for 91% of clasts counted. Black, reddish-brown, greenish-gray, and gray volcanic clasts with aphanitic, aphanitic-porphyritic, and amygdaloidal textures are most common (andesite and basalt 54%). White, green, and tan laminated tuff, crystal-vitric tuff, welded tuff, and pumice make up 37% of the counted clasts. Minor sedimentary (3%) and metavolcanic (5%) clasts include greenstone, chert, and volcanic-lithic sandstone.

Sandstone Composition

Standard petrographic thin-sections were made from 60 medium-grained sandstone samples that were obtained while measuring stratigraphic sections. Thin sections of the least altered samples (n = 34) were stained for K-feldspar and Ca-plagioclase feldspar, and point counted (400–450 grains per section) according to a modified Gazzi-Dickinson method (Dickinson, 1970), in which crystals larger than silt sized in lithic fragments are counted as monocrystalline grains (Ingersoll et al., 1984). Point-counted sandstones are texturally immature with moderately to poorly sorted, angular to subrounded framework grains contained in a matrix of clay, silt, and devitrified glass. Figure 11 summarizes key compositional trends in the point-counted samples. Sandstones are compositionally immature with mainly unstable lithic fragments and plagioclase feldspar (quartz, feldspar, lithics, Q:F:L—14:24:62). Volcanic fragments are especially common (volcanic lithics, metamorphic lithics, sedimentary lithics, Lm:Lv:Ls—6:84:9) and include mainly basalt and andesite. Argillite, shale, quartzofeldspathic siltstone, and sparse carbonate grains make up the sedimentary lithic grain population. Metamorphic lithic grains include mica schist, quartz-mica schist, gneiss, and slate.

U/Pb Zircon Ages from Sandstone

Two samples of moderately sorted, medium- to coarse-grained volcanic-lithic sandstone were processed for detrital U/Pb geochronologic analyses. Figure 5 shows the stratigraphic positions of the samples. Spot analyses were collected from 39–41 randomly selected zircon grains per sample (80 ages total) using the Stanford–U.S. Geological Survey sensitive high-resolution ion microprobe (SHRIMP; Fig. 12). Supplemental Table 1[5] presents U/Pb isotopic age data; analytical details are described in Appendix 1. U/Th ratios are <9 for all analyzed zircons and <5 for 73 of 80 grains indicative of an igneous origin (Supplemental Table 1 [see footnote 5]). Five major age populations are documented: 12–9 Ma (Late Miocene, 40% of grains analyzed), 25–14 Ma (Late Oligocene–Middle Miocene, 21%), 89–70 Ma (Late Cretaceous, 8%), 118–98 Ma (Late Early Cretaceous, 4%), and 181–135 Ma (Early Jurassic–Early Cretaceous, 24%). Single Eocene (53 Ma), Permian (289 Ma), and Devonian (374 Ma) grains are present. Sample PIL yields Late Oligocene to Late Miocene grains (Fig. 12A), whereas sample DBT exhibits a broader distribution of ages (Fig. 12B).

GEOCHRONOLOGY AND STRATIGRAPHIC CORRELATION

We report isotopic ages from 12 lavas, 2 tuffs, and 2 sandstones in Table 2 and Supplemental Tables 1 (see footnote 5), 2[6], and 3[7]; analytical details are described in Appendix 1. The U/Pb zircon age determinations were conducted at the Stanford–U.S. Geological Survey Microisotopic Analytical Center using the SHRIMP reverse geometry. Individual zircon crystals were separated from tuffs and analyzed through individual spot analyses. Results for individual crystals were used to calculate a weighted mean

---

[5]Supplemental Table 1. PDF file of SHRIMP U-Pb isotopic data and apparent ages for sandstone from the Frederika Formation. If you are viewing the PDF of this paper or reading it offline, please visit http://dx.doi.org/10.1130/GES00762.S5 or the full-text article at www.gsapubs.org to view Supplemental Table 1.

[6]Supplemental Table 2. PDF file of SHRIMP U-Pb isotopic data and apparent ages for tuff from the Frederika Formation. If you are viewing the PDF of this paper or reading it offline, please visit http://dx.doi.org/10.1130/GES00762.S6 or the full-text article at www.gsapubs.org to view Supplemental Table 2.

[7]Supplemental Table 3. PDF file of ${}^{40}Ar/{}^{39}Ar$ analytical data. If you are viewing the PDF of this paper or reading it offline, please visit http://dx.doi.org/10.1130/GES00762.S7 or the full-text article at www.gsapubs.org to view Supplemental Table 3.

---

average age for each sample (Fig. 13). The ${}^{40}Ar/{}^{39}Ar$ age determinations were performed at the Lehigh University (Bethlehem, Pennsylvania) geochronology laboratory on plagioclase feldspar crystals separated from porphyritic lavas and groundmass separated from aphanitic lavas (Fig. 14).

The sampled volcanic rocks yield isotopic ages that range from ca. 11.2 to 5.3 Ma. Two tuffs from the middle of eastern sections yield 11.2–11.1 Ma U/Pb zircon ages (Fig. 13); 10 lavas from both eastern and western sections yield 10.0–8.3 Ma ${}^{40}Ar/{}^{39}Ar$ ages (Fig. 14). Two lavas from western sections yield ${}^{40}Ar/{}^{39}Ar$ ages of 5.39 ± 0.70 Ma and 5.29 ± 1.24 Ma (Fig. 14). Detrital zircons from sandstone exhibit minimum age clusters that are consistent with the isotopic ages obtained from volcanic rocks. The minimum U/Pb detrital zircon age population in sample DBT-207 centers at 10.6 Ma (Fig. 12B), compatible with the 11.2 Ma U/Pb zircon age of a tuff located 104 m lower in the stratigraphy (Figs. 5 and 13). Zircons from sandstone sample PIL-72 yield a minimum age population centered at 10.7 Ma (Fig. 12A), consistent with the 8.4 Ma ${}^{40}Ar/{}^{39}Ar$ age of a lava exposed 268 m higher in the section (Figs. 5 and 14). Ages young westward from 11.2–9.5 Ma near Castle Mountain, to 9.6–8.3 Ma at Chimney Mountain, to 8.7–8.3 Ma near the West Fork Glacier. Two samples from sections 3 and 6 in the western and southwestern part of the study area yield even younger ages of ca. 5.3 Ma. The 5.3 Ma ages are statistically indistinguishable from with 5.7–5.4 Ma ${}^{40}Ar/{}^{39}Ar$ ages previously reported from two sills that intrude Mesozoic strata a few kilometers southwest of section 3 (Figs. 3 and 4). In summary, integration of our new ages with previously reported ages support progressive westward migration of volcanism from ca. 11.2 to 5.3 Ma (Figs. 3 and 4; Table 2).

GEOCHEMISTRY

In order to characterize the range of lava compositions present in the central WVB and to compare magmatism in this region with existing data for the western and eastern WVB and the nearby Sonya Creek volcanic field, lavas and a few hypabyssal intrusive samples were collected from across the area shown in Figure 3. The vast majority of these were collected in the context of the measured sections detailed in Figures 5 and 6 and Supplemental Figures 1–4 (see footnotes 1–4). General descriptions of the igneous units are given in Table 1, and the geochemical data keyed to section and location within section are provided in Table 3. Analytical methods are described in Notes section in Table 3. As illustrated in Figures 4–6 and Supplemental Figures

TABLE 2. ISOTOPIC AGE DATA FOR MIOCENE VOLCANIC AND INTRUSIVE ROCKS OF THE CENTRAL WRANGELL VOLCANIC FIELD

Sample and lithology	Latitude (°N)	Longitude (°W)	Section	Height* (m)	Material dated[†]	Age[§] (Ma)	Notes, references
*This study (U-Pb single-grain SHRIMP)***							
DBT-207 (tuff)	61°34′01″	142°20′15″	13	207	ZR	11.1 ± 0.4	14 spot analyses on 14 grains
FDN-109 (tuff)	61°41′17″	142°10′06″	15	109	ZR	11.2 ± 0.1	3 spot analyses on 3 grains
This study ([40]Ar/[39]Ar)[††]							
MGA-2 (lava)	61°37′17″	142°50′24″	3	25	PL	5.26 ± 1.10	Inverse isochron age
PIL-335 (lava)	61°37′07″	142°45′05″	4	335	GM	8.24 ± 0.18	Plateau age
BK1-654 (lava)	61°39′09″	142°42′07″	5	654	GM	8.72 ± 0.21	Plateau age
NZM-67 (lava)	61°36′36″	142°32′23″	6	67	PL	5.30 ± 0.64	Inverse isochron age
CHM-4 (lava)	61°42′33″	142°31′29″	7	20	PL	9.62 ± 0.28	Inverse isochron age
CHM-39 (lava)	61°43′21″	142°28′55″	9	410	PL	9.64 ± 0.39	Plateau age
CHM-38 (lava)	61°43′44″	142°29′32″	9	442	PL	8.34 ± 0.22	Plateau age
57-6877 (lava)	61°31′26″	142°23′17″	12	310	GM	10.95 ± 0.42	Plateau age
FDN-8 (lava)	61°41′19″	142°09′24″	15	440	PL	9.45 ± 1.47	Inverse isochron age
FDN-3 (lava)	61°41′19″	142°09′47″	15	270	GM	9.93 ± 0.24	Plateau age
SKO-28A (lava)	61°36′50‴	142°06′31″	18	515	PL	9.74 ± 0.34	Inverse isochron age
SKO-3 (lava)	61°37′03″	142°00′57″	18	50	GM	10.02 ± 0.22	Plateau age
Previous studies (K-Ar ages)							
4 (andesite flow)	61°46′8″	142°49′8″	n/a	n/a	GM[§§]	10.0 ± 0.3	Denton and Armstrong, 1969
2 (andesite flow)	61°46′2″	142°50′1″	n/a	n/a	GM[§§]	9.8 ± 0.3	Denton and Armstrong, 1969
5 (andesite flow)	61°46′4″	141°47′9″	n/a	n/a	GM[§§]	8.6 ± 0.7	Denton and Armstrong, 1969
3 (andesite flow)	61°46′7″	142°50′0″	n/a	n/a	GM[§§]	8.8 ± 0.9	Denton and Armstrong, 1969
81ASj12 (lava)	61°39′0″	142°00′3″	n/a	n/a	GM	9.8 ± 0.3; 9.8 ± 0.3	Richter et al., 1990
81ASj36 (lava)	61°34′7″	142°14′1″	n/a	n/a	GM	8.9 ± 0.3, 9.0 ± 0.3	Richter et al., 1990
Chitistone (granodiorite)	61°22′0″	142°03′0″	n/a	n/a	HB, BI	8.6 ± 0.3, 8.6 ± 0.3	MacKevett, 1970a, 1970b
74AMs17 (rhyolite porphyry)	61°29′2″	142°49′5″	n/a	n/a	SA	6.7 ± 0.2	Silberman et al., 1976
74AMs14 (dacite porphyry)	61°25′1″	142°47′9″	n/a	n/a	PL, HB	9.4 ± 0.7, 15.2 ± 0.5	Silberman et al., 1977

Note: SHRIMP—sensitive high-resolution ion microprobe; n/a—Information not available.
*Height above base of measured section; see Figures 3 and 5 for sample locations and sections.
[†]BI—biotite; GM—groundmass; HB—hornblende; PL—plagioclase feldspar; SA—sanidine; ZR—zircon.
[§]See text and Tables DR1, DR2, DR3 (see text footnote 1) for geochronologic details.
**Ages referenced to R-33 zircon (540 Ma); 2σ uncertainties.
[††]Ages referenced to GA-1550 biotite (98.79 Ma); 2σ uncertainties, including 1% uncertainty in J-factor.
[§§]Samples exhibit moderate amounts of alteration; ages considered minimum ages.

1–4 (see footnotes 1–4), lava flows are most common in the upper portion of the Frederika Formation (lithofacies 3) and the overlying Wrangell Lava (lithofacies 4). Because no clear geochemical distinctions are identified between lavas from these lithofacies associations, and no systematic geographically controlled chemical variation is observed (Fig. 15A), for geochemical and petrologic purposes the samples are treated as a single time-transgressive suite.

Although considerable care was taken in the field to collect the freshest possible volcanic materials, it is clear from LOI (total volatiles lost on ignition at 950 °C for 45 min) values in excess of 5 wt% in some cases and some analytical totals outside a generally accepted range of 98.5–101 wt% that a number of samples have been affected by secondary hydrothermal and/or meteoric fluid migration. Based on a combination of (1) petrographic characteristics including high abundances of secondary phyllosilicate and/or carbonate phases, (2) LOI > 3.5 wt%, and (3) anomalous (nonigneous) relationships between Mg, Fe, Ni, Cr, V, and Sc, 17 samples are interpreted to possess nonprimary geochemical traits and thus are eliminated from further geochemical and petrologic discussion. Figure 15A illustrates that the bulk compositions of these excluded samples generally are within the

range of other samples in the suite; we therefore believe that our interpretations are based on a representative data set. Data for the excluded samples are presented in Supplemental Table 4[8].

Figures 15B–15D portray important basic classification and nomenclature attributes of the Frederika and Wrangell magmatic suite. For these and all other geochemical plots, major element data have been normalized to 100% anhydrous prior to plotting. Using a variety of widely accepted elemental parameters and relationships, the data define a subalkaline basaltic andesite through rhyolite suite with predominantly calc-alkaline affinity, in line with a convergent plate margin setting. Figure 16 includes selected major (wt%) and trace (ppm) element concentrations plotted versus wt% SiO_2. Many of the trends observed are common for fractionation-dominated differentiation in igneous suites, for example, the overall decreases in MgO, TiO_2, Ni, and Sr and increase in K_2O with increasing SiO_2. Diverging trends in Y and Zr with increasing

[8]Supplemental Table 4. PDF file of additional geochemical data for Miocene rocks of the central Wrangell volcanic field. If you are viewing the PDF of this paper or reading it offline, please visit http://dx.doi.org/10.1130/GES00762.S8 or the full-text article at www.gsapubs.org to view Supplemental Table 4.
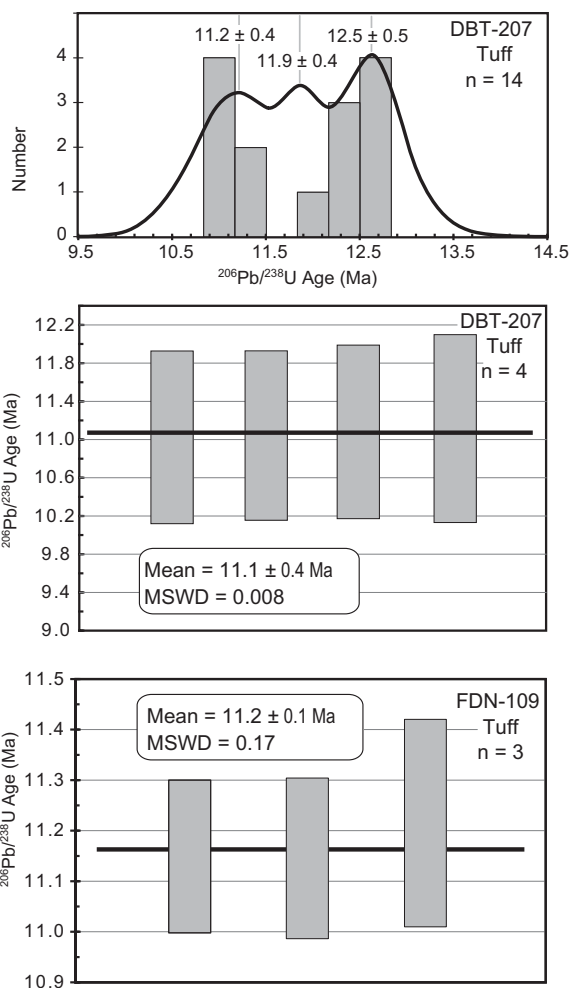
SiO_2 coupled with broad ranges in concentration for a number of elements at the more mafic (basaltic andesite) end of the compositional spectrum are characteristics that the Frederika-Wrangell suite share with eruptive products of the younger than 5 Ma Wrangell Volcanic Field (predominantly western WVB). As discussed in Preece and Hart (2004), these traits may suggest one or more of variable source, melting, or early differentiation histories.

DISCUSSION

Provenance

Active intrabasinal volcanoes were the primary source of sediment deposited in the central WVB, based on provenance data. Texturally immature volcanic-lithic clasts, plagioclase feldspar, embayed monocrystalline quartz, and unstable accessory minerals (Figs. 10 and 11) reflect erosion of volcanic edifices and limited transport through depositional environments (e.g., Critelli and Ingersoll, 1995). Mafic- to intermediate-composition volcanic clasts in conglomerate are texturally and mineralogically identical to intrabasinal lavas that crop out in the central WVB. The youngest detrital zircon age population (11.7–9.3 Ma) closely matches

Figure 13. Relative age probability histograms for zircons from tuff samples reflecting Miocene ages. Plots calculated with Isoplot software (Ludwig, 2006). Errors are 1 σ. Refer to Figures 3 and 5 for geographic and stratigraphic position of samples. Age determinations represent individual spot analyses from individual zircons; n—total number of concordant zircons. MSWD—mean square of weighted deviates.

Cretaceous detrital zircons may have been recycled from Jurassic–Cretaceous sedimentary strata that underlie the central WVB and crop out north and south of the central WVB (Figs. 3 and 7B). Mesozoic strata exposed <5–15 km south of the central WVB contain 153–152 Ma granitic clasts (Trop et al., 2002); similar strata exposed <30 km to the north yield 159–147 Ma detrital zircons (Manuszak et al., 2007). However, Mesozoic sedimentary strata were subordinate sources compared to igneous sources, given the paucity of sedimentary lithic grains in conglomerate and sandstone together with the dominance of Miocene detrital zircons in central WVB strata. Potential sources exposed north of the Denali fault would have contributed metamorphic clasts and Precambrian–Paleozoic detrital zircons (Foster et al., 1994; Dusel-Bacon and Williams, 2009; Hampton et al., 2010) that are not observed in central WVB provenance data. Similarly, potential sources exposed south of the Border Range fault (Chugach terrane, Fig. 1) would have provided metasedimentary clasts and a broader population of Early to middle Cretaceous detrital ages (Amato and Pavlis, 2010; Kochelek et al., 2011).

Central WVB Basin Development

Stratigraphic and geochronologic data demonstrate that the depositional and stratigraphic evolution of the central WVB was closely linked to construction of intrabasinal volcanic centers, active crustal subsidence, and extensional deformation. Volcanic eruptions routinely influenced environments of deposition based on the intercalation of volcanic breccia, lahars, volcaniclastic and/or pyroclastic deposits, and lavas with alluvial-fluvial-lacustrine siliciclastic deposits. Stratigraphic data demonstrate that volcanic aprons and alluvial fans prograded across fluvial-lacustrine environments (Figs. 17 and 18). Fluvial-lacustrine strata with thin volcanic interbeds (associations 1 and 2) are progressively replaced upsection by volcanic apron strata with thick-bedded lavas and lahars (associations 3 and 4) that increase in abundance and thickness upsection until only volcanic strata are preserved (e.g., sections 4 and 5 in Fig. 5 and Supplemental Figs. 1 and 2 [see footnotes 1 and 2]). We attribute progradation to topographic expansion of volcanic centers coeval with basin subsidence. The vertical stratigraphic pattern is consistent with tectonically controlled models of basin stacking patterns (e.g., Blair and Bilodeau, 1988). Volcanism was characterized by outpouring of lavas interrupted by less common, small-volume pyroclastic eruptions. The predominance of lavas compared with pyroclastic deposits suggests a volcanic field

the age of volcanic interbeds in the Frederika Formation and Wrangell Lavas (11.2–8.4 Ma; Figs. 3 and 12; Table 2), and most detrital zircons exhibit euhedral to subhedral grain shapes, oscillatory zoning, and U/Th ratios <6, indicative of an igneous origin (Williams, 2001; Rubatto et al., 2001). Subordinate detritus was eroded from inactive eruptive centers that remained topographically elevated in the eastern part of the central WVB. Sandstone sample PIL-72 yields 25–14 Ma detrital zircons (Fig. 12A) that overlap the age of volcanic rocks and intrusions exposed <20 km northeast of the central WVB near the Alaska-Yukon border in the Sonya Creek and Rocker Creek area (Figs. 1 and 4; Skulski et al., 1992; Richter et al., 2000).

Local Mesozoic–Paleozoic igneous and sedimentary sources contributed subordinate detritus to the central WVB. Late Cretaceous detrital zircons (89–70 Ma) match the age of plutons that crop out across southern Alaska and western Canada (Breitsprecher and Mortensen, 2004a, 2004b), including <50 km north of the central WVB near the Denali fault
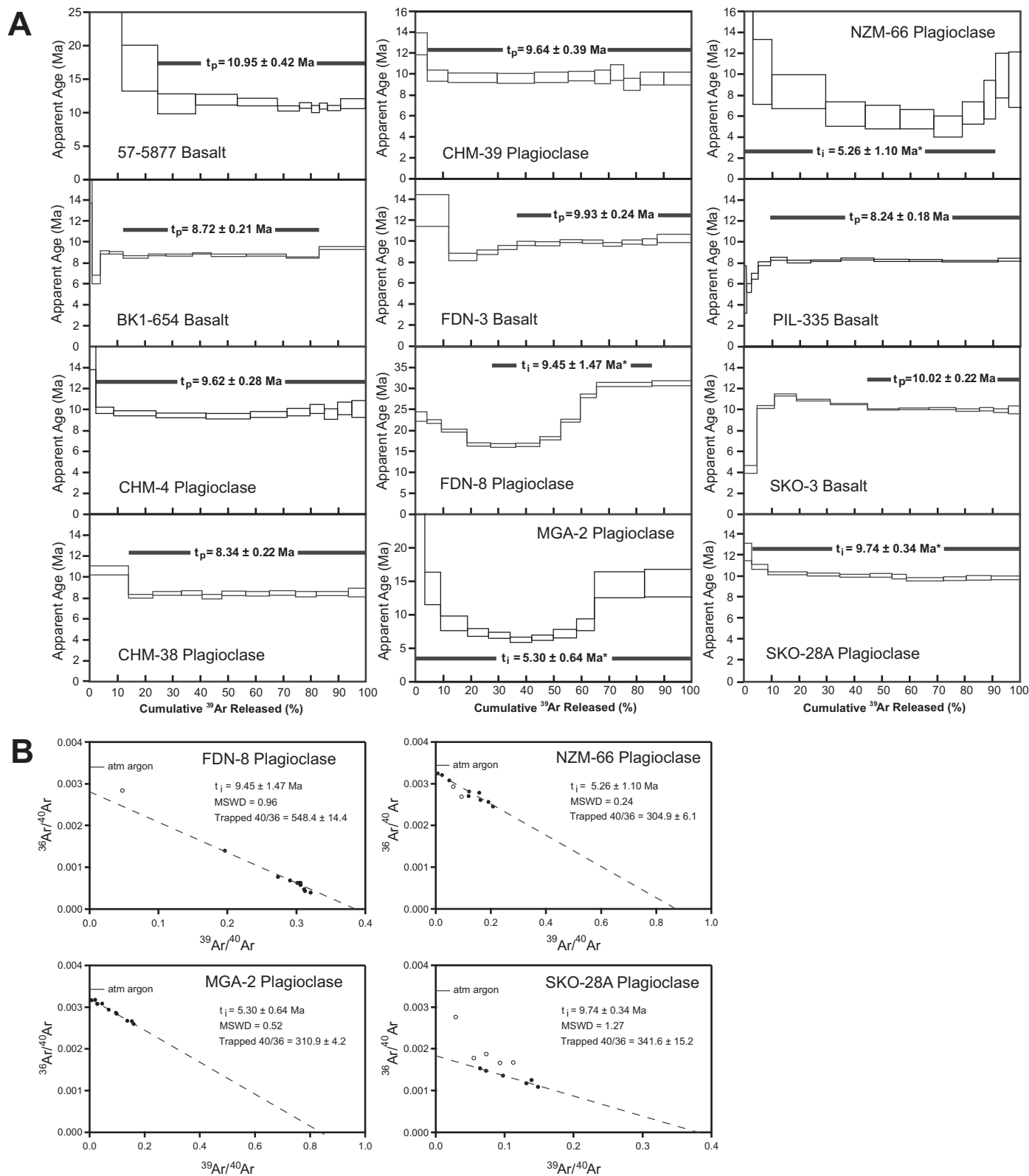
(Richter, 1976). Mid-Cretaceous detrital zircons (118–97 Ma) overlap the age range of 123–85 Ma plutons exposed along the north flank of the Wrangell Mountains (Snyder and Hart, 2007) and more distant areas of eastern Alaska and Yukon Territory (Richter et al., 1975; Foster et al., 1994; Israel et al., 2006; Israel and Cobbett, 2008). Middle Jurassic–Early Cretaceous detrital zircons (169–136 Ma) overlap the age of 170–130 Ma plutons that crop out along the south flank of the Wrangell Mountains (Roeske et al., 2003; Richter et al., 2006). Detrital zircon grains with Permian (289 Ma) and Devonian (374 Ma) ages match the ages of plutonic-metamorphic belts that crop out across eastern Alaska and adjacent parts of Canada (Aleinikoff et al., 1988; Nokleberg et al., 1994). In the central WVB, this belt includes 320–282 Ma plutons and metavolcanic rocks, including the Barnard and Ahtell plutons (Gardner et al., 1988; Richter et al., 1975) and gneiss with 380–340 Ma isotopic ages that crops out >50 km north of the WVB in eastern Alaska and Yukon Territory (Dusel-Bacon and Williams, 2009). Jurassic–

Figure 14. Age spectrum and selected inverse isochron diagrams for $^{40}Ar/^{39}Ar$ age samples of lava flows reflecting Miocene ages. Plateau ages (t_p) are quoted for all samples except for FDN-8, MGA-2, NZM-66, and SKO-28A (noted by asterisks), which did not yield acceptable plateaus and show evidence of excess ^{40}Ar contamination. Inverse isochron ages (t_i) are quoted for these samples. Heating steps represented by open circles were not included in the isochron regressions. Refer to Figure 5 for stratigraphic and geographic position of samples. MSWD—mean square of weighted deviates.

TABLE 3. GEOCHEMICAL DATA FOR MIOCENE VOLCANIC AND INTRUSIVE ROCKS OF THE CENTRAL WRANGELL VOLCANIC FIELD

Sample	SOU-1	SOU-2	SOU-6	PIL-335	PIL-340	CHM-4	CHM-5	CHM-6	CHM-7	CHM-14
Type	Intrusive	Intrusive	Intrusive	Lava	Lava	Lava	Lava	Lava	Lava	Lava
Section	n/a	n/a	n/a	4	4	7	7	7	7	7
Number	1	2	3	5	6	8	9	10	11	12
Latitude (dd)	61.427917	61.427917	61.427917	61.634533	61.634533	61.706944	61.709278	61.709639	61.709861	61.720417
Longitude (dd)	142.671972	142.671972	142.671972	142.769733	142.769733	142.521639	142.524944	142.525972	142.526139	142.512722
SiO_2 (wt%)	65.48	66.16	71.84	59.11	58.71	54.24	52.79	61.68	62.43	54.52
TiO_2	0.41	0.42	0.09	1.55	1.59	1.20	1.51	1.36	1.35	1.28
Al_2O_3	16.64	16.74	15.21	16.70	16.73	16.89	16.73	15.25	14.80	17.68
$Fe_2O_3(t)$	3.35	3.38	1.21	3.28	3.48	7.64	8.33	7.07	6.76	8.07
MnO	0.07	0.06	0.04	0.14	0.13	0.11	0.13	0.08	0.11	0.21
MgO	1.38	1.39	0.21	2.56	2.63	5.07	3.50	1.67	1.33	4.09
CaO	3.43	3.32	1.51	5.88	5.67	7.82	8.90	3.95	3.94	7.26
Na_2O	4.91	4.98	4.67	4.65	4.73	3.80	3.58	4.12	3.93	4.32
K_2O	1.74	1.77	2.50	1.62	1.56	1.15	1.24	2.94	2.86	0.88
P_2O_5	0.15	0.15	0.08	0.45	0.46	0.31	0.40	0.52	0.52	0.28
LOI	1.55	1.09	1.48	0.89	0.49	1.14	2.05	0.94	1.30	0.36
Total	99.10	99.45	98.83	96.82	96.18	99.37	99.16	99.57	99.32	98.95
Rb (ppm)	43	42	63	27	33	<5	<5	83	106	12
Sr	492	513	349	546	522	543	588	365	356	525
Ba	636	618	941	620	624	445	463	922	947	352
Zr	84	87	63	230	224	146	161	346	355	133
Y	10	8	8	31	31	25	29	43	42	26
Zn	39	46	66	82	85	70	70	75	78	95
Ni	9	11	<5	<5	<5	76	71	7	11	16
Cr	<5	<5	<5	9	<5	150	141	<5	<5	<5
Cu	15	13	<5	20	23	28	37	59	46	35
V	62	46	7	166	169	196	189	126	179	190
Sc	5.1	3.7	<0.5	17	17	18	21	18	13	21

Sample	CHM-31	CHM-39	CHM-38	CHM-41	CHM-42	CHM-43	CHM-44	CHM-35	KRS-WP50	MAR-WP47
Type	Lava	Lava	Lava	Lava	Lava	Lava	Lava	Lava	Lava	Lava
Section	9	9	9	9	9	9	9	9	14	16
Number	13	15	16	17	18	19	20	21	29	30
Latitude (dd)	61.725361	61.722417	61.728944	61.717444	61.731167	61.715583	61.715389	61.730667	61.667722	61.710722
Longitude (dd)	142.477417	142.482000	142.492333	142.497972	142.497889	142.498444	142.498194	142.495111	142.165111	142.184444
SiO_2 (wt%)	56.31	53.59	63.92	53.15	52.97	53.92	52.54	53.50	51.83	51.84
TiO_2	0.83	1.48	0.88	1.18	1.42	1.19	1.16	1.22	1.61	1.24
Al_2O_3	16.48	16.77	15.84	15.60	18.34	18.61	17.32	17.07	16.52	16.96
$Fe_2O_3(t)$	6.43	8.37	4.75	7.08	8.93	8.02	8.18	8.27	9.22	8.44
MnO	0.10	0.12	0.08	0.11	0.14	0.12	0.13	0.17	0.15	0.15
MgO	5.00	5.01	1.66	5.73	4.96	4.80	6.40	5.51	5.32	5.76
CaO	6.81	8.16	4.10	9.06	8.09	8.25	9.52	9.32	7.93	8.61
Na_2O	3.59	3.63	4.23	3.39	4.20	4.02	3.53	3.48	3.59	3.72
K_2O	1.62	1.11	2.26	0.95	0.73	0.45	0.36	0.61	1.07	0.97
P_2O_5	0.22	0.35	0.23	0.39	0.27	0.23	0.22	0.19	0.33	0.30
LOI	2.74	1.17	2.40	1.46	0.54	0.97	0.66	0.67	1.96	1.85
Total	100.16	99.77	100.35	98.10	100.58	100.58	100.02	100.01	99.53	99.84
Rb (ppm)	28	15	50	29	12	14	6	12	40	<5
Sr	590	510	387	693	533	564	445	367	401	481
Ba	527	450	821	518	276	301	256	268	409	389
Zr	144	185	261	171	132	123	130	133	179	136
Y	16	26	25	21	25	23	26	25	32	27
Zn	70	76	61	70	75	109	68	65	74	60
Ni	118	59	19	83	16	29	68	35	38	39
Cr	153	119	10	206	9	20	200	53	105	150
Cu	52	41	17	84	32	42	58	52	32	18
V	134	183	95	186	205	182	185	188	177	170
Sc	19	22	11	25	25	23	29	29	24	24

(continued)

characterized by multiple vents scattered along fissures and hypabyssal intrusions that fed into volcanic deposits (Condit and Connor, 1996; Walker, 2000; Cole et al., 2006). The basin fill is not interpreted as one or more calderas given that lowermost strata overlie Mesozoic strata along a basin-wide unconformity, thick silicic ignimbrites typical of caldera fills are not evident, and ring faults and ring fracture intrusions are not observed. Miocene dikes strike parallel to north-striking normal faults that cut Miocene sedimentary and volcanic strata throughout the study area (Figs. 3 and 17; MacKevett, 1970a, 1970b), indicating that normal faults may have been conduits for magma ascent. The north-striking normal faults dip steeply and strata do not exhibit substantial postdepositional rotation (note dominance of bedding dips from 0° to 10° in Fig. 3), indicating limited displacement along nonlistric faults. Localized thickening of vol-canic and sedimentary strata across some faults (Fig. 7A) indicates syndepositional displacement, but growth strata are not well developed; for example, intraformational unconformities are not evident. The north-striking orientation of normal faults is consistent with syndepositional extension in a zone of right-lateral shear between northwest-striking strike-slip faults that cut strata along the northeastern and southwestern margins of the outcrop belt (Totschunda fault

TABLE 3. GEOCHEMICAL DATA FOR MIOCENE VOLCANIC AND INTRUSIVE ROCKS OF THE CENTRAL WRANGELL VOLCANIC FIELD (*continued*)

Sample	FDN-WP41	FDN-3	FDN-4	FDN-6	FDN-10	FDN-11	MAR-8	SKO-1	SKO-3	SKO-9
Type	Lava	Lava	Lava	Lava	Lava	Lava	Lava	Lava	Lava	Lava
Section	15	15	15	15	15	15	16	18	18	18
Number	31	32	33	34	36	37	38	39	40	41
Latitude (dd)	61.688167	61.688472	61.688361	61.688583	61.687556	61.685250	61.711528	61.617778	61.617361	61.616861
Longitude (dd)	142.165583	142.162944	142.161444	142.159917	142.154111	142.147444	142.163306	142.016833	142.015750	142.050611
SiO_2 (wt%)	53.38	51.93	52.09	52.15	52.43	62.06	59.71	57.19	56.91	61.40
TiO_2	1.26	1.28	1.31	1.29	1.46	0.72	0.86	1.03	0.95	0.69
Al_2O_3	15.86	17.34	17.52	17.21	17.27	16.51	16.66	16.94	16.73	16.41
$Fe_2O_3(t)$	8.10	8.47	8.72	8.45	9.40	4.57	6.08	6.80	6.55	4.73
MnO	0.13	0.14	0.12	0.12	0.17	0.09	0.08	0.12	0.12	0.08
MgO	5.48	5.76	5.60	5.37	3.59	2.26	3.46	4.24	4.76	3.67
CaO	7.41	8.81	8.63	8.70	7.08	4.77	5.91	6.94	7.18	5.54
Na_2O	3.64	3.65	3.61	3.69	4.17	4.13	4.16	3.96	3.72	4.22
K_2O	1.36	0.82	0.97	0.98	1.20	1.75	1.51	1.54	1.60	1.51
P_2O_5	0.28	0.30	0.30	0.31	0.33	0.23	0.30	0.33	0.27	0.22
LOI	2.84	1.24	1.01	1.31	2.16	2.24	1.12	0.38	0.51	0.77
Total	99.71	99.74	99.89	99.60	99.26	99.33	99.86	99.46	99.31	99.23
Rb (ppm)	26	20	22	22	18	97	34	35	39	38
Sr	381	484	464	476	458	506	611	518	474	541
Ba	499	379	371	362	501	732	656	588	591	549
Zr	145	159	154	156	188	170	179	184	174	135
Y	28	28	28	30	31	18	21	23	22	15
Zn	73	76	80	77	95	45	75	74	62	54
Ni	69	36	35	31	13	19	55	33	42	29
Cr	159	139	133	104	<5	30	96	80	154	108
Cu	30	28	25	27	20	26	24	21	19	20
V	185	172	194	165	202	73	107	134	132	92
Sc	21	25	27	26	20	10	14	18	19	13

| Sample	SKO-10	SKO-14	SKO-16	SKO-17	SKO-23	SKO-26	SKO-29	SKO-30	SKO-31
Type	Lava	Lava	Lava	Lava	Lava	Lava	Intrusive	Intrusive	Intrusive
Section	18	18	18	18	18	18	n/a	n/a	n/a
Number	42	43	44	45	46	47	48	49	50
Latitude (dd)	61.616472	61.623500	61.620944	61.620444	61.619361	61.619917	61.634639	61.633194	61.632806
Longitude (dd)	142.051833	142.085806	142.085250	142.084806	142.107972	142.107278	142.060944	142.046528	142.047028
SiO_2 (wt%)	61.42	54.85	59.96	53.51	68.54	69.71	70.97	71.54	71.28
TiO_2	0.62	1.07	0.93	1.52	0.19	0.19	0.19	0.19	0.19
Al_2O_3	16.76	17.38	16.84	18.15	14.80	14.94	15.39	14.72	15.54
$Fe_2O_3(t)$	4.46	7.40	5.84	8.06	2.39	2.13	2.07	1.78	1.93
MnO	0.08	0.11	0.12	0.09	0.08	0.07	0.04	0.09	0.04
MgO	3.33	3.85	3.00	3.32	0.93	0.87	0.34	0.25	0.14
CaO	5.27	7.23	5.23	7.58	1.89	1.65	1.60	1.69	1.55
Na_2O	4.39	3.70	4.30	4.12	4.05	3.87	4.85	4.64	4.84
K_2O	1.17	2.15	2.00	1.03	3.22	3.32	2.90	2.91	2.99
P_2O_5	0.21	0.45	0.31	0.39	0.13	0.12	0.12	0.12	0.12
LOI	1.66	0.55	0.97	1.23	2.91	2.96	0.64	0.98	0.76
Total	99.37	98.72	99.49	99.00	99.14	99.81	99.09	98.90	99.38
Rb (ppm)	50	45	47	13	85	84	78	81	80
Sr	578	873	446	555	276	265	267	266	271
Ba	637	752	776	463	1104	1095	1120	1159	1160
Zr	131	213	228	212	193	188	180	183	243
Y	15	25	25	30	17	18	17	19	17
Zn	55	74	68	88	50	55	56	55	51
Ni	33	19	21	29	7	5	<5	9	<5
Cr	90	28	48	50	<5	<5	<5	<5	<5
Cu	20	38	29	34	<5	<5	<5	<5	<5
V	81	164	109	182	<5	<5	<5	<5	<5
Sc	12	19	16	22	1.7	1.8	1.5	1.6	0.8

Note: Section and number correspond to the measured section location (Fig. 3) and sampling location within section (Figs. 5,6, DR1–DR4), respectively. All samples were crushed to powder using a steel jaw crusher and alumina-ceramic disc mill and shatterbox assemblies. Analytical data were acquired via direct current argon plasma spectrometry techniques as described in Katoh et al. (1999) and Brueseke and Hart (2008). LOI is loss on ignition; dd is decimal degrees.

and an unnamed fault that truncates the northeast side of Porphyry and Sourdough Mountains in Fig. 3). Alternatively, extensional deformation may have been unrelated to strike-slip tectonics and initiated mainly by thermal weakening from ascending magmatic bodies. Unfortunately, the timing and kinematics of faults that cut the basin fill are not well established. Additional field studies of faults and their relationship with Miocene volcanic and sedimentary rocks are needed to accurately and completely understand magma ascent mechanisms and basin development.

Stratigraphic evidence, including paludal coal seams and lacustrine deposits, indicate that sediment accumulation was accommodated by active subsidence rather than being simply a response to ponding by volcanic stratigraphy. Subsidence is attributable to extensional deformation along intrabasinal normal faults and heat flow associated with intrabasinal volcanic centers. Well-developed progradational stacking patterns (Figs. 5, 17, and 18) together with the limited thickness of coal and lacustrine strata indicate that subsidence was outpaced by supply of sediment and volcanic deposits. Topographic expansion of intrabasinal volcanoes may have
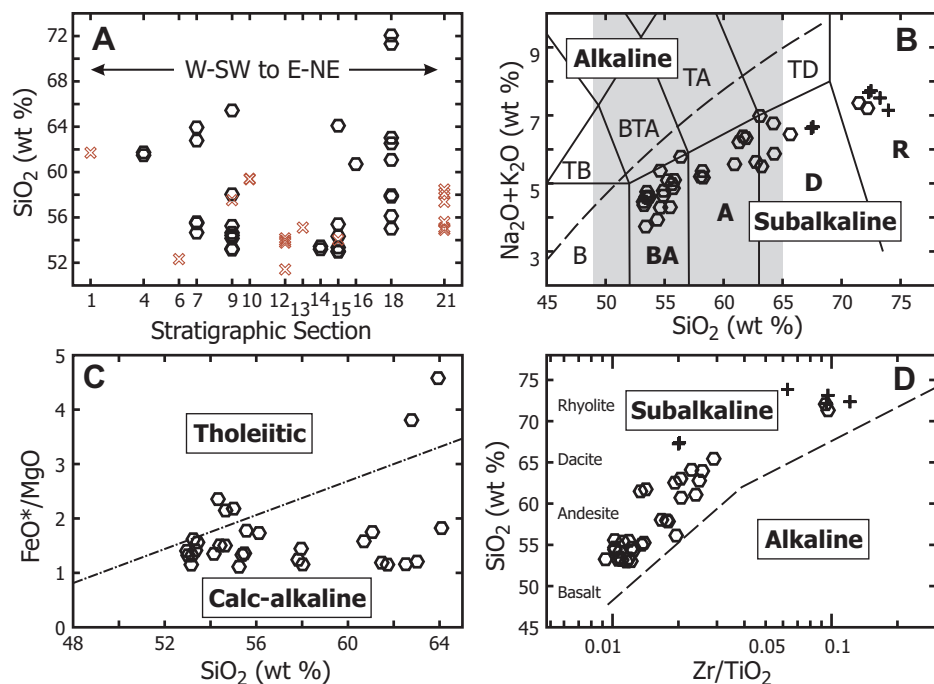
Figure 15. Sample distribution and classification and nomenclature. (A) Within and between stratigraphic section locality (Figs. 3 and 5) variations in SiO₂ (wt%). Note that overall range from ~52–72 wt% does not systematically correlate with geographic location. All analyzed extrusive samples are plotted for reference; the red crosses represent highly altered samples that are not used in subsequent plots or for interpretations (see text for details). (B) Total alkalies versus silica volcanic classification diagram after LeBas et al. (1986) with dashed line representing approximate division between alkaline and subalkaline rock series. Note that all samples are subalkaline and range from basaltic andesite (BA) to andesite (A), dacite (D), and rhyolite (R). Other abbreviations: B—basalt; BTA—basaltic andesite; TA—trachyandesite; TB—trachybasalt; TD—trachydacite. The shaded region depicts the SiO₂ range portrayed in C. Hexagons indicate extrusive material; plus signs indicate shallow intrusive material. (C) FeO*/MgO (total Fe as FeO = FeO*) versus SiO₂ diagram after Miyashiro (1974) illustrating that the vast majority of the sample suite is calc-alkaline. (D) Zr/TiO₂ diagram modified after Winchester and Floyd (1977), further illustrating the strongly subalkaline nature of the entire sample suite from this study.

eventually prompted development of an internally drained intramontane basin through damming of fluvial-lacustrine systems, but erosion of basin margin outcrops hampers detailed reconstruction of the basin paleogeography.

Our new stratigraphic, geochronologic, and lithofacies data from the central WVB (Fig. 5) document localized distribution of vent-proximal volcanic-sedimentary strata (<3200 km²), high accumulation rates of sedimentary-volcanic strata (>0.5 mm/yr), brief duration of sedimentary-volcanic accumulation (<3 m.y.), complex lateral lithofacies patterns, and evidence for lateral shifts in volcanism and basin development. These attributes are consistent with models of intraarc basin development (e.g., Smith and Landis, 1995). Similar intraarc successions are reported from continental arcs in Oregon-Washington-Idaho (Smith et al., 1987; Carlson and

Moye, 1990; Smith and Landis, 1995; Janecke et al., 1997), Mexico (Righter et al., 1995), New Zealand (Stern, 1985), and Arizona (Bassett and Busby, 2005; Busby and Bassett, 2007). The depocenter likely originated as a transtensional intraarc basin if basin-bounding right-lateral faults and intrabasinal normal faults were active during sediment deposition (e.g., Polliand et al., 2005; Busby et al., 2005). With oblique convergence of only 10° from orthogonal or more, strike-slip faults may form in the upper plate (Jarrard, 1986), especially in thermally weakened crust of volcanic belts (Cole and Lewis, 1981; Geist et al., 1988; McCaffrey, 1992; Weinberg, 1992; Bellier and Sebrier, 1994; Van Dijk, 1994; Israde-Alcantara and Garduno-Monroy, 1999), resulting in transtensional intraarc basins (e.g., Polliand et al., 2005; Busby et al., 2005). Establishment of the timing and kinematics of

central WVB deformation by future structural studies will help us to better evaluate the tectonic setting of basin development.

WVB Volcanism

The previous section outlined a scenario whereby the volcanic-sedimentary stratigraphy, complex lithofacies changes, and overall structural setting argue for volcanism and basin development in an intraarc setting. Using the chemistry of the lavas in conjunction with all of the other data presented herein can place first-order constraints on tectonic interpretations, particularly when compared to other WVB geochemical information. The older eastern WVB and the younger western WVB have been examined in some detail down to a volcano by volcano or at least volcanic field by volcanic field basis (e.g., Skulski et al., 1991, 1992; Richter et al., 1994, 1995; Preece and Hart 2004; and numerous references therein). We utilize the larger geochemical data sets and tectonomagmatic interpretations from these studies as a backdrop to our understanding of the central WVB Frederika-Wrangell magmatism.

Figure 19 uses major element data recalculated to cation percent values in order to compare central and western WVB data to those presented for the eastern WVB by Skulski et al. (1991). Plots A and B illustrate Na + K and Fe/Mg versus Si relationships for the central (this study and Sonya Creek field) and eastern (Saint Claire Creek field) WVB, and plots C and D illustrate the same parameters for the central and western (young western Wrangell and Mount Churchill) WVB. These plots convey the same general information depicted in Figures 15B and 15C. In addition, the Frederika-Wrangell data show little if any overlap with transitional subalkaline to alkaline (eastern Wrangell, EW-T) and more strongly alkaline (EW-A) lavas associated with leaky transform magmatic activity in the Saint Claire field or to lavas with strong intraplate geochemical signatures from the northwestern Canadian Cordillera (Skulski et al., 1991; Thorkelson et al., 2011). In contrast, note the strong overlap of the Frederika-Wrangell data with calc-alkaline and hybrid suites from Saint Claire Creek (EW-C; eastern), Sonya Creek (SC; central) and the young western (WW-1 and combined WW-2a, WW-2b) WVB. Using the interpretations of Skulski et al. (1991, 1992) and Preece and Hart (2004), these overlaps suggest magma genesis and evolution associated with subduction and intraarc extensional processes. A subduction as opposed to intraplate association for the central WVB is supported by the recent regional geochemical synthesis forwarded by Thorkelson et al. (2011).

Figure 16. Selected major (wt% MgO, TiO₂, K₂O, P₂O₅) and trace (ppm Ni, Y, Zr, Sr) element concentrations versus wt% SiO₂. Hexagons indicate extrusive material; plus signs indicate shallow intrusive material. See text for discussion.
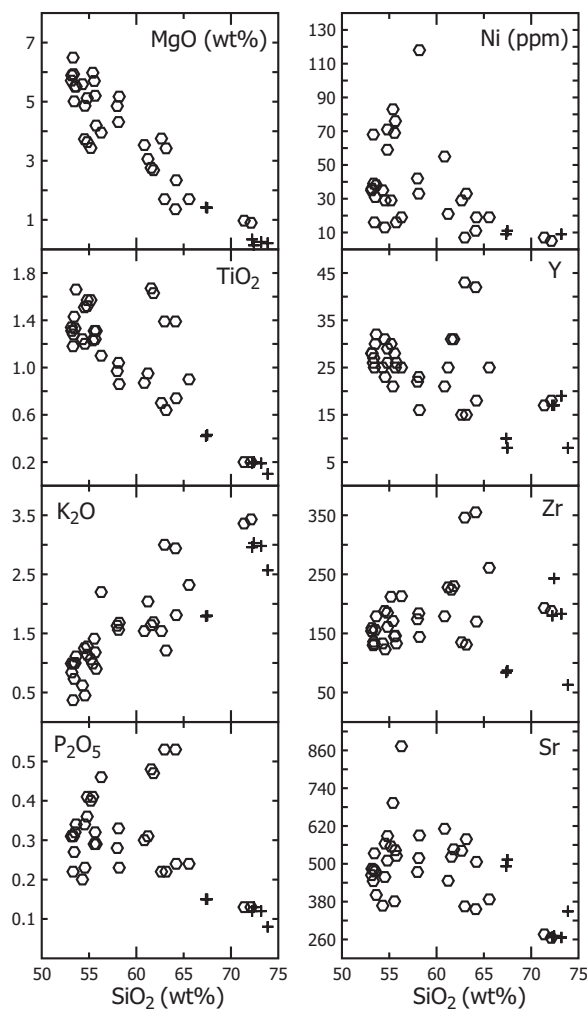
In order to further explore these associations and their implications, more detailed comparisons are drawn between the central (this study) and western (Preece and Hart, 2004) WVB in Figures 20 and 21. Both figures illustrate the three suites or trends defined in Preece and Hart (2004): WW-1—trend 1 calc-alkaline to tholeiitic suite; WW-2a—trend 2a strongly calc-alkaline suite; WW2b—trend 2b dominantly adakitic suite. Along with TiO₂, Y concentration strongly differentiates between the trend 1 and trend 2 lavas, particularly at increased levels of differentiation (Fig. 20A). This distinction at least in part reflects a role for early amphibole fractionation in trend 2 materials, implying higher fluid concentrations in the trend 2 magma sources and/or chambers. All lavas from the Frederika-Wrangell suite can be grouped with the trend 1 (WW-1) and trend 2a (WW-2a) materials of the younger than 5 Ma western WVB, suggesting a tectonomagmatic setting akin to either the interior (intraarc extensional regime and decompression melting of subduction modified mantle) or back side (trench dis-

tal portion of a magmatic arc and/or melting of recently slab fluid–enriched mantle) of the western region illustrated in Figure 2 (Fig. 20B).

Figure 21 illustrates a series of element and element ratio versus Y (ppm) plots that are employed to place additional qualitative constraints on Frederika-Wrangell tectonomagmatism. Figure 21A highlights the WW-1 and WW-2a association and also serves as a reminder that even the low SiO₂ members of the suite presented in this study have undergone considerable differentiation, so care must be taken when commenting on mantle sources. The K/P ratio versus Y plot (Fig. 21B) illustrates the dominance of trend 1 characteristics (low K/P), suggesting a less prominent role for slab fluid and/or felsic crustal influences (e.g., Carlson and Hart, 1987) than is common for the majority of trend 2a and 2b materials. Similarly, the Sr/P ratio (normalized to primitive mantle; Borg et al., 1997) versus Y plot (Fig. 21C) offers additional evidence for subduction-related but possibly not active subduction-driven magma genesis; for example, the dashed line at $(Sr/P)_{PM} = 5.5$ is suggested to

distinguish between magmas strongly enriched in components derived from subducting lithosphere (>5.5) from those enriched in these components (1–5.5). The Sr/Y versus Y plot (Fig. 21D) clearly distinguishes the lavas of this study from adakitic lavas that often are interpreted to result from partial melting of subducted mafic oceanic crust (e.g., Defant et al., 1991) due to various factors, including a young, hot slab with a shallow dip, plate margin effects, and development of a slab window (e.g., Yogodzinski et al., 2001). Such factors seem reasonable for present-day southern Alaska, where shallow slab geometries are documented. By analogy and/or comparison to studies in the western and eastern WVB, these geochemical signatures are taken to indicate that Miocene central WVB magmatism was a result of variable degrees of partial melting of a heterogeneous slab component–enriched mantle wedge source locally in response to development of an intraarc extensional regime.

WVB VOLCANISM AND BASIN DEVELOPMENT IN THE CONTEXT OF REGIONAL TECTONICS

Neogene deformation, volcanism, and basin development in south-central Alaska are linked to oblique convergence and flat-slab subduction between North America and the Yakutat microplate (Plafker, 1987; Plafker et al., 1994). In earlier tectonic models, oceanic crust along the inboard (northern) part of the Yakutat microplate was inferred to have been subducted beneath eastern Alaska and adjacent parts of Canada from Early Oligocene (ca. 30 Ma) to Middle Miocene time, with the onset of subduction based on the age of the oldest WVB lavas (Rocker and Sonya Creeks in Figs. 1, 4, 22A, and 22B). These early models infer that more buoyant continentalized crust of the southern part of the Yakutat microplate was subducted at a shallow angle beneath southern Alaska starting in Middle Miocene time (Plafker et al., 1994). Recent geophysical data, however, indicate that both the subducted and unsubducted parts of the Yakutat microplate consist of thick buoyant crust. The subducted northwestern portion of the microplate is 11–22 km thick, the unsubducted portion is 15–30 km thick, and both exhibit high ratios of P-wave to S-wave velocities typical of overthickened oceanic crust (Ferris et al., 2003; Eberhart-Phillips et al., 2006; Gulick et al., 2007; Christeson et al., 2010; Worthington et al., 2012), possibly representing an oceanic plateau (Pavlis et al., 2004). Recent integration of geologic data sets from south-central Alaska documents crustal shortening, regional exhumation, cessation of magma-
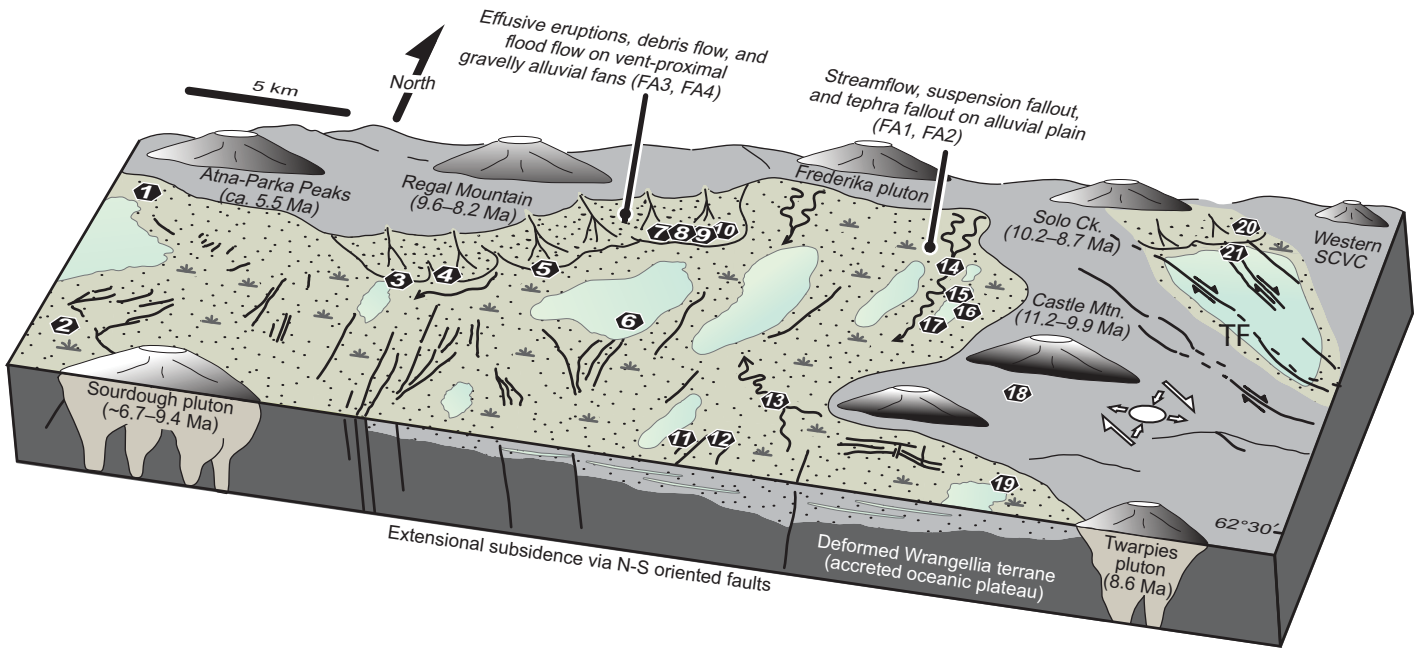
Figure 17. Schematic paleogeographic model showing inferred depositional environments and volcanic centers in the central Wrangell volcanic belt during Middle Miocene time. Hexagons indicate locations of measured sections from this study (Fig. 5). Ages of volcanic centers are based on new geochronologic ages from volcanic rocks (Table 2). Intrabasinal plutons (Twarpies, Porphyry, Frederika) overlap in age with spatially associated volcanic strata. Note syndepositional north-striking normal faults (originally mapped by MacKevett, 1970a, 1970b) interpreted as contributing to basin subsidence and serving as conduits for magmas. The orientation of the north-striking normal faults is consistent with east-west extension associated with right-lateral displacement along northwest-striking strike-slip faults such as the Totschunda fault (TF). SCVC—Sonya Creek volcanic center.
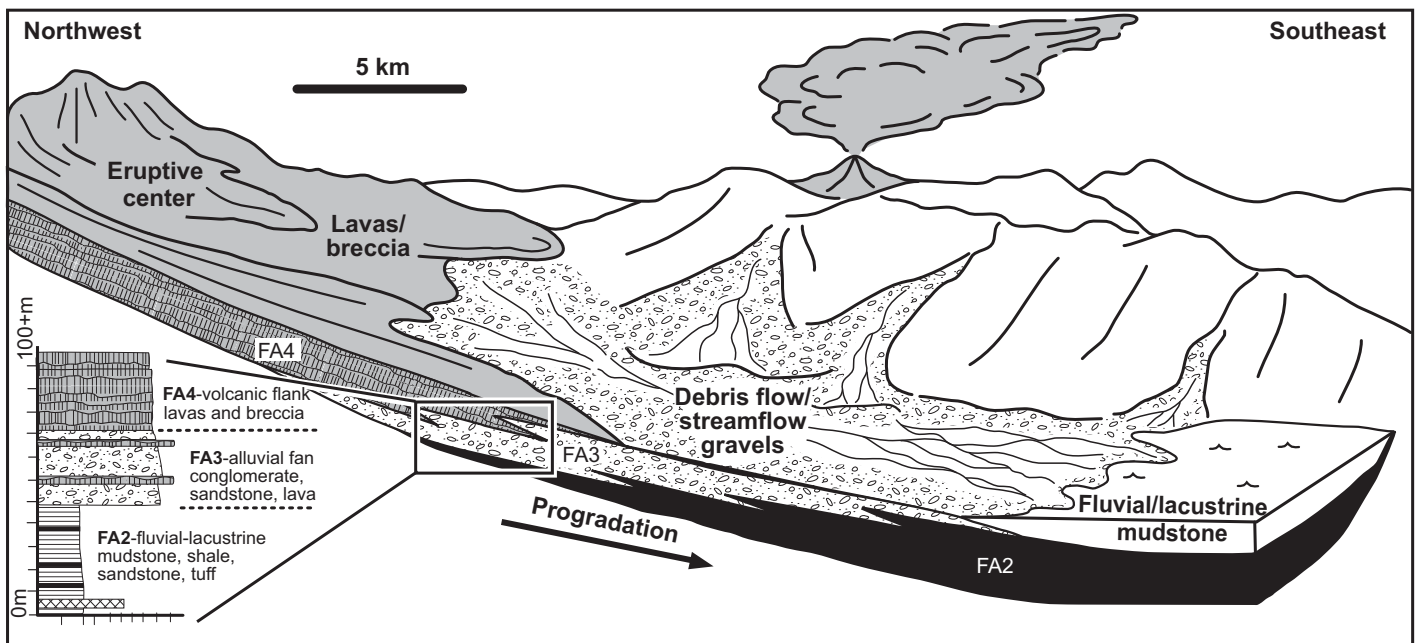
Figure 18. Schematic depositional model of upsection lithofacies transition resulting from progradation of vent-proximal volcanics (facies association 4) across gravelly alluvial fan strata (association 3) and finer grained fluvial-lacustrine deposits (associations 1 and 2). Schematic section in lower left characterizes sections 3–5 and 21 in the northwestern part of the basin. Refer to Figure 5 for measured sections. Sections in the southeastern part of the basin exhibit similar upsection transitions from fluvial-lacustrine strata to volcanic flanks but do not contain intervening alluvial strata (sections 11–17 in Fig. 5). FA—facies association. See sections 3–6 on Fig. 5 for detailed sections.

Figure 19. Cation percent (after Skulski et al., 1991) bulk chemical comparisons between samples from this study (central Wrangell volcanic belt, WVB; Fig. 2) and from the eastern and western (EW, WW) portions of the WVB (Fig. 2). (A) Total alkalies versus silica plot emphasizing subalkaline character of the sample suite of this study. This suite is also compared to calc-alkaline and hybrid (EW-C), transitional subalkaline-alkaline (EW-T), and alkaline (EW-A) lavas from the eastern WVB (Saint Clare Creek field; Skulski et al., 1991), to intraplate volcanism in the northwestern Cordillera (NWC; Skulski et al., 1991), and to samples from the nearby Sonya Creek field (SC; Richter et al., 2000). (B) Fe/Mg ratio versus silica plot comparing data from this study to other eastern and central WVB lava suites indicated in A. (C) Total

alkalies versus silica plot as in A, but comparing present sample suite to the SC and to volcanic suites defined by Preece and Hart (2004) for the younger than 5 Ma predominantly western WVB (plus Mount Churchill; Fig. 2); WW-1 is the trend 1 calc-alkaline to predominantly tholeiitic suite and WW-2a,b represents a combined field for two separate trend 2 suites with strongly calc-alkaline to adakitic geochemical signatures. (D) Fe/Mg ratio versus silica plot comparing data from this study to other eastern and central WVB lava suites indicated in C. Hexagons indicate extrusive material; plus signs indicate shallow intrusive material. See text for discussion.
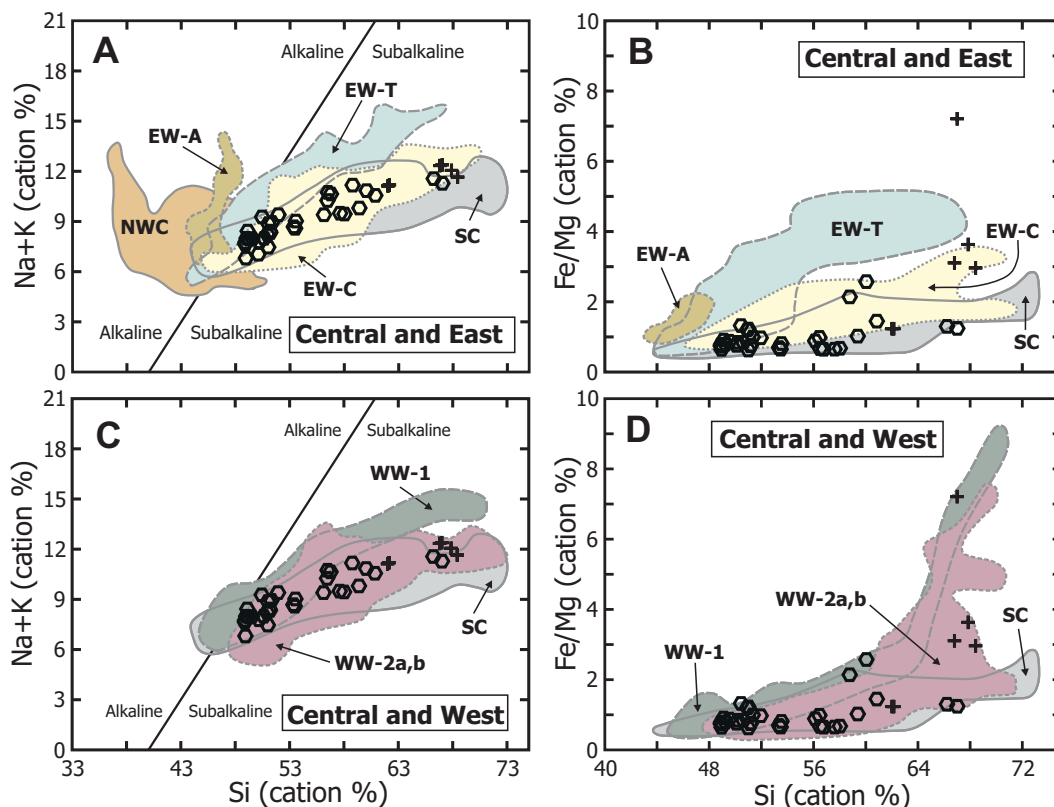
tism, and inversion of sedimentary basins above the flat-slab region since Oligocene time (Enkelmann et al., 2008, 2010; Benowitz et al., 2011; Finzel et al., 2011). Sedimentary basins located along the western and northern perimeter of the flat-slab region record enhanced sediment accumulation rates and sediment delivery from bedrock sources exhumed above the flat-slab region beginning in Late Oligocene–Middle Miocene time (Cook Inlet and Tanana basins; Ridgway et al., 2007; Finzel et al., 2011). Together, these studies indicate shallow subduction of the Yakutat microplate since Oligocene time. Along the eastern perimeter of the flat-slab region, diachronous Oligocene–Quaternary volcanism and basin development in the WVB are consistent with progressive northwestward insertion of the northward-tapering slab into the arcuate continental margin of eastern Alaska. Oligocene–Miocene basin development and volcanism in the eastern WVB are linked to right-lateral displacement along the Duke River and Dalton faults in Yukon Territory and British Columbia (Figs. 22A, 22B). Eocene–Oligocene alluvial fan, fan-delta, and lacustrine strata >900 m thick

record strike-slip basin development (Ridgway and DeCelles, 1993a, 1993b; Ridgway et al., 1992, 1996). Progressive extensional deformation within strike-slip basins permitted construction of intrabasinal volcanic centers and progradation of >1000-m-thick successions of 18–15 Ma lava flows and pyroclastic rocks (Wrangell Lavas) upon underlying sedimentary successions (Miocene Stanley Creek, Alsek, Nines Creek fields in Figs. 22A, 22B; Skulski et al., 1991; Cole and Ridgway, 1993). The predominance of transitional to alkaline geochemical compositions of volcanic rocks together with their limited spatial distribution along strike-slip faults indicates volcanism related to extensional strike-slip faulting (i.e., leaky transform volcanism; Skulski et al., 1991, 1992). Age-equivalent volcanic centers in the Saint Clare field (Yukon Territory) and Sonya Creek–Rocker Creek area record a spatial transition from strike-slip to subduction tectonics (Fig. 22B). The presence of shield volcanoes that produced materials with transitional to calc-alkaline geochemical compositions indicates derivation from a mid-oceanic ridge basalt (MORB) like

mantle wedge heterogeneously enriched via the addition of slab-derived components. We interpret transtensional basins and volcanic centers along northwest-striking strike-slip faults as the products of initial orogen-parallel translation of the leading edge of the Yakutat microplate along the eastern, northwest-striking part of the arcuate continental margin (southern Alaska syntaxis). Coeval subduction-related volcanic centers are interpreted to represent northwestward subduction of oceanic crust (the inboard margin of the Yakutat microplate) beneath the central part of the syntaxis (Saint Clare and Sonya Creek fields in Figs. 22A, 22B).

Sedimentary and volcanic strata exposed in the Wrangell Mountains record a progressive northwestward shift in the position of volcanism and basin development ca. 12–8 Ma (Fig. 22C; this study). Sampled volcanic suites exhibit transitional to calc-alkaline geochemical compositions that suggest generation from subduction-modified mantle sources. Basinal strata record progradation of volcanic strata (Wrangell Lavas) across alluvial-lacustrine strata (Frederika Formation) in response to

Figure 20. Comparison of central Wrangell volcanic belt (WVB) (this study) magmatism with that of the western WVB (Preece and Hart, 2004). (A) Y versus SiO$_2$ plot showing fields for the three western WVB volcanic groups (trends) introduced in Figure 19. Here, distinction is made between trend 2a (WW-2a; strongly calc-alkaline) and trend 2b (WW-2b; adakitic). (B) Histograms of western WVB geochemical groups (trends) illustrating distinctions in the relative proportions of samples from the different trends (1, 2a, 2b) with geographic location approximately perpendicular to the strike of the continental margin. The data set is dominated by samples from Mounts Drum, Wrangell, and Churchill (front side); Mount Sanford and interior cinder cones and/or mesas (interior); and Skookum Creek, Tanada Peak, and Capital Mountain (back side) (see Fig. 2). Hexagons indicate extrusive material; plus signs indicate shallow intrusive material. See text for discussion.
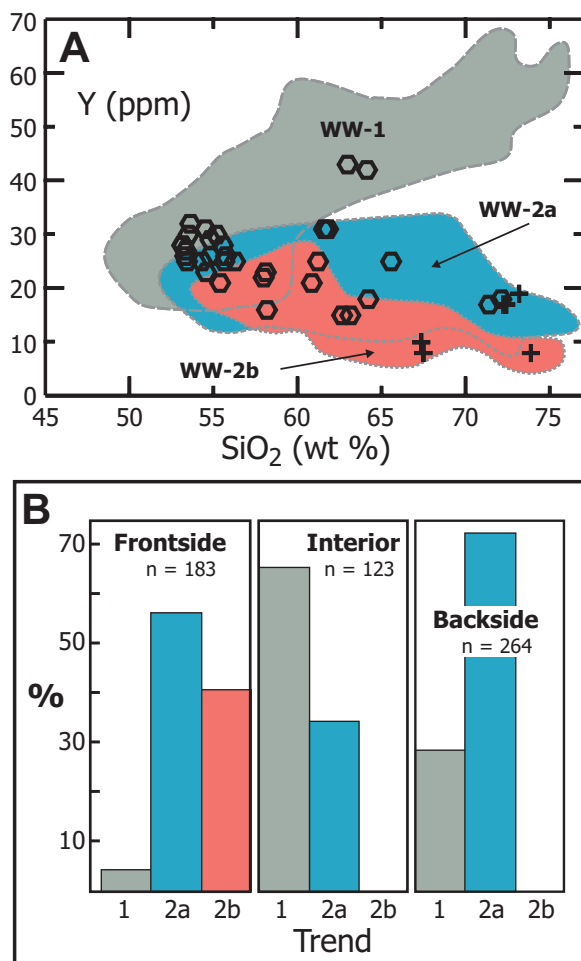
topographic expansion of eruptive centers. We interpret this spatial-temporal shift in the location of volcanism and basin development as a consequence of insertion of progressively thicker crust (documented by recent geophysical studies; e.g., Worthington et al., 2012) into the eastern part of the syntaxis synchronous with a documented change in plate motion (Fig. 22C; Stock and Molnar, 1988). Volcanic centers originating from subduction-related processes and sources would be expected to migrate northwestward as thicker, more buoyant crust entered the subduction zone from the southeast along the Queen Charlotte–Fairweather transform fault and the leading edge of the subducting slab migrated northwestward. We infer that intraarc basin development and volcanism were accommodated by extensional deformation along north-striking normal faults and, more speculatively, that transtensional basin development was associated with basin-bounding, northwest-striking, right-lateral strike-slip faults.

Volcanism continued to migrate northwestward during Late Miocene–Holocene time based on the spatial distribution of younger than 5 Ma to Holocene volcanoes in the western Wrangell Mountains (Figs. 4 and 22D; Richter et al., 1990, 2006; Preece and Hart, 2004). Continued northwestward migration of magmatism is consistent with thermochronologic data that document exhumation in the central WVB ca. 5–4 Ma (Enkelmann et al., 2010). An exception to the northwestward-younging pattern of volcanism is Mount Churchill, a Holocene stratovolcano in the central WVB that erupted large-volume silicic fallout deposits as recently as 1147 yr ago (Clague et al., 1995; Richter et al., 1995). It is not known whether sedimentary basin development preceded volcanism in the western WVB, as documented in the central and eastern WVB, because the subvolcanic stratigraphy remains largely obscured by Holocene volcanoes (Richter et al., 2006). Western WVB volcanism records subduction-related processes based on complex spatial-chemical variations above a modern geophysically imaged, north-dipping slab (Preece and Hart, 2004; Fuis et al., 2008). All sampled western WVB volcanic suites contain mafic parental compositions consistent with derivation from a MORB-like mantle wedge that

has been heterogeneously enriched via the addition of slab-derived components. Large shield volcanoes and stratovolcanoes (Fig. 2; front-side and back-side in Fig. 20) surround the interior region and exhibit calc-alkaline mafic suites that indicate higher degrees of partial melting catalyzed by active fluid fluxing into the mantle wedge. High-TiO$_2$ transitional tholeiitic eruptive products emplaced along the inboard part of the volcanic field (interior in Figs. 2 and 20) indicate relatively low degrees of partial melting resulting from an intraarc extensional regime.

Northwestward migration of subduction-related magmatism is supported by the spatial extent of a present-day subducted slab deeper than 50 km beneath only the westernmost WVB (Fuis et al., 2008), although some studies indicate that a present-day deeply subducted slab (>50 km) is not present beneath any part of the WVB (Eberhart-Phillips et al., 2006; Qi et al., 2007). Subduction-related fluids implicated in magma generation and evolution processes in the central and western WVB were likely derived from shallowly subducting portions of the Yakutat slab. Steady dehydration of a shallow slab would release fluids that would be expected to migrate laterally from the slab and into the western WVB (Gutscher et al., 2000; Preece and Hart, 2004; Eberhart-Phillips et al., 2006). Adakitic, amphibole dacite magmas documented in samples from Mounts Drum and Churchill (Fig. 2) are consistent with partial melting of the Yakutat slab (Preece and Hart, 2004). Adakite melts commonly form by slab melting when the downgoing slab is young and at shallow depths, the dip of the downgoing plate is very shallow, or the plate margin is characterized by elevated shear stresses (Drummond et al., 1996; Gutscher et al., 2000; Yogodzinski et al., 1995, 2001), conditions that characterize the present-day flat-slab region of southern Alaska (Ferris et al., 2003; Eberhart-Phillips et al., 2006).

Northwestward insertion of progressively thicker crust into the syntaxis during Miocene to Holocene time is also consistent with the evolution of deformation and sediment accumulation outboard (southward) of the WVB. Thermochronologic data from the Chugach, Saint Elias, and Fairweather Ranges document exhumation starting ca. 26 Ma with pulses ca. 20 Ma and ca. 11 Ma followed by rapid, deep-seated, and focused exhumation in the corner of the syntaxis beginning ca. 6–5 Ma (Berger et al., 2008a, 2008b; McAleer et al., 2009; Enkelmann et al., 2008, 2010). Rapid exhumation was synchronous with Late Miocene to Pleistocene crustal shortening and synorogenic sedimentation in the adjacent Gulf of Alaska (Lagoe et al., 1993; Gulick et al., 2007; Witmer, 2009; Worthington et al., 2010). The Yakataga Formation consists of
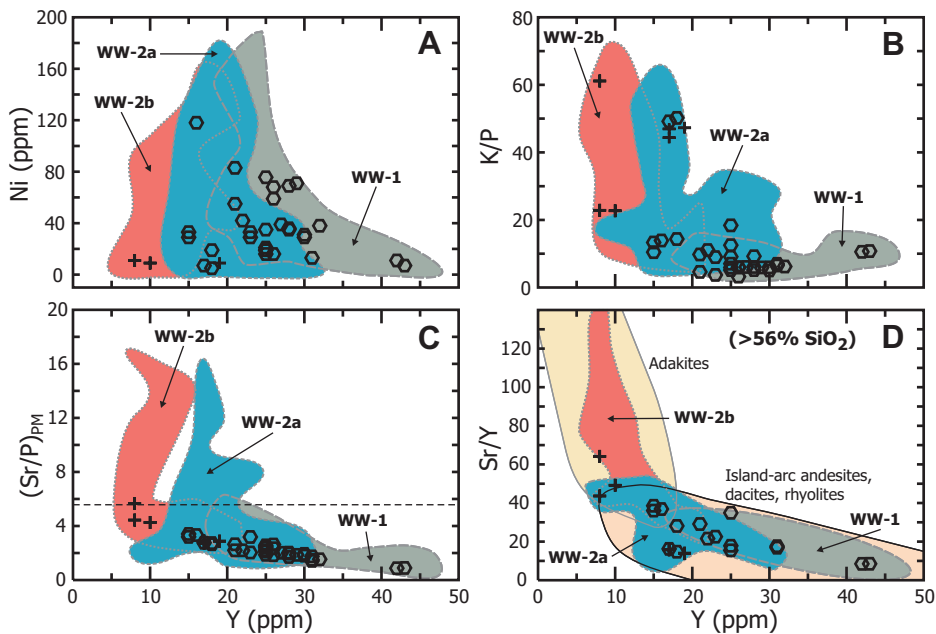
Figure 21. Selected geochemical parameters versus ppm Y for samples from this study and for the three young western Wrangell volcanic belt suites and/or trends (i.e., WW-) previously defined. (A) Ni (ppm) as an indicator of overall degree of magmatic differentiation. (B) K/P ratio. This ratio can be an effective indicator of felsic crustal assimilation (solid or melt) and/or slab fluid contributions to a magma source (e.g., Carlson and Hart, 1987). (C) Sr/P ratio normalized to primitive mantle values (after Borg et al., 1997). Horizontal dashed line at $(Sr/P)_{PM} = 5.5$ separates magmas enriched (1–5.5) from those strongly enriched in components derived from subducting lithosphere. (D) Sr/Y ratio for samples with >56 wt% SiO_2. Diagram modified after Defant et al. (1991) and Preece and Hart (2004); yellow and beige shaded fields indicate characteristics associated with adakitic lavas and more typical arc andesites, dacites, and rhyolites, respectively. Hexagons indicate extrusive material; plus signs indicate shallow intrusive material. See text for discussion.

a siliciclastic succession as much as 10 km thick with intraformational angular unconformities reflecting syndepositional deformation; the succession reflects enhanced sediment accumulation rates following deposition of the Eocene–Early Miocene Poul Creek and Kulthieth Formations (Plafker, 1987; Witmer, 2009; Worthington et al., 2010). Magnetostratigraphic data suggest that the base of the Yakataga Formation was deposited during Late Miocene time (later than 11.6 Ma; Lagoe et al., 1993; Zellers and Gary, 2007), concurrent with the shift in WVB volcanism and basin development from the eastern part of the syntaxis to the central WVB.

The Miocene–recent evolution of the southern Alaska syntaxis has been compared with syntaxes that define the Himalaya-Tibetan orogenic belt (Enkelmann et al., 2010). The Alaskan and Himalaya-Tibetan syntaxes are similarly characterized by extreme local relief resulting from rapid exhumation and deformation at the spatial transition from strike-slip tectonics to convergence (Zeitler et al., 1993, 2001; Stewart et al., 2008). Both regions exhibit Mio-

cene–Quaternary volcanic centers with complex spatial-geochemical-age patterns, including calc-alkaline volcanism linked to slab dehydration and diachronous alkaline volcanism and basin development associated with transtensional deformation along regional strike-slip faults (e.g., Maury et al., 2004; Wang et al., 2006, 2007; Yang et al., 2007; Lee et al., 2010). We speculate that similar patterns of deformation, volcanism, and basin development shaped pre-Cenozoic syntaxial margins, especially during assembly of supercontinents, and may be distinguishable from typical continental margin processes through integrated geochemical, geochronological, and stratigraphic data sets.

CONCLUSIONS

Sedimentology, provenance, geochemistry, and geochronology document construction of the central WVB and link this event to Neogene tectonic processes that shaped the northern Pacific plate margin. Lithofacies associations identified in the Frederika Formation and lower

Wrangell Lavas indicate deposition by volcanic aprons, alluvial fans, and more distal braided streams and floodplain channels, lakes, and mires. Stratigraphic and topographic relationships along the basal unconformity show that accumulation occurred on a high-relief (400+ m) erosional surface developed on deformed Mesozoic marine strata. Upward-coarsening stratigraphic successions record progradation of volcanic aprons onto fluvial-lacustrine deposystems in response to topographic growth of intrabasinal volcanic centers. Paleoclimate conditions were sufficiently warm and moist to support abundant vegetation, peat formation, and perennial aqueous depositional processes. Compositional, paleocurrent, and detrital ages link deposition of the Frederika Formation chiefly to erosion of active intrabasinal volcanoes. Local eruptive centers provided juvenile volcanic detritus, including volcanic-lithic clasts, plagioclase feldspar crystals, tuffaceous matrix, and 12–9 Ma detrital zircons. Subordinate sediment was derived from remnant volcanoes currently exposed along the Alaska-Yukon border as well as Mesozoic plutons and marine strata that underlie or crop out adjacent to central WVB strata. Central WVB lavas exhibit calc-alkaline geochemical compositions ranging from basaltic andesite to rhyolite. The sampled lavas broadly overlap Pliocene–Quaternary phases of the western WVB interpreted as the product of subduction-related volcanism. In contrast, Miocene volcanic rocks from the eastern WVB are attributable to magmatism along leaky strike-slip faults and exhibit higher Fe/Mg ratios and total alkalies at a given silica content. The U/Pb and $^{40}Ar/^{39}Ar$ age analyses of tuffs and lavas indicate that sediment accumulation and volcanism in the central WVB commenced by ca. 12.5–11.2 Ma and shifted westward to younger vents from ca. 8.3–9.6 Ma. Samples from two western sections yield even younger ages of ca. 5.3 Ma. Integration of these new ages with published ages supports northwestward migration of volcanism and basin development across the eastern (ca. 26–10.4 Ma), central (12.5–5 Ma), and western (5 or later to 0.8 Ma) WVB. Stratigraphic evidence, including coal and lacustrine deposits, indicates active tectonic subsidence during basin development. Likely subsidence mechanisms include heat flow from intrabasinal volcanoes and extensional deformation linked to intrabasinal normal faults. The orientation of the normal faults is consistent with east-west extension associated with right-lateral displacement along basin-bounding northwest-striking strike-slip faults that cut the basinal strata. WVB basin development and volcanism initiated in western Canada during northward translation of the Yakutat terrane along orogen-parallel, northwest-

Figure 22. Paleogeographic sketch maps (A–D) showing inferred links between Wrangell volcanic belt volcanism and basin development, subduction of the Yakutat microplate, and right-lateral displacement along strike-slip faults. Sedimentary basins (yellow): BL—Bates Lake, BW—Burwash, FB—Frederika, SH—Sheep Creek (in A), TG—Three Guardsmen. Volcanic centers (red): SC—Saint Clare (in B), NC—Nines Creek, AL—Alsek, ST—Stanley. Accreted terranes: WCT—Wrangellia composite, YCT—Yukon composite. Faults: CPT—Chugach-Prince William terranes, CSF—Chugach–Saint Elias, FF—Fairweather, CF—Totschunda-Fairweather connector, TF—Totschunda. Plate motion: P-NA—Pacific–North America, WW—Western Wrangell volcanic belt. Refer to text for discussion.
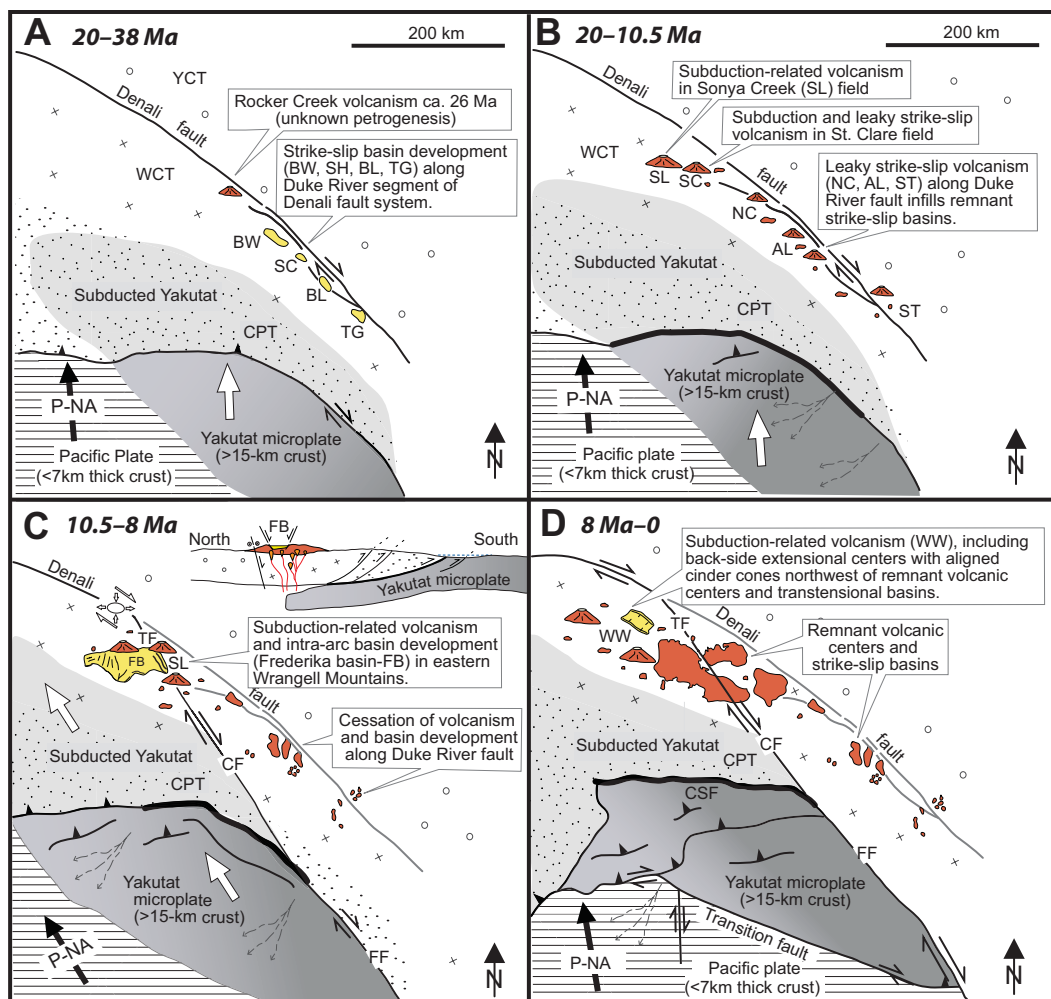
striking strike-slip faults. Volcanism and basin development shifted northwestward into eastern Alaska in response to insertion of progressively thicker crust into the southern Alaska plate corner synchronous with a shift in plate motions to more northwestward-directed convergence. Volcanism persists today in the westernmost WVB above a weakly imaged north-dipping subducted slab along the northeastern edge of the subducted portion of the Yakutat microplate. The stratigraphic, geochemical, and geochronologic attributes of the WVB and their links to regional tectonic elements in southern Alaska contribute to our growing understanding of the complex processes responsible for crustal accretion and recycling. In particular, WVB strata offer an exceptional example of diachronous volcanism, basin development, and deformation associated with subduction of thickened oceanic crust into a syntaxial plate margin characterized by a spatial transition from strike-slip deformation to shallow-slab subduction. Our analysis highlights the importance of integrated

multidisciplinary data sets to distinguish ancient stratigraphic successions associated with slab-edge volcanism and deformation generated by subduction-collision of thickened oceanic crust along a syntaxial plate margin from volcanic-arc complexes produced by subduction of typical oceanic crust.

APPENDIX 1.

U/Pb Geochronology Methods

We completed 107 zircon U/Pb sensitive high-resolution ion microprobe (SHRIMP) analyses from 2 tuff samples and 2 sandstone samples. (Refer to Supplemental Tables 1 and 2 [see footnotes 5 and 6] for U-Th-Pb data for all analyses.) Zircons were separated using standard sample-preparation methods, and U/Pb SHRIMP analyses, data reduction and plotting using Squid and Isoplot, respectively (Ludwig, 2006). No morphologic or color differentiation was made during hand-picking for the sample mount. Zircon mounts were examined through scanning electron microscope-cathodoluminescent imaging to detect structures correlated with zircon trace element concentrations. U-Th-Pb isotopic ratios and elemental abundance of zircon grains were determined by Trop

at the Stanford-U.S. Geological Survey Microisotopic Analytical Center using the reverse geometry SHRIMP, following standard operating procedures. The primary beam spot size was 20–40 μm in diameter, and the spot was placed over the middle of the grain, avoiding cracks, inclusions, and broken edges of grain fragments. Analyses consisted of 4–6 scans through each isotope mass, counting 2 s on Zr_2O, 7 s on background, 12 s on ^{206}Pb, 16 s on ^{207}Pb, 10 s on ^{208}Pb, 5 s on ^{238}U, 3 s on $^{248}(ThO)$, and 3 s on $^{254}(UO)$. Pb/U ratios were calibrated with reference to standard zircon R33, which was analyzed after every fourth or fifth analysis of an unknown zircon. Reported ages are based on $^{204}Pb/^{206}Pb$-corrected $^{206}/^{238}U$ ratios because errors of the $^{207}Pb/^{235}Ua$ and $^{206}Pb/^{207}Pb$ ratios are significantly greater. The $^{206}Pb/^{207}Pb$ ages for these Paleozoic–Cenozoic zircon grains are less reliable, given the relatively low concentration of ^{207}Pb. The Pb/U ratios were calibrated with reference standard zircon R33 (419 Ma), which was analyzed after every fourth or fifth unknown analysis.

$^{40}Ar/^{39}Ar$ Geochronology Methods

Ages for 12 basalt samples were determined by the $^{40}Ar/^{39}Ar$ method at Lehigh University (Bethlehem, Pennsylvania). Plagioclase phenocrysts were separated for dating from seven samples, and ground-

mass material was prepared from five aphanitic lavas that exhibit relatively little evidence of alteration and interstitial glass. Olivine and pyroxene phenocrysts were removed from the groundmass separates prior to irradiation in order to reduce trapped ^{40}Ar contamination. The samples were irradiated two batches. Samples BK1–654, CHM-38, CHM-39, FDN-3, FDN-8, SKO-3, SKO-16, and SKO-28A were irradiated in position 5C of the McMaster University reactor for 6 h. The Oregon State University (OSU) TRIGA reactor was used for samples 57–6877, CHM-4, MGA-1, NZM-66, and PIL-335, which were subjected to a 10 h irradiation in the CLICIT (cadmium-lined, in-core irradiation tube) facility. The neutron flux within the irradiation containers was monitored with GA1550 biotite (98.79 ± 0.54 Ma; Renne et al., 1998). CaF_2 and K_2SO_4 were also included in the irradiation packages to monitor neutron-induced interferences from Ca and K, respectively.

Argon was extracted from the samples by stepwise heating in a double-vacuum resistance furnace, and purified using a cold finger cooled to liquid nitrogen temperature and two SAES ST101 getters. The analyses were performed with a VG3600 noble gas mass spectrometer equipped with an electron multiplier operated in the pulse-counting mode. The mass spectrometer sensitivity during the dating experiments was $\sim1.154 \times 10^{-19}$ mol/count/second ^{40}Ar. Extraction line blanks were typically $\sim2.5 \times 10^{-15}$ mol ^{40}Ar at 1350 °C and $<1 \times 10^{-15}$ mol ^{40}Ar at temperatures <1000 °C, and were approximately atmospheric in composition. The isotopic data were corrected for extraction line blank, mass spectrometer background, mass discrimination, radioactive decay of ^{37}Ar and ^{39}Ar, neutron-induced interferences, and atmospheric contamination prior to calculation of the ages. The neutron interference correction factors determined for the McMaster irradiation were $(^{36}Ar/^{37}Ar)_{Ca} = 0.000280$, $(^{39}Ar/^{37}Ar)_{Ca} = 0.000699$, and $(^{40}Ar/^{39}Ar)_K = 0.026$; for the OSU irradiation the corrections were $(^{36}Ar/^{37}Ar)_{Ca} = 0.000264$, $(^{39}Ar/^{37}Ar)_{Ca} = 0.000680$, and $(^{40}Ar/^{39}Ar)_K = 0.00075$. Mass discrimination ranged from 0.06 to 0.19%/atomic mass units over the course of the experiments (average measured atmospheric $^{40}Ar/^{36}Ar = 296.26 \pm 0.75\%$ for the McMaster samples and $297.76 \pm 0.23\%$ for the OSU samples). Ages were calculated using the decay constants and isotopic abundances of Steiger and Jager (1977). A complete tabulation of the analytical data is presented in Supplemental Table 3 (see footnote 7).

The final results of the dating experiments are summarized in Table 2. We report plateau ages for 8 samples yielding acceptable plateaus and atmospheric trapped $^{40}Ar/^{36}Ar$. These plateau ages are the inverse-error weighted mean ages of contiguous steps that compose 50% or more of the gas released from a sample and define individual ages statistically indistinguishable from the weighted mean at the 2σ analytical error level. Inverse isochron ages are reported for samples FDN-8, MGA-2, NZM-66, and SKO-28A, which contain trapped argon of nonatmospheric composition. The isochron ages were determined by regressing blank-corrected isotope data using the method of York (1968).

REFERENCES CITED

Aleinikoff, J.N., Plafker, G., and Nokleberg, W.J., 1988, Middle Pennsylvanian plutonic rocks along the southern margin of Wrangellia, *in* Hamilton, T.D., and Galloway, J.P., eds., The U.S. Geological Survey in Alaska: Accomplishments during 1987: U.S. Geological Survey Circular 1016, p. 110–113.

Amato, J., and Pavlis, T.L., 2010, Detrital zircon ages from the Chugach terrane, southern Alaska, reveal multiple episodes of accretion and erosion in a subduction complex: Geology, v. 38, p. 459–462, doi:10.1130/G30719.1.

Bassett, K.N., and Busby, C.J., 2005, Tectonic setting of the Glance Conglomerate along the Sawmill Canyon fault zone, southern Arizona: A sequence analysis of an intra-arc strike-slip basin, *in* Anderson, T.H., et al., eds., The Mojave-Sonora megashear hypothesis: Development, assessment, and alternatives: Geological Society of America Special Paper 393, p. 377–400, doi:10.1130/0-8137-2393-0.377.

Bellier, O., and Sebrier, M., 1994, Relationship between tectonism and volcanism along the Great Sumatran fault system deduced from SPOT image analyses: Tectonophysics, v. 233, p. 215–231, doi:10.1016/0040-1951(94)90242-9.

Benowitz, J.A., Layer, P., Armstrong, P., Perry, S., Haeussler, P., Fitzgerald, P., and VanLaningham, S., 2011, Spatial variations in focused exhumation along a continental-scale strike-slip fault: The Denali fault of the eastern Alaska Range: Geosphere, v. 7, p. 455–467, doi:10.1130/GES00589.1.

Berger, A.L., Gulick, S.P.S., Spotila, J.A., Upton, P., Jaeger, J.M., Chapman, J.B., Worthington, L.A., Pavlis, T.L., Ridgway, K.D., Willems, B.A., and McAleer, R.J., 2008a, Quaternary tectonic response to intensified glacial erosion in an orogenic wedge: Nature Geoscience, v. 1, p. 793–799, doi:10.1038/ngeo334.

Berger, A.L., Spotila, J.A., Chapman, J.B., Pavlis, T.L., Enkelmann, E., Ruppert, N.A., and Buscher, J.T., 2008b, Architecture, kinematics, and exhumation of a convergent orogenic wedge: A thermochronological investigation of tectonic-climatic interactions within the central Saint Elias orogen, Alaska: Earth and Planetary Science Letters, v. 270, p. 13–24, doi:10.1016/j.epsl.2008.02.034.

Berry, E.W., 1928, Paleontological report on F.H. Moffit's fossil collections 27AM-F16 (U.S.G.S. locality 4042) and 27AM-F20 (U.S.G.S. locality 7905): U.S. Geological Survey Paleontological Report, p. 5452–5455.

Blair, T.C., and Bilodeau, W.L., 1988, Development of tectonic cyclothems in rift, pull-apart, and foreland basins: Sedimentary response to episodic tectonism: Geology, v. 16, p. 517–520, doi:10.1130/0091-7613(1988)016<0517:DOTCIR>2.3.CO;2.

Borg, L.E., Clynne, M.A., and Bullen, T.D., 1997, The variable role of slab-derived fluids in the generation of a suite of primitive calc-alkaline lavas from the southernmost Cascades, California: Canadian Mineralogist, v. 35, p. 425–452.

Breitsprecher, K., and Mortensen, J.K., 2004a, BCAge 2004A–1a; A database of isotopic age determinations for rock units from British Columbia: British Columbia Ministry of Energy and Mines, British Columbia Geological Survey, Open-File 2004–3 (Release 3.0).

Breitsprecher, K., and Mortensen, J.K., 2004b, YukonAge 2004; A database of isotopic age determinations for rock units from Yukon Territory: Yukon Geological Survey, Department of Energy, Mines and Resources, Government of Yukon, CD-ROM.

Bru<seke, M.E., and Hart, W.K., 2008, Geology and petrology of the mid-Miocene Santa Rosa–Calico Volcanic Field, northern Nevada: Nevada Bureau of Mines and Geology Bulletin 113, 48 p., http://www.nbmg.unr.edu/dox/dox.htm.

Bruhn, R.L., Pavlis, T.L., Plafker, G., and Serpa, L., 2004, Deformation during terrane accretion in the Saint Elias orogen, Alaska: Geological Society of America Bulletin, v. 116, p. 771–787, doi:10.1130/B25182.1.

Busby, C.J., and Bassett, K.N., 2007, Volcanic facies architecture of an intra-arc strike-slip basin, Santa Rita Mountains, southern Arizona: Bulletin of Volcanology, v. 70, p. 85–103, doi:10.1007/s00445-007-0122-9.

Busby, C.J., Bassett, K.N., Steiner, M.B., and Riggs, N.R., 2005, Climatic and tectonic controls on Jurassic intra-arc basins related to northward drift of North America, *in* Anderson, T.H., et al., eds., The Mojave-Sonora megashear hypothesis: Development, assessment, and alternatives: Geological Society of America Special Paper 393, p. 359–376, doi:10.1130/0-8137-2393-0.359.

Carlson, D.H., and Moye, F.J., 1990, The Colville igneous complex: Paleogene volcanism, plutonism, and extension in northeastern Washington, *in* Anderson, J.L., ed., The nature and origin of Cordilleran magmatism: Geological Society of America Memoir 174, p. 375–394.

Carlson, R.W., and Hart, W.K., 1987, Crustal genesis on the Oregon Plateau: Journal of Geophysical Research, v. 92, p. 6191–6206, doi:10.1029/JB092iB07p06191.

Cas, R.A.F., and Wright, J.V., 1987, Volcanic successions, modern and ancient: A geological approach to processes products and successions: Chapman, London, 544 p.

Chapman, J.B., and 14 others, 2008, Neotectonics of the Yakutat collision: Changes in deformation driven by mass redistribution, *in* Freymueller, J.T. et al., eds., Active tectonics and seismic potential of Alaska: American Geophysical Union Geophysical Monograph 179, p. 65–82, doi:10.1029/GM179.

Christeson, G.L., Gulick, S.P.S., Van Avendonk, H.J.A., Worthington, L.L., Reece, R.S., and Pavlis, T.L., 2010, The Yakutat terrane: Dramatic change in crustal thickness across the Transition fault, Alaska: Geology, v. 38, p. 895–898, doi:10.1130/G31170.1.

Clague, J.J., Evans, S.G., Rampton, V.N., and Woodsworth, G.J., 1995, Improved age estimates for the White River and Bridge River tephras, western Canada: Canadian Journal of Earth Sciences, v. 32, p. 1172–1179, doi:10.1139/e95-096.

Cole, J.W., and Lewis, K.B., 1981, Evolution of the Taupo-Hikurangi subduction system: Tectonophysics, v. 72, p. 1–21, doi:10.1016/0040-1951(81)90084-6.

Cole, R.B., and Ridgway, K.D., 1993, The influence of volcanism on fluvial depositional systems in a Cenozoic strike-slip basin, Denali fault system, Yukon Territory, Canada: Journal of Sedimentary Petrology, v. 63, p. 152–166, doi:10.1306/D4267AB4-2B26-11D7-8648000102C1865D.

Cole, R.B., Nelson, S.W., Layer, P.W., and Oswald, P., 2006, Eocene volcanism above a depleted slab window in southern Alaska: Geological Society of America Bulletin, v. 118, p. 140–158, doi:10.1130/B25658.1.

Collinson, J.D., 1996, Alluvial sediments, *in* Reading, H.G., ed., Sedimentary environments: Processes, facies, and stratigraphy: Oxford, Blackwell Science, p. 37–82.

Condit, C.D., and Connor, C.B., 1996, Recurrence rates of volcanism in basaltic volcanic fields: An example from the Springerville volcanic field, Arizona: Geological Society of America Bulletin, v. 108, p. 1225–1241, doi:10.1130/0016-7606(1996)108<1225:RROVIB>2.3.CO;2.

Critelli, S., and Ingersoll, R.V., 1995, Interpretation of neovolcanic versus palaeovolcanic sand grains: An example from Miocene deep-marine sandstone of the Topanga Group (Southern California): Sedimentology, v. 42, p. 783–804, doi:10.1111/j.1365-3091.1995.tb00409.x.

Defant, M.J., Richerson, P.M., De Boer, J.Z., Stewart, R.H., Maury, R.C., Bellon, H., Drummond, M.S., Feigenson, M.D., and Jackson, T.E., 1991, Dacite genesis via both slab melting and differentiation: petrogenesis of La Yeguada Volcanic Complex, Panama: Journal of Petrology, v. 32, p. 1101–1142, doi:10.1093/petrology/32.6.1101.

Delaney, M.R., 2006, A stratigraphic study of the Miocene Frederika Formation, Wrangell–Saint Elias Mountains, south-central Alaska [B.S. thesis]: Lewisburg, Pennsylvania, Bucknell University, 52 p.

Denton, G.H., and Armstrong, R.L., 1969, Miocene-Pliocene glaciations in southern Alaska: American Journal of Science, v. 267, p. 1121–1142.

Dickinson, W.R., 1970, Interpreting detrital modes of greywacke and arkose: Journal of Sedimentary Petrology, v. 40, p. 695–707, doi:10.1306/74D72018-2B21-11D7-8648000102C1865D.

Dickinson, W.R., 1985, Interpreting provenance relations from detrital modes of sandstones, *in* Zuffa, G.G., ed., Provenance of arenites: Dordrecht, Netherlands, Reidel, p. 333–361.

Doser, D.I., and Lomas, R., 2000, The transition from strike-slip to oblique subduction in southeastern Alaska from seismological studies: Tectonophysics, v. 316, p. 45–65, doi:10.1016/S0040-1951(99)00254-1.

Drummond, M.S., Defant, M.J., and Kepezhinskas, P.K., 1996, Petrogenesis of slab-derived trondhjemite-tonalite-dacite/adakite magmas: Royal Society of Edinburgh Transactions, Earth Sciences, v. 87, p. 205–215, doi:10.1017/S0263593300006611.

Dusel-Bacon, C., and Williams, I.S., 2009, Evidence for prolonged mid-Paleozoic plutonism and ages of crustal sources in east-central Alaska from SHRIMP U/Pb dating of syn-magmatic, inherited, and detrital zircon: Canadian Journal of Earth Sciences, v. 46, p. 21–39, doi:10.1139/E09-005.

Eberhart-Phillips, D., and 28 others, 2003, The 2002 Denali fault earthquake, Alaska: A large magnitude, slip-partitioned event: Science, v. 300, p. 1113–1118, doi:10.1126/science.1082703.

Eberhart-Phillips, D., Christensen, D.H., Brocher, T.M., Hansen, R., Ruppert, N.A., Haeussler, P.J., and Abers, G.A., 2006, Imaging the transition from Aleutian subduction to Yakutat collision in central Alaska with local earthquakes and active source data: Journal of Geophysical Research, v. 111, B11303, doi:10.1029/2005JB004240.

Enkelmann, E., Garver, J.I., and Pavlis, T.L., 2008, Rapid exhumation of ice-covered rocks of the Chugach–Saint Elias orogen, southeast Alaska: Geology, v. 36, p. 915–918, doi:10.1130/G2252A.1.

Enkelmann, E., Zeitler, P.K., Pavlis, T.L., Garver, J.I., and Ridgway, K.D., 2009, Intense localized rock uplift and erosion in the Saint Elias orogen of Alaska: Nature Geoscience, v. 2, p. 360–363, doi:10.1038/ngeo502.

Enkelmann, E., Zeitler, P.K., Garver, J.I., Pavlis, T.L., and Hooks, B.P., 2010, The thermochronological record of tectonic and surface process interaction at the Yakutat–North American collision zone in southeast Alaska: American Journal of Science, v. 310, p. 231–260, doi:10.2475/04.2010.01.

Eyles, C.H., and Eyles, N., 1989, The upper Cenozoic White River "tillites" of southern Alaska: Subaerial slope and fan-delta deposits in a strike-slip setting: Geological Society of America Bulletin, v. 101, p. 1091–1102, doi:10.1130/0016-7606(1989)101<1091:TUCWRT>2.3.CO;2.

Eyles, N., and Kocsis, S., 1988, Sedimentology and clast fabric of subaerial debris flow facies in a glacially influenced alluvial fan: Sedimentary Geology, v. 59, p. 15–28, doi:10.1016/0037-0738(88)90098-X.

Ferris, A., Abers, G.A., Christensen, D.H., and Veenstra, E., 2003, High resolution image of the subducted Pacific plate beneath central Alaska, 50–150 km depth: Earth and Planetary Science Letters, v. 214, p. 575–588, doi:10.1016/S0012-821X(03)00403-5.

Fisher, R.V., and Schmincke, H.U., 1984, Pyroclastic rocks: Berlin, Springer-Verlag, 472 p.

Finzel, E.S., Trop, J.M., and Ridgway, K.D., 2011, Upper-plate proxies for flat-slab subduction processes in southern Alaska: Earth and Planetary Science Letters, v. 303, p. 348–360, doi:10.1016/j.epsl.2011.01.014.

Foster, H.L., Keith, T.E.C., and Menzie, W.D., 1994, Geology of the Yukon-Tanana area of east-central Alaska, *in* Plafker, G., and Berg, H.C., eds., The geology of Alaska: Boulder, Colorado, Geological Society of America, The geology of North America, v. G-1, p. 205–240.

Freundt, A., Wilson, C.J.N., and Carey, S.N., 2000, Ignimbrites and block-and-ash flow deposits, *in* Sigurdsson, H., et al., eds., Encyclopedia of volcanoes: San Diego, California, Academic Press, p. 581–600.

Fuis, G.S., and 13 others, 2008, Trans-Alaska crustal transect and continental evolution involving subduction underplating and synchronous foreland thrusting: Geology, v. 36, p. 267–270, doi:10.1130/G24257A.1.

Gardner, M.C., Bergman, S.C., Cushing, G.W., MacKevett, E.M., Plafker, G., Campbell, R.B., Dodds, C.J., McClelland, W.C., and Mueller, P.A., 1988, Pennsylvanian pluton stitching of Wrangellia and the Alexander terrane, Wrangell Mountains, Alaska: Geology, v. 16, p. 967–971, doi:10.1130/0091-7613(1988)016<0967:PPSOWA>2.3.CO;2.

Geist, E.L., Childs, J.R., and Scholl, D.W., 1988, The origin of summit basins of the Aleutian Ridge: Implications for block rotation of an arc massif: Tectonics, v. 7, p. 327–341, doi:10.1029/TC007i002p00327.

Gradstein, F.M., Ogg, J.G., and Smith, A.G., 2004, A geologic time scale 2004: London, Cambridge University Press, 610 p.

Gulick, S.P., Lowe, L.A., Pavlis, T.L., Gardner, J.V., and Mayer, L.A., 2007, Geophysical insights into the Transition fault debate: Propagating strike slip in response to stalling Yakutat block subduction in the Gulf of Alaska: Geology, v. 35, p. 763–766, doi:10.1130/G23585A.1.

Gutscher, M.-A., Maury, R., Eissen, J.-P., and Bourdon, E., 2000, Can slab melting be caused by flat subduction?: Geology, v. 28, p. 535–538, doi:10.1130/0091-7613(2000)28<535:CSMBCB>2.0.CO;2.

Hampton, B.A., Ridgway, K.D., and Gehrels, G.E., 2010, A detrital record of Mesozoic island arc accretion and exhumation in the North American Cordillera: U-Pb geochronology of the Kahiltna basin, southern Alaska: Tectonics, v. 29, doi:10.1029/2009TC002544.

Haeussler, P.J., 2008, An overview of the neotectonics of interior Alaska: Far-field deformation from the Yakutat microplate collision, *in* Freymueller, J.T., et al., eds., Active tectonics and seismic potential of Alaska: American Geophysical Union Geophysical Monograph 179, p. 269–285, doi:10.1029/GM179.

Ingersoll, R.V., Bullard, T.F., Ford, R.L., Grimm, J.P., Pickle, J.D., and Sares, S.W., 1984, The effect of grain size on detrital modes: A test of the Gazzi-Dickinson point-counting method: Journal of Sedimentary Petrology, v. 54, p. 103–116, doi:10.1306/212F83B9-2B24-11D7-8648000102C1865D.

Israde-Alcantara, I., and Garduno-Monrov, V.H., 1999, Lacustrine record in a volcanic-arc setting: The evolution of the late Neogene Cuitzeo basin system (central-western Mexico, Michoacan): Palaeogeography, Palaeoclimatology, Palaeoecology, v. 151, p. 209–227, doi:10.1016/S0031-0182(99)00024-3.

Israel, S., and Cobbett, R., 2008, Kluane Ranges bedrock geology, White River area (Parts of NTS 115F/9, 15 and 16; 115G/12 and 115K/1, 2), *in* Emond, D.S., et al., eds., Yukon exploration and geology 2007: Yukon Geological Survey, Exploration and Geological Services Division, Yukon Region, Indian and Northern Affairs Canada, p. 153–167.

Israel, S., Tizzard, A., and Major, J., 2006, Bedrock geology of the Duke River area, parts of NTS 115G/2, 3, 4, 6, and 7, southwestern Yukon, *in* Emond, D.S., et al., eds., Yukon exploration and geology 2005: Yukon Geological Survey, Exploration and Geological Services Division, Yukon Region, Indian and Northern Affairs Canada, p. 139–154.

Janecke, S.U., Hammond, B.F., Snee, L.W., and Geissman, J.W., 1997, Rapid extension in an Eocene volcanic arc: Structure and paleogeography of an intra-arc half graben in central Idaho: Geological Society of America Bulletin, v. 109, p. 253–267, doi:10.1130/0016-7606(1997)109<0253:REIAEV>2.3.CO;2.

Jarrard, R.D., 1986, Relations among subduction parameters: Reviews of Geophysics, v. 24, p. 217–284, doi:10.1029/RG024i002p00217.

Johnson, C.L., and Graham, S.A., 2004, Cycles in perilacustrine facies of late Mesozoic rift basins, southeastern Mongolia: Journal of Sedimentary Research, v. 74, p. 786–804, doi:10.1306/051304740786.

Kalbas, J.L., Freed, A.M., and Ridgway, K.D., 2008, Contemporary fault mechanics in southern Alaska, *in* Freymueller, J.T. et al., eds., Active tectonics and seismic potential of Alaska: American Geophysical Union Geophysical Monograph 179, p. 321–336, doi:10.1029/GM179.

Katoh, S., Danhara, T., Hart, W.K., and WoldeGabriel, G., 1999, Use of sodium polytungstate solution in the purification of volcanic glass shards for bulk chemical analysis: Nature and Human Activities, v. 4, p. 45–54.

Kochelek, E.J., Amato, J.M., Pavlis, T.L., and Clift, P.D., 2011, Flysch deposition and preservation of coherent bedding in an accretionary complex, detrital zircon ages from the Upper Cretaceous Valdez Group, Chugach terrane, Alaska: Lithosphere, v. 3, p. 265–274, doi:10.1130/L131.1.

Koons, P.O., Hooks, B.P., Pavlis, T., Upton, P., and Barker, A.D., 2010, Three-dimensional mechanics of Yakutat convergence in the southern Alaskan plate corner: Tectonics, v. 29, TC4008, doi:10.1029/2009TC002463.

Lagoe, M.B., Eyles, C.H., Eyles, N., and Hale, C., 1993, Timing of late Cenozoic tidewater glaciation in the far North Pacific: Geological Society of America Bulletin, v. 105, p. 1542–1560, doi:10.1130/0016-7606(1993)105<1542:TOLCTG>2.3.CO;2.

Le Bas, M.J., Le Maitre, R.W., Streckeisen, A., and Zanettin, B., 1986, A chemical classification of volcanic rocks based on the total alkali-silica diagram: Journal of Petrology, v. 27, p. 745–750, doi:10.1093/petrology/27.3.745.

Lee, H.Y., Chung, S.L., Yang, H.M., Chu, C.H., Lo, C.H., and Mitchell, A.H.G., 2010, Age and geochemical constraints on the petrogenesis of late Cenozoic volcanism in Myanmar, *in* Abstracts with Programs, Tectonic Crossroads: Evolving Orogens of Eurasia–Africa–Arabia, Ankara, Turkey, October 2010: Boulder, Colorado, Geological Society of America, p. 53.

Leonard, L.J., Hyndman, R.D., Mazzotti, S., Nykolaishen, L., Schmidt, M., and Hippchen, S., 2007, Current deformation in the northern Canadian Cordillera inferred from GPS measurements: Journal of Geophysical Research, v. 112, doi:10.1029/2007JB005061.

Ludwig, K.R., 2006, Isoplot 3.7: Berkeley, California, Berkeley Geochronology Center Special Publication.

Lunt, I.A., and Bridge, J.S., 2004, Evolution and deposits of a gravelly braid bar, Sagavanirktok River, Alaska: Sedimentology, v. 51, p. 415–432, doi:10.1111/j.1365-3091.2004.00628.x.

MacKevett, E.M., Jr., 1970a, Geologic map of the McCarthy C-4 quadrangle: U.S. Geological Survey Geologic Quadrangle Map GQ-0844, scale 1:63,360.

MacKevett, E.M., Jr., 1970b, Geologic map of the McCarthy C-5 quadrangle: U.S. Geological Survey Geologic Quadrangle Map GQ-0899, scale 1:63,360.

MacKevett, E.M., Jr., 1978, Geologic map of the McCarthy quadrangle, Alaska: U.S. Geological Survey Miscellaneous Investigation Series I-1032, scale 1:250,000.

Makaske, B., 2001, Anastomosing rivers: A review of their classification, origin, and sedimentary products: Earth-Science Reviews, v. 53, p. 149–196, doi:10.1016/S0012-8252(00)00038-6.

Manuszak, J.D., Ridgway, K.D., Trop, J.M., and Gehrels, G.E., 2007, Sedimentary record of the tectonic growth of a collisional continental margin: Upper Jurassic–Lower Cretaceous Nutzotin Mountains sequence, eastern Alaska Range, Alaska, *in* Ridgway, K.D., et al., eds., Tectonic growth of a collisional continental margin: Crustal evolution of southern Alaska: Geological Society of America Special Paper 431, p. 345–377, doi:10.1130/2007.2431(14).

Matmon, A., Schwartz, D.P., Haeussler, P.J., Lienkaemper, J.J., Stenner, H.D., and Dawson, T.E., 2006, Denali fault slip rates and Holocene–late Pleistocene kinematics of central Alaska: Geology, v. 34, p. 645–648, doi:10.1130/G22361.1.

Maury, R.C., Pubellier, M., Rangin, C., Wulput, L., Cotton, J., Socquet, A., Bellon, H., Gullaud, J.P., and Htun, H.M., 2004, Quaternary calc-alkaline and alkaline vol-

canism in a hyper-oblique convergence setting, central Myanmar and western Yunnan: Bulletin de la Société Géologique de France, v. 175, p. 461–472, doi:10.2113/175.5.461.

McAleer, R.J., Spotila, J.A., Enkelmann, E., and Berger, A.L., 2009, Exhumation along the Fairweather fault, southeastern Alaska, based on low-temperature thermochronometry: Tectonics, v. 28, doi:10.1029/2007TC002240.

McCabe, P.J., 1984, Depositional environments of coal and coal-bearing strata, *in* Rahmani, R.A., and Flores, R.M., eds., Sedimentology of coal and coal-bearing sequences: International Association of Sedimentologists Special Publication 7, p. 13–42.

McCabe, P.J., 1991, Geology of coal; environments of coal deposition, *in* Gluskoter, H.J., et al., eds., Economic Geology: U.S.: Boulder, Colorado, Geological Society of America, The Geology of North America, v. P-2, p. 469–482.

McCaffrey, R., 1992, Oblique plate convergence, slip vectors, and forearc deformation: Journal of Geophysical Research, v. 97, p. 8905–8915, doi:10.1029/92JB00483.

Meigs, A., Johnston, S., Garver, J., and Spotila, J., 2008, Crustal-scale structural architecture, shortening, and exhumation of an active eroding orogenic wedge (the Chugach/Saint Elias Range, southern AK): Tectonics, v. 27, doi:10.1029/2007TC002168.

Melchor, R.N., 2007, Changing lake dynamics and sequence stratigraphy of synrift strata in a half-graben: An example from the Triassic Ischigualasto–Villa Union Basin, Argentina: Sedimentology, v. 54, p. 1417–1446, doi:10.1111/j.1365-3091.2007.00887.x.

Miall, A.D., 1978, Lithofacies types and vertical profile models in braided river deposits: A summary, *in* Miall, A.D., ed., Fluvial Sedimentology: Canadian Society of Petroleum Geologists Memoir 5, p. 597–604.

Miall, A.D., 2006, The Geology of Fluvial Deposits: Berlin, Springer, 582 p.

Miller, T.P., and Richter, D.H., 1994, Quaternary volcanism in the Alaska Peninsula and Wrangell Mountains, Alaska, *in* Plafker, G., and Berg, H.C., eds., The Geology of Alaska: Boulder, Colorado, Geological Society of America, The Geology of North America, v. G-1, p. 759–779.

Miyashiro, A., 1974, Volcanic rock series in island arcs and active continental margins: American Journal of Science, v. 274, p. 321–355, doi:10.2475/ajs.274.4.321.

Morozova, G.S., and Smith, N.D., 1999, Holocene avulsion history of the lower Saskatchewan fluvial system, Cumberland Marshes, Saskatchewan-Manitoba, Canada, *in* Smith, N.D., and Rogers, J., eds., Fluvial sedimentology 6: International Association of Sedimentologists Special Publication 28, p. 231–249, doi:10.1002/9781444304213.ch18.

Nadon, G.C., 1994, The genesis and recognition of anastomosed fluvial deposits: Data from the Saint Mary River Formation, southwestern Alberta, Canada: Journal of Sedimentary Research, v. B64, p. 451–463, doi:10.1306/D4267FE1-2B26-11D7-8648000102C1865D.

Nokleberg, W.J., Plafker, G., and Wilson, F.H., 1994, Geology of south-central Alaska, *in* Plafker, G., and Berg, H.C., eds., The Geology of Alaska: Boulder, Colorado, Geological Society of America, The Geology of North America, v. G-1, p. 311–365.

Page, R.A., Stephens, C.D., and Lahr, J.C., 1989, Seismicity of the Wrangell and Aleutian Wadati-Benioff zones and the North American plate along the Trans-Alaska Crustal Transect, Chugach Mountains and Copper River Basin, southern Alaska: Journal of Geophysical Research, v. 94, p. 16,059–16,082, doi:10.1029/JB094iB11p16059.

Page, R.A., Biswas, N.N., Lahr, J.C., and Hulpan, H., 1991, Seismicity of continental Alaska, *in* Slemmons, D.B., et al., eds., Neotectonics of North America: Geological Society of America, Decade of North America map volume 1, p. 47–68.

Pavlis, T.L., and Roeske, S.M., 2007, The Border Ranges fault system, southern Alaska, *in* Ridgway, K.D., et al., eds., Tectonic Growth of a Collisional Continental Margin: Crustal Evolution of Southern Alaska: Geological Society of America Special Paper 431, p. 95–127, doi:10.1130/2007.2431(05).

Pavlis, T.L., Picornell, C., Serpa, L., Bruhn, R.L., and Plafker, G., 2004, Tectonic processes during oblique collision: Insights from the Saint Elias orogen, northern North American Cordillera: Tectonics, v. 23, doi:10.1029/2003TC001557.

Perry, S.E., Garver, J.I., and Ridgway, K.D., 2009, Transport history of the Yakutat terrane: Evidence from sediment petrology and detrital zircon fission-track and U/Pb double dating: Journal of Geology, v. 117, p. 156–173, doi:10.1086/596302.

Pierson, T.C., and Scott, K.M., 1985, Downstream dilution of a lahar: Transition from debris flow to hyperconcentrated streamflow: Water Resources Research, v. 21, p. 1511–1524, doi:10.1029/WR021i010p01511.

Pietras, J.T., and Carroll, A.R., 2006, High-resolution stratigraphy of an underfilled lake basin: Wilkins Peak Member, Eocene Green River Formation, Wyoming, U.S.A.: Journal of Sedimentary Research, v. 76, p. 1197–1214, doi:10.2110/jsr.2006.096.

Plafker, G., 1987, Regional geology and petroleum potential of the northern Gulf of Alaska continental margin: Geology and resource potential of the continental margin of western North America and adjacent ocean basins, Beaufort Sea to Baja California: Circum-Pacific Council for Energy and Mineral Resources Earth Science Series, v. 6, p. 229–268.

Plafker, G., Hudson, T., and Richter, D.H., 1977, Preliminary observations on late Cenozoic displacements along the Totschunda and Denali fault systems, *in* Blean, K.M., ed., The United States Geological Survey in Alaska; Accomplishments during 1976: U.S. Geological Survey Circular 751B, p. B67–B69.

Plafker, G., Moore, J.C., and Winkler, G.R., 1994, Geology of the southern Alaska margin, *in* Plafker, G., and Berg, H.C., eds., The Geology of Alaska: Boulder, Colorado, Geological Society of America, The Geology of North America, v. G-1 p. 389–450.

Platt, N.H., 1989, Lacustrine carbonates and pedogenesis: Sedimentology and origin of palustrine deposits from the Early Cretaceous Rupelo Formation, W. Cameros Basin, N. Spain: Sedimentology, v. 36, p. 665–684, doi:10.1111/j.1365-3091.1989.tb02092.x.

Polliand, M., Schaltegger, U., Frank, M., and Fontebote, L., 2005, Formation of intra-arc volcanosedimentary basins in the western flank of the central Peruvian Andes during Late Cretaceous oblique subduction: Field evidence and constraints from U-Pb ages and Hf isotopes: International Journal of Earth Sciences, v. 94, p. 231–242, doi:10.1007/s00531-005-0464-5.

Postma, G., 1984, Mass flow conglomerates in a submarine canyon, Abrioja fan-delta, Pliocene, southeast Spain, *in* Koster, E.H., and Steel, R.J., eds., Sedimentology of gravels and conglomerates: Canadian Society of Petroleum Geologists Memoir 10, p. 237–258.

Preece, S.J., and Hart, W.K., 2004, Geochemical variations in the <5 Ma Wrangell Volcanic Field, Alaska: Implications for the magmatic and tectonic development of a complex continental arc system: Tectonophysics, v. 392, p. 165–191, doi:10.1016/j.tecto.2004.04.011.

Qi, C., Zhao, D.P., and Chen, Y., 2007, Search for deep slab segments under Alaska: Physics of the Earth and Planetary Interiors, v. 165, p. 68–82, doi:10.1016/j.pepi.2007.08.004.

Renne, P.R., Swisher, C.C., Deino, A.L., Karner, D.B., Owens, T.L., and DePaolo, D.J., 1998, Intercalibration of standards, absolute ages and uncertainties in ⁴⁰Ar-³⁹Ar dating: Chemical Geology, v. 145, p. 117–152, doi:10.1016/S0009-2541(97)00159-9.

Richter, D.H., 1976, Geologic map of the Nabesna quadrangle, Alaska: U.S. Geological Survey Miscellaneous Geological Investigations Series Map I-932, scale 1:250,000.

Richter, D.H., and Matson, N.A., Jr., 1971, Quaternary faulting in the eastern Alaska Range: Geological Society of America Bulletin, v. 82, p. 1529–1540, doi:10.1130/0016-7606(1971)82[1529:QFITEA]2.0.CO;2.

Richter, D.H., Lanphere, M.A., and Matson, N.A., Jr., 1975, Granitic plutonism and metamorphism, eastern Alaska Range, Alaska: Geological Society of America Bulletin, v. 86, p. 819–829, doi:10.1130/0016-7606(1975)86<819:GPAMEA>2.0.CO;2.

Richter, D.H., Smith, J.G., Lanphere, M.A., Dalrymple, G.B., Reed, B.L., and Shew, N., 1990, Age and pro-

gression of volcanism, Wrangell volcanic field, Alaska: Bulletin of Volcanology, v. 53, p. 29–44, doi:10.1007/BF00680318.

Richter, D.H., Moll-Stalcup, E.J., Miller, T.P., Lanphere, M.A., Dalrymple, G.B., and Smith, R.L., 1994, Eruptive history and petrology of Mount Drum volcano, Wrangell Mountains, Alaska: Bulletin of Volcanology, v. 56, p. 29–46, doi:10.1007/BF00279727.

Richter, D.H., Preece, S.J., McGimsey, R.G., and Westgate, J.A., 1995, Mount Churchill, Alaska: source of the late Holocene White River Ash: Canadian Journal of Earth Sciences, v. 32, p. 741–748, doi:10.1139/e95-063.

Richter, D.H., Ratté, J.C., Leeman, W.P., and Menzies, M., 2000, Geologic map of the McCarthy D-1 quadrangle, Alaska: U.S. Geological Survey Geologic Investigations Series I-2695, scale 1:63,360.

Richter, D.H., Preller, C.C., Labay, K.A., and Shew, N.B., 2006, Geologic map of the Wrangell– Saint Elias Park and Preserve, Alaska: U.S. Geological Survey Scientific Investigations Map 2877, scale 1:350,000.

Ridgway, K.D., and DeCelles, P.G., 1993a, Stream-dominated alluvial-fan and lacustrine depositional systems in Cenozoic strike-slip basins, Denali fault system, Yukon Territory: Sedimentology, v. 40, p. 645–666, doi:10.1111/j.1365-3091.1993.tb01354.x.

Ridgway, K.D., and DeCelles, P.G., 1993b, Petrology of mid-Cenozoic strike-slip basins in an accretionary orogen, Saint Elias Mountains, Yukon Territory, Canada, *in* Johnsson, M.J., and Basu, A., eds., Processes controlling the composition of clastic sediments: Geological Society of America Special Paper 284, p. 67–89.

Ridgway, K.D., Skulski, T., and Sweet, A.R., 1992, Cenozoic displacement along the Denali fault system, Yukon Territory: Eos (Transactions, American Geophysical Union), fall meeting supplement, v. 73, p. 534.

Ridgway, K.D., Skulski, T., and Sweet, A.R., 1996, Cenozoic strike-slip tectonics along the Duke River Fault, St. Elias Mountains; Intracontinental transform fault response to terrane accretion: Geological Society of America Abstracts with Programs, v. 28, no. 7, p. 313.

Ridgway, K.D., Thoms, E.E., Layer, P.W., Lesh, M.E., White, J.M., and Smith, S.V., 2007, Neogene transpressional foreland basin development on the north side of the central Alaska Range, Usibelli Group and Nenana Gravel, Tanana basin, *in* Ridgway, K.D., et al., eds., Tectonic growth of a collisional continental margin: Crustal evolution of southern Alaska: Geological Society of America Special Paper 431, p. 507–547, doi:10.1130/2007.2431(20).

Righter, K., Carmichael, I.S.E., Becker, T.A., and Renne, P.R., 1995, Pliocene–Quaternary volcanism and faulting at the intersection of the Gulf of California and the Mexican volcanic belt: Geological Society of America Bulletin, v. 107, p. 612–626, doi:10.1130/0016-7606(1995)107<0612:PQVAFA>2.3.CO;2.

Rioux, M., Hacker, B., Mattinson, J., Kelemen, P., Blusztajn, K., and Gehrels, G., 2007, Magmatic development of an intra-oceanic arc: High-precision U-Pb zircon and whole-rock isotopic analyses from the accreted Talkeetna arc, south-central Alaska: Geological Society of America Bulletin, v. 119, p. 1168–1184, doi:10.1130/B25964.1.

Roeske, S.M., Snee, L.W., and Pavlis, T.L., 2003, Dextral-slip reactivation of an arc-forearc boundary during Late Cretaceous–early Eocene oblique convergence in the northern Cordillera, *in* Sisson, V.B., et al., eds., Geology of a transpressional orogen developed during ridge-trench interaction along the north Pacific margin: Geological Society of America Special Paper 371, p. 141–169, doi:10.1130/0-8137-2371-X.141.

Rubatto, D., Williams, I.S., and Buck, I.S., 2001, Zircon and monazite response to prograde metamorphism in the Reynolds Range, central Australia: Contributions to Mineralogy and Petrology, v. 140, p. 458–468, doi:10.1007/PL00007673.

Sheaf, M.A., Serpa, L., and Pavlis, T.L., 2003, Exhumation rates in the Saint Elias Mountains, Alaska: Tectonophysics, v. 367, p. 1–11, doi:10.1016/S0040-1951(03)00124-0.

Silberman, M.L., Potter, R.W., II, and Nissenbaum, A., 1976, Stable isotope, sulfide mineralogy, fluid inclusion, and K/Ar age study of the massive sulfide deposits at

Kennecott, *in* Cobb, E.H., ed., The United States Geological Survey in Alaska: Accomplishments during 1975: U.S. Geological Survey Circular 733, p. 51–52.

Silberman, M.L., Mathews, A., Potter, R.W., and Nissenbaum, A., 1977, Stable isotope geochemistry, sulfide mineralogy, and potassium-argon ages of the Kennecott massive sulfide deposits, Alaska, *in* Blean, K.M., ed., The United States Geological Survey in Alaska: Accomplishments during 1976: U.S. Geological Survey Circular 751, p. 56–58.

Skulski, T., Francis, D., and Ludden, J., 1991, Arc-transform magmatism in the Wrangell volcanic belt: Geology, v. 19, p. 11–14, doi:10.1130/0091-7613(1991)019<0011:ATMITW>2.3.CO;2.

Skulski, T., Francis, D., and Ludden, J., 1992, Volcanism in an arc-transform transition zone: The stratigraphy of the Saint Clare Creek volcanic field, Wrangell volcanic belt, Yukon, Canada: Canadian Journal of Earth Sciences, v. 29, p. 446–461, doi:10.1139/e92-039.

Smith, D.G., 1983, Anastomosed fluvial deposits: Modern examples from western Canada, *in* Collinson, J.D., and Lewin, J.D., eds., Modern and ancient fluvial systems: International Association of Sedimentologists Special Publication 6, p. 155–168.

Smith, G.A., 1986, Coarse-grained nonmarine volcaniclastic sediment: Terminology and depositional processes: Geological Society of America Bulletin, v. 97, p. 1–10, doi:10.1130/0016-7606(1986)97<1:CNVSTA>2.0.CO;2.

Smith, G.A., 1987, Sedimentology of volcanism-induced aggradation in fluvial basins: Examples from the Pacific Northwest, U.S.A., *in* Ethridge, F.G., et al., eds., Recent developments in fluvial sedimentology: Society of Economic Paleontologists and Mineralogists Special Publication 39, p. 217–229.

Smith, G.A., and Landis, C.A., 1995, Intra-arc basins, *in* Busby, C.J., and Ingersoll, R.V., eds., Tectonics of sedimentary basins: Oxford, Blackwell Science, p. 263–298.

Smith, G.A., and Lowe, D.R., 1991, Lahars: Volcanohydrologic events and deposition in the debris flow-hyperconcentrated flow continuum, *in* Fisher, R.V., and Smith, G.A., eds., Sedimentation in volcanic settings: Society for Sedimentary Geology (SEPM) Special Publication 45, p. 59–70.

Smith, G.A., Snee, L.W., and Taylor, E.M., 1987, Stratigraphic, sedimentologic, and petrologic record of late Miocene subsidence of the central Oregon High Cascades: Geology, v. 15, p. 389–392, doi:10.1130/0091-7613(1987)15<389:SSAPRO>2.0.CO;2.

Snyder, D.E., and Hart, W.K., 2007, The White Mountain granitoid suite: Isotopic constraints on source reservoirs for Cretaceous magmatism within the Wrangellia Terrane, *in* Ridgway, K.D., et al., eds., Tectonic Growth of a Collisional Continental Margin: Crustal Evolution of Southern Alaska: Geological Society of America Special Paper 431, p. 379–400, doi:10.1130/2007.2431(15).

Souther, J.G., and Stanciu, C., 1975, Operation Saint Elias, Yukon Territory: Tertiary volcanic rocks, *in* Report of activities, part A: Geological Society of Canada Paper 74–1A, p. 39–41.

Steiger, R.H., and Jäger, E., 1977, Subcommission on geochronology: Convention on the use of decay constants in geo- and cosmochronology: Earth and Planetary Science Letters, v. 36, p. 359–362, doi:10.1016/0012-821X(77)90060-7.

Stern, T.A., 1985, A back-arc basin formed within continental lithosphere: The central volcanic region of New Zealand: Tectonophysics, v. 112, p. 385–409, doi:10.1016/0040-1951(85)90187-8.

Stewart, R.J., Hallet, B., Zeitler, P.K., Malloy, M.A., Allen, C.M., and Trippett, D., 2008, Brahmaputra sediment flux dominated by highly localized rapid erosion from the easternmost Himalaya: Geology, v. 36, p. 711–714, doi:10.1130/G24890A.1.

Stock, J., and Molnar, P., 1988, Uncertainties and implications of the Late Cretaceous and Tertiary positions of North America relative to the Farallon, Kula, and Pacific plates: Tectonics, v. 7, p. 1339–1384, doi:10.1029/TC007i006p01339.

Talbot, M.R., and Allen, P.A., 1996, Lakes, *in* Reading, H.G., ed., Sedimentary environments: Processes, facies, and stratigraphy: Oxford, Blackwell Science, p. 83–124.

Thorkelson, D.J., Madsen, J.K., and Sluggett, C.L., 2011, Mantle flow through the Northern Cordilleran slab window revealed by volcanic geochemistry: Geology, v. 39, p. 267–270, doi:10.1130/G31522.1.

Tidmore, R.S., 2004, Sedimentologic and petrologic investigation of the Miocene Frederika Formation: A record of the initial construction of the Wrangell volcanic field, Alaska [B.S. thesis]: Lewisburg, Pennsylvania, Bucknell University, 206 p.

Trop, J.M., 2000, Sedimentary basin development within the Wrangellia composite terrane, Mesozoic Wrangell Mountains basin, southern Alaska: A long-term record of terrane migration and arc construction [PhD thesis]: West Lafayette, Indiana, Purdue University, 310 p.

Trop, J.M., 2008, Latest Cretaceous forearc basin development along an accretionary convergent margin: South-central Alaska: Geological Society of America Bulletin, v. 120, p. 207–224, doi:10.1130/B26215.1.

Trop, J.M., and Ridgway, K.D., 2007, Mesozoic and Cenozoic tectonic growth of southern Alaska: A sedimentary basin perspective, *in* Ridgway, K.D., et al., eds., Tectonic Growth of a Collisional Continental Margin: Crustal Evolution of Southern Alaska: Geological Society of America Special Paper 431, p. 55–94, doi:10.1130/2007.2431(04).

Trop, J.M., Ridgway, K.D., Manuszak, J.D., and Layer, P.W., 2002, Sedimentary basin development on the allochthonous Wrangellia composite terrane, Mesozoic Wrangell Mountains basin, Alaska: A long-term record of terrane migration and arc construction: Geological Society of America Bulletin, v. 114, p. 693–717, doi:10.1130/0016-7606(2002)114<0693:MSBDOT>2.0.CO;2.

Van der Plas, L., and Tobi, A.C., 1965, A chart for judging the reliability of point counting results: American Journal of Science, v. 263, p. 87–90, doi:10.2475/ajs.263.1.87.

Van Dijk, J.P., 1994, Late Neogene kinematics of intra-arc oblique shear zones: The Petilia-Rizzuto fault zone (Calabrian arc, central Mediterranean): Tectonics, v. 13, p. 1201–1230, doi:10.1029/93TC03551.

Walker, G.P.L., 2000, Basaltic volcanoes and volcanic systems, *in* Sigurdsson, H., et al., eds., Encyclopedia of Volcanoes: San Diego, California, Academic Press, p. 283–289.

Wang, F., Zicheng, P., Zhu, R., He, H., and Yang, L., 2006, Petrogenesis and magma residence time of lavas from Tengchong volcanic field (China): Evidence from U series disequilibria and ^{40}Ar/^{39}Ar dating: Geochemistry Geophysics Geosystems, v. 7, Q01002, doi:10.1029/2005GC001023.

Wang, Y., Zhang, X., Jiang, C., Wei, H., and Wan, J., 2007, Tectonic controls on the late Miocene–Holocene volcanic eruptions of the Tengchong volcanic field along the southeastern margin of the Tibetan plateau: Journal of Asian Earth Sciences, v. 30, p. 375–389, doi:10.1016/j.jseaes.2006.11.005.

Waythomas, C.F., and Wallace, K.L., 2002, Flank collapse at Mount Wrangell, Alaska, recorded by volcanic mass-flow deposits in the Copper River lowland: Canadian Journal of Earth Sciences, v. 39, p. 1257–1279.

Weinberg, R.F., 1992, Neotectonic development of western Nicaragua: Tectonics, v. 11, p. 1010–1017, doi:10.1029/92TC00859.

Williams, I.S., 2001, Response of detrital zircon and monazite, and their U/Pb isotopic systems to regional metamorphism and host-rock partial melting, Cooma complex, southeastern Australia: Journal of Earth Sciences, v. 48, p. 557–580, doi:10.1046/j.1440-0952.2001.00883.x.

Winchester, J.A., and Floyd, P.A., 1977, Geochemical discrimination of different magma series and their differentiation products using immobile elements: Chemical Geology, v. 20, p. 325–343, doi:10.1016/0009-2541(77)90057-2.

Witmer, J.W., 2009, Neogene deposition, provenance, and exhumation along a tectonically active, glaciated continental margin, Yakataga and Redwood formations, southern Alaska syntaxis [M.S. thesis]: West Lafayette, Indiana, Purdue University, 313 p.

Worthington, L.L., Gulick, S.P.S., and Pavlis, T.L., 2010, Coupled stratigraphic and structural evolution of a glaciated orogenic wedge, offshore St. Elias orogen, Alaska: Tectonics, v. 29, doi:10.1029/2010TC002723.

Worthington, L.L., Van Avendonk, H.J.A., Gulick, S.P.S., Christeson, G.L., and Pavlis, T.L., 2012, Crustal structure of the Yakutat terrane and the evolution of subduction and collision in southern Alaska: Journal of Geophysical Research, v. 117, B01102, doi:10.1029/2011JB008493.

Yang, H., Chung, S., Chu, C., Gallet, S., and Mitchell, A., 2007, Quaternary volcanic rocks from Central Burma: Geochemical characteristics and petrogenesis: Eos (Transactions, American Geophysical Union), v. 88, no. 52, fall meeting supplement, abs. T31B–0470.

Yogodzinski, G.M., Kay, R.W., Volynets, O.N., Klolskov, A.V., and Kay, S.M., 1995, Magnesian andesite in the western Aleutian Komandorsky region: Implications for slab melting and processes in the mantle wedge: Geological Society of America Bulletin, v. 107, p. 505–519, doi:10.1130/0016-7606(1995)107<0505:MAITWA>2.3.CO;2.

Yogodzinski, G.M., Lees, J.M., Churikova, T.G., Dorendorf, F., Wöerner, G., and Volynets, O.N., 2001, Geochemical evidence for the melting of subducting oceanic lithosphere at plate edges: Nature, v. 409, p. 500–504, doi:10.1038/35054039.

York, D., 1968, Least squares fitting of a straight line with correlated errors: Earth and Planetary Science Letters, v. 5, p. 320–324, doi:10.1016/S0012-821X(68)80059-7.

Zeitler, P.K., Chamberlain, C.P., and Smith, H.A., 1993, Synchronous anatexis, metamorphism, and rapid denudation at Nanga Parbat, Pakistan Himalaya: Geology, v. 21, p. 347–350, doi:10.1130/0091-7613(1993)021<0347:SAMARD>2.3.CO;2.

Zeitler, P.K., and 19 others, 2001, Crustal reworking at Nanga Parbat, Pakistan: Metamorphic consequences of thermal-mechanical coupling facilitated by erosion: Tectonics, v. 20, p. 712–728, doi:10.1029/2000TC001243.

Zellers, S.D., and Gary, A.C., 2007, Unmixing foraminiferal assemblages: Polytopic vector analysis applied to Yakataga Formation sequences in the offshore Gulf of Alaska: Palaios, v. 22, p. 47–59, doi:10.2110/palo.2005.p05-041r.